5-2013

Study of Immobilizing Cadmium Selenide Quantum Dots in Selected Polymers for Application in Peroxyoxalate Chemiluminescence Flow Injection Analysis

Christopher S. Moore
East Tennessee State University

Follow this and additional works at: https://dc.etsu.edu/etd

Part of the Analytical Chemistry Commons, Bioimaging and Biomedical Optics Commons, and the Nanoscience and Nanotechnology Commons

Study of Immobilizing Cadmium Selenide Quantum Dots in Selected Polymers for Application

in Peroxyoxalate Chemiluminescence Flow Injection Analysis

_____

A thesis

presented to

the faculty of the Department of Chemistry

East Tennessee State University

In partial fulfillment

of the requirements for the degree

Master of Science in Chemistry

_____

by

Christopher S. Moore

May 2013

_____

Dr. Cassandra Eagle, Chair

Dr. Alesky Vasiliev

Dr. Jeffrey Wardeska

ABSTRACT

Study of Immobilizing Cadmium Selenide Quantum Dots in Selected Polymers for Application

in Peroxyoxalate Chemiluminescence Flow Injection Analysis

by

Christopher S. Moore

Two batches of CdSe QDs with different sizes were synthesized for immobilizing in

polyisoprene (PI), polymethylmethacrylate (PMMA), and low-density polyethylene (LDPE).

The combinations of QDs and polymer substrates were evaluated for their analytical fit-for-use

in applicable immunoassays. Hydrogen peroxide standards were injected into the flow injection

analyzer (FIA) constructed to simulate enzyme-generated hydrogen peroxide reacting with *bis*-

(2,4,6-trichlorophenyl) oxalate.

Linear correlations between hydrogen peroxide and chemiluminescent intensities yielded

regression values greater than 0.9750 for hydrogen peroxide concentrations between 1.0×10^{-4}

M and 1.0×10^{-1} M. The developed technique's LOD was approximately 10 ppm. Variability of

the prepared QD-polymer products was as low as 3.2% throughout all preparations. Stability of

the preparations was tested during a 30-day period that displayed up to a four-fold increase in the

first 10 days. The preparations were decently robust to the FIA system demonstrating up to a

15.20% intensity loss after twenty repetitive injections.

ACKNOWLEDGEMENTS

I would like to acknowledge several important collections of people that helped make this thesis and supporting graduate work possible.

I will begin by thanking my family first and foremost. My parents and grandparents have been of the greatest influence in emphasizing the importance of an education. Without that emphasis I would not appreciate the true value in continuing my education. They also instilled a desire to always strive for more out of life.

Thanks also go to my professional colleagues. They provided much wisdom and encouragement during my graduate career. Many thanks go to Mr. John Harrison and Dr. Spencer Hochstetler for mentoring me in the profession of analytical chemistry. Their guidance has inspired me to be intrigued with the observations that chemistry provides and to think rationally about the causes that create the effects. My academic colleagues also deserve acknowledgement as collegiate careers cannot be completed without their support.

Finally, I would like to acknowledge several professors I have had the opportunity to cross paths with along my academic journey. Thank you to my research advisors, both undergraduate and graduate, for introducing me to different levels of academic research, and allowing me to apply my classroom knowledge to laboratory practices. This has taught me how to work and think independently, while not forgetting how to collaborate with others. This is of great importance in my profession now and onward. Also thanks to them for the opportunities to perform research in areas of high interests and intriguing discoveries. Many thanks go to both Dr. Jeffrey Wardeska and Dr. Chu-Ngi Ho for their guidance.

DEDICATION

The work presented is dedicated to my niece, Rebecca Shay.

TABLE OF CONTENTS

6

8

LIST OF TABLES

LIST OF FIGURES

CHAPTER 1

NANOCHEMISTRY PRINCIPLES AND APPLICATIONS

Introduction

Nanotechnology has become a household word in the recent decades. The innovation of

nanotechnology has been expanded across industries such as medical, electronics, and optics (1, 2). The

effects of nanotechnology on society, now and in the future, have been portrayed as the "Second

Industrial Revolution" (3). The possibilities and applications of nanotechnology continue to emerge as

scientists and engineers explore deeper into the principles of nanochemistry.

Results of nanochemistry have been on display for centuries as immense red colors from gold

nanoparticles on stained-glass art works (4). Prior to the twentieth century, nanochemistry had not been

proposed; therefore not understood. Renowned physicists Erwin Schrodinger and Richard Feynman

initiated the concept of building up to nanoparticles rather than dissecting down to them (3,5). Advances

in chemical instrumentation helped re-ignite nanochemistry first proposed decades before (2).

The basis of nanochemistry lies in the syntheses and properties of near-atomic-sized particles

termed nanoparticles. A nanoparticle is defined as a collection of atoms or molecules that is less than 100

nanometers in one of its three directional dimensions (2,6). These collections can contain up to one

million atoms or molecules in a variety of geometries. Such geometries can include spheres, cylindrical

tubes, and triangular disks (2,6).

The shape and size of a synthesized nanoparticle affects both its physical and chemical properties

(2,4,6). The effect on the properties is inversely proportional to the nanoparticle size. Learning to control

the size and properties of nanoparticles, nanotechnology can influence human life tremendously. Figure 1

compares a 10 nm nanoparticle to atomic components and other nanoparticles.
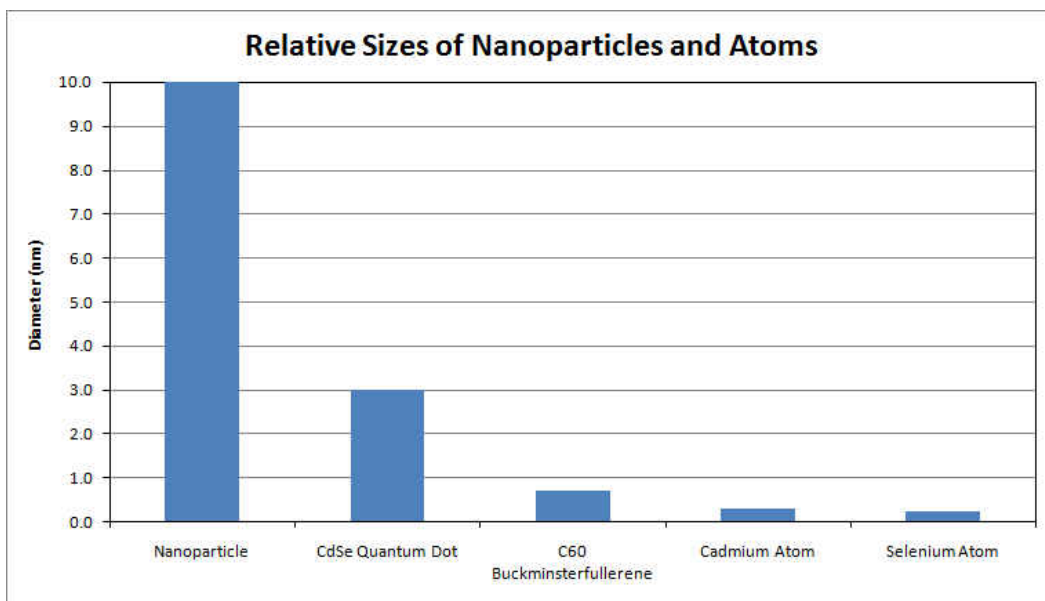
Figure 1. Chart of size comparison of nanoparticles and atoms

Social impacts of nanotechnology can be both positive and negative (3,6,7). Research and application of nanotechnology in the electronic and medical industries have been two of the most studied fields. Considering advances in computational processing, Gordon Moore of IBM proclaimed an expectation that processing power capability of electronics approximately doubles per year (3). This expectation or prediction was termed Moore's Law. Extrapolation of Moore's Law predicts miniaturized power production sources by the mid-twenty-first century (3). Trends in this direction can be seen with the advent of solar cells using nanoparticles.

It has been seen that nanotechnology can provide enormous benefits to society. The majority of society, however, remains blind to the implications of nanochemistry on the present and upcoming future (1). Environmental and health concerns arise whenever new materials are produced. Waste containing nanoparticles have been rigorously studied with governmental funding (8). Quantum dot toxicity on human cellular uptake and environmental bacteria functions create additional areas of concern (9,10). On the other hand, silver ion nanoparticles have been employed in many anti-microbial applications (8) while biocompatible quantum dots are being synthesized for luminescent medical imaging (7,11).

14

<u>Synthesis of Nanoparticles and Quantum Dots</u>

Nanoparticles exist in a unique size region between the everyday bulk materials and the atomic components that the bulk is comprised of. To reach the size of these particles, one can follow either a "top-down" or "bottom-up" approach (2,5-7). Working from bulk material, nanoparticles are synthesized using mechanical methods of precise milling and grinding. Though the mechanical methods do create nanoparticles, control of their size and shape is hindered (2). Some procedures require the assistance of surfactants to minimize the aggregation of the particles during machining (6).

To produce nanoparticles of desired characteristics, many work from the atomic level building upwards. This "bottom-up" approach offers several techniques and advantages for to controlling the expected properties during synthesis of designed nanoparticles. The synthesis of nanoparticles can be carried out in either a gaseous or liquid phase.

<u>Gaseous Synthesis</u>

Nanoparticles of metals and metal oxides typically employ gaseous syntheses (2,6). All gaseous syntheses follow similar routes by condensing the particles from a supersaturated atmosphere (7). Initiation of gaseous syntheses, however, can follow several routes based on the energy source employed. Once initiated through a thermal, sputtering, or laser method, the elements condensed begin nucleation and growth into the desired particles (2,6).

The most beneficial gaseous, or vapor, synthesis is the vapor deposition technique. This synthesis proceeds via a decomposition of metal or semiconductor precursor (6). Pyrolysis immediately vaporizes the precursor under an inert atmosphere. Depending on defined configurations of the apparatus used for synthesis, condensation of the vapor releases the precursors into their zero-valent states (7). Soon after condensation of the elements, agglomeration occurs to begin building the nanonparticles. Collecting on a cool or charged surface, vapor deposition is a useful method for producing nanoparticle

films of high purity (2). Disadvantages in using vapor deposition are commonly found in the cost and operational integrity.

Colloidal Synthesis

In contrast to the gaseous synthesis, liquid syntheses are considered easier, cheaper, and more controllable. Dispersive solutions are used to serve as media for self-assembly or to promote precipitation of the nanoparticles (6). Molecular self-assembly synthesis provides the benefit for polymers to agglomerate for nanoparticle synthesis. The colloidal synthesis, however, is more commonly employed among published works (12).

As mentioned, many reports of the synthesis of nanoparticles have been carried out in colloids suggesting its popularity among researchers. This popularity implies a need to better understand how nanoparticles evolve from the colloidal approach. Formation of nanoparticles typically follows a two-step process, nucleation and growth (12). The nucleation step occurs first precipitating a collection of monomers produced from thermal decomposition and precursors and their stabilization. Common monomers from precursors involve cadmium and selenium (9,13-15).

The nucleation of a nanoparticle is governed by the energy potential between crystalline and liquid states (12). When the potential of the crystalline state falls below that of the liquid state nucleation is favored as the calculated Gibbs free energy potential is negative. To induce spontaneous nucleation, hot-injection methods into organic solvents are commonly practiced (12-14). Hot injection techniques exhibit an advantage of immediate nucleation prior to any growth of the nuclei formed. This advantage is important for size-selective syntheses.

The second half of the nanoparticle synthesis in colloids is growth. Complete nucleation prior to growth is preferred to minimize the dispersity of particle size (12). Migration and diffusion of monomers to the nuclei surface are important to the nanoparticle growth. In methods using high-concentrated injections of precursor monomers, diffusion becomes a negligible factor. This is due to lack of a

16

distinguishable concentration gradient surrounding the nuclei surface. Therefore the limiting factor lies in the speed of reaction between the nuclei surface and surrounding surplus of injected monomers.

As the nuclei growth progresses forming nanoparticles, diffusion of monomers becomes more prominent. Monomer depletion increases with reaction time minimizing the availability of monomers within close proximity of the growing nanoparticles (12). Continued growth relies on the concentration gradient formed between the nanoparticle region and bulk solution. Diffusion from the bulk solution into the less concentrated nanoparticle region allows this continued growth. The Nernst-Planck equation and Fick's Law for diffusion can be applied to help study and predict growth patterns and rates (16,17).

By permitting the colloidal solution to continue reacting in the growth stage the smaller nanoparticles can decompose releasing monomers under the extreme synthesis conditions. The available monomers become collected by larger nanoparticles. This process known as Ostwald ripening (12) provides smaller dispersities in particle sizes, but the average particle size is not commonly of small dimensions. If particle size, however, holds a greater importance than size dispersity temperature quenching during synthesis or size extraction methods can be applied.

<u>Band Gap Chemistry</u>

The chemistry of electron movement through solids, such as semiconductors and metals, revolves around the existence of the band gap (18,19). Molecular orbitals are created from the combination of individual atomic orbitals. As the valence electrons combine to form low-energy and occupied orbitals, opposing unoccupied orbitals of higher energy are formed. The increasing number of molecular orbitals decreases the space between orbitals of the same category, occupied and unoccupied. This creates a "band" of energy levels for electrons to move freely. Bands for both occupied orbitals and unoccupied orbitals are produced. Electron occupied bands are known as valence bands, and unoccupied bands are referred to as conduction bands. The gap between the bands is known as the "band gap".

Band gaps can vary based on the molecule size, or number of atoms. The gap decreases with an increase in the number of atoms until bulk properties are reached. Dense and conductive metals for example, have little or no band gaps for electrons to transition across. Semiconductors have moderate band gaps with transition energies similar to those associated with visible light (19). Wavelengths of light can be expressed as energy in electron volts, eV. Most semiconductor band gap energies exist up to 4 eV (20). Their band gap energies, E_g, can be tuned by particle size (21) and surface chemistry.

<div align="center">Surface Chemistry of Nanoparticles</div>

Nanoparticles can exhibit electrical and optical properties that are dependent upon the surface chemistry involved. Respective surface chemistry involves the use of various ligands to stabilize and functionalize the synthesized nanoparticles of interest (6). Stabilization of the nanoparticle can be performed to increase photostability, or even inhibit aggregation within dispersed solutions. The functionalization of surfaces creates numerous possibilities and applications for material properties existing from a single nanoparticle core.

Effect of Organic Ligands

Organic ligands are used in nanoparticle syntheses to stabilize or functionalize the surface. Bulky organic molecules such as tri-n-octyl phosphine and oleic acid are used to coordinate and aid dissolution of the semiconductor elements (13,14,22). During synthesis nanoparticles can agglomerate or group together, making it difficult to produce smaller particles. Boatman et al. (13) used 1-octadecene as a high-temperature solvent while simultaneously taking advantage of its ability to inhibit sudden agglomeration.

Other uses of organic ligands relate to functionalizing surfaces for solvent compatibility and tuning optical properties. Semiconductor quantum dots in organic solvents have exceptional luminescent properties. Their application in the biological sciences, however, requires aqueous compatibility and biocompatibility. Beta-cyclodextrin has been employed (23) to produce water-soluble CdSe and

CdSe/CdS quantum dots. The modified quantum dots were observed to be soluble as the solution became an orange-red during synthesis. The core CdSe fluorescence emission was recorded at 550 nm with a quantum yield of 0.65%.

An amphiphilic polymer to mediate aqueous compatibility was evaluated by Pellergrino et al. (24). Different nanoparticles including CdSe/ZnS were synthesized in organic media with hydrophobic ligands attached to the surface. The maleic anhydride polymer was reacted with the hydrophobic chains to form a surrounding shell with hydrophilic groups exposed. Diameters of the nanoparticles were observed to more than double with the addition of the polymer shell.

It has been reported that organic ligands can also alter the optical properties of nanoparticles. Research groups have used CdSe quantum dots to examine these influences of organic ligand exchange. Tri-n-octylphosphine (TOP) and its oxide form (TOPO) were substituted with pyridine by Hyun-Ju et al. (25) to measure surface effects. Upon ligand exchange the quantum dot solution was exposed to UV light for 3 days. The effect was a red shift in emission wavelength. Two explanations were manifested to determine why the shift occurred. The first was the ability of pyridine to participate in electron transfer unlike that of the phosphine and phosphine oxide. The second was the absorption of oxygen during the 3 days of of UV exposure. Oxygen was suspected to react with surface cadmium forming CdO.

Several years later, Luo et al. (26) revisited pyridine-capping of CdSe quantum dots. Four sizes of CdSe capped with TOPO were synthesized. The TOPO ligands were exchanged with pyridine. Blue shifts to higher energy were observed after the ligand exchange. The smallest quantum dots synthesized saw a 46.1 meV shift, while the other three sizes shifted by less than 10 meV. A red shift was also noted to occur by approximately 23 meV due the change in surface electron density.

Effect of Inorganic Ligands

Core quantum dots synthesized are susceptible to reactions that decrease emission intensities and quantum yields. The surfaces of core quantum dots may also be imperfect with surface states that trap

mobile electrons. Inorganic shells of semiconductors different than that of the core have been applied to passivate surfaces (27).

Many research groups have studied the effects of capping CdSe quantum dots with semiconductors of wider band gap. The effects reported were reproducible increases in photoluminescence intensities and quantum efficiencies. CdSe quantum dots were synthesized by Hao et al. (28) with low quantum yields via a microemulsion technique. Attempts were made to create an outer shell of CdS to improve the quantum yield. The addition of Na_2S as a sulfide source to for a CdS shell on CdSe quantum dots failed to improve the yield. The CdS-capped CdSe quantum dots also synthesized by Hao's group demonstrated efficiencies up to 15%. This efficiency was low compared to 20-80% yields by prior preparations using an epitaxial growth technique (28). The epitaxial growth of CdS on CdSe by Lin et al. (29) only yielded an efficiency of 2.4% with the addition of thioacetamide as the sulfur source. Exposure to UV light increased the yield immensely to 60% and caused a luminescent 14 nm blue shift.

Semiconductors of ZnSe (30) and ZnTe (31) were used to form a shell around core CdSe quantum dots. The CdSe quantum dots coated with ZnSe fluoresced near 580 nm. The CdSe/ZnSe emission was a red shifted approximately 40 nm from the core emission. The peak intensity was also increased approximately 10 fold. These observations were suggestive of the CdSe surface becoming passivated by the ZnSe shell eliminating surface imperfections. The electrogenerated luminescence spectrum was also compared to that of photoluminescence (30). The overlapping spectra provided insight that luminescence stemmed from the core CdSe quantum dot when core-shell interfaces were ideal.

A ZnTe shell on CdSe was used to study electron-hole separation. Increasing the ZnTe shell thickness increased fluorescent lifetimes confirming the relocation of the vacant hole from the core to the shell (31). The displacement of the hole to an energy band of the shell provided an indirect fluorescence upon recombination of the electron from the CdSe conduction band and hole from the ZnTe valence band.

Extensions of the core-shell structures to core-shell-shell structures have improved photoluminescence efficiencies and stabilities (32,33). The addition of a ZnS shell restricts the exposure of electrons to the surrounding environment due to a large band gap. Efficiencies, however, can be diminished when ZnS and the underlying semiconductor has a mismatch in the crystalline lattice structures (32). The lattice mismatch between CdSe and ZnS creates interfacial imperfections allowing for electron trapping or oxidation via diffusion. By inserting a semiconductor material between the core and outer shell, the mismatch can be minimized or eliminated. The mediating semiconductor material used must be composed of either the cationic or anionic of the core or previous shell. Talapin et al. (32) used CdS and ZnSe as the mediating semiconductors between CdSe and ZnS. Emission wavelengths were red-shifted by approximately 50 nm from the CdSe core emission, and effeciencies increased to near 80%.

The use of ZnS also is important for dispersion in aqueous media. CdTe/CdSe quantum dots have been examined for their application in biological imaging (33). The CdTe core quantum dots, when coated with a monolayer of CdSe exhibited an impressive efficiency of 94%.   Upon transfer to aqueous solutions, the photoluminescence of CdTe/CdSe was completely quenched. Zhang et al. (33) reported that the quenching in aqueous conditions could be due to electrons reaching the CdSe surface or extremeties. Intriguingly the CdTe/CdSe quantum dots were prepared in chloroform. This suggests the solvent conductivity aids to separate the electron-hole pair far enough apart that recombination is improbable. By coating the CdTe/CdSe with ZnS to confine the electron-hole pair, dispersion in aqueous media restored photoluminescence efficiency to 84%.

Effect of Oxygen

Oxygen makes up approximately one-fifth of our planet's atmosphere. This environmental factor makes oxidation a concern when performing inert-condition syntheses. As nanoparticle syntheses employ the reduction of metals and salts, their potential to form oxides exists. With dimensions of nanoparticles

less than 10 nm, the atomic affects are much stronger from oxidation. This alters the semiconductor's band gap energy as oxygen reacts as an n-type dopant.

Several research groups have discussed the concerns of quantum dot photodegradation by oxygen (23,25,32). The best approach to combat oxidation of the quantum dot surface has been to add a semiconductor layer with larger band gap energy. Though coatings with ZnS (31,32,34) drastically improved the stability of CdSe quantum dots; diffusion of oxygen through lattice mismatch was still observed (32). This provides evidence that a better understanding of oxygen interaction with quantum dot surfaces is required.

Investigations into the role of oxygen from air (35) and solvent (36) exposures were carried out. CdSe quantum dots dispersed in chloroform exhibited an intensity increase. Myung et al. (35) prepared the quantum dots in a colloidal solution using tri-octylphosphine oxide as a stabilizing ligand. After precipitation and re-dispersion into chloroform the quantum dots were stored free of light. Air exposure over time caused irreversible photoluminescence observations upon additional precipitation and dispersion routines. Sparging the chloroform dispersion with oxygen increased the rate of increasing intensity, and provided sound evidence that oxygen was adsorbing to the quantum dot surface forming cadmium and selenium oxides.

Dissolved oxygen in coordination with solvent molecules was found to affect the optical properties of CdSe quantum dots (36). The absorption of a CdSe quantum dot dispersion in toluene approximately tripled in absorbance when saturating with dissolved oxygen. Removing the dissolved oxygen with argon returned the absorbance to near the pre-oxygenated levels. Quantum dots dispersed in air-saturated solvents exposed to UV illumination were observed to undergo photooxidation. It was suggestive that decomposition of the organic capping agents such as tri-octylphosphine oxide rendered surface sites available for oxide formation (36).

Quantum Dot Optical Applications

The optical properties expressed by quantum dots are unique to most light-emitting species. Synthesized quantum dots offer tunable emission colors and impressive efficiencies through size control and surface chemistry, respectively. These properties have gained attention for application in display lighting and medical use.

Quantum Dot Light-Emitting Diodes (QLEDs)

Light emitting diodes (LEDs) have been an increasing trend in the past couple of decades. The recent initiative to go "green" has influenced many to evaluate ways to reduce energy consumption. LEDs provide comparable performance to incandescent and fluorescent lighting; however, only using a fraction of the energy. Bulk semiconductor materials are used in the construction of LEDs (37). Band gap properties of the semiconductors allow for light to be produced when an electrical current is applied. Continuing interest in LEDs has led to application research of quantum dot light emitting diodes (QLEDs), where LEDs can be fabricated on the nanoscale with desirable characteristics (38).

Colloidal CdSe quantum dots were tested for construction of QLED devices (39-41). Surface-attached molecules of oleic acid from synthesis were exchanged with a block copolymer (39). Three-fold improvements in device efficiency were observed when compared to unmodified quantum dots. Zorn et al. (39) also discovered that the stability of blue-emitting dots coated with the copolymer increased approximately one order of magnitude when continuously exposed to UV light.

QLED configurations are sandwich-like devices. The outer layers consist of an aluminum-based anode and indium tin oxide (ITO) cathode (39-40), while transport layers and quantum dots reside between. These electrodes transport electrons and holes, respectively. The electrons and holes combine within the middle-layered quantum dots releasing luminescence. Bae et al. (40) produced a multi-layer region of CdSe/ZnS dots between the electrodes. Alternating the layers between green and red emitting quantum dots, electroluminescent spectra showed that all emission was from the two layers closest to the

anode. The majority of emission was from the quantum dot layer adjacent to the anode. Intensities of the device were stated to be 600 times brighter than others previously reported.

Inverted device configurations were examined by Kwak et al. (41) to yield red, green, and blue emissions. A zinc oxide layer was inserted between the ITO electrode and quantum dot layers. The zinc layer aided electron injection and transport from the ITO electrode. It also provided a foundation for deposition of succeeding quantum dot layers by spin-coating (41). Overall device efficiencies for red, green, and blue emissions were 7.3%, 5.8%, and 1.7%, respectively. Substituting hole transport layers with different HOMO energies; an increase in efficiency was observed when the orbital energy increased. The inverted configurations also exhibited improved stabilities by three orders of magnitude.

Aside from improving emission colors in the visible spectrum, QLEDs emitting in the infrared spectrum region were of interest. Monat et al. spin-casted above-average sized InAs/GaAs quantum dots into a QLED device (42). Electroluminescence spectra showed two distinct peaks near 1300 nm with currents less than one microamp. The intensity of luminescence saw a linear increase by 100-fold between 0.1 microamp and 10 microamps. The group suggested QLEDs of this emission type be used in quantum cryptography (42).

Biosensors and Probes

Sensitivity and selectivity of luminescent techniques make them appealing to biological detection schemes and applications. Biosensors and bioprobes have been investigated for molecular–level detection with ease and fast response. Sensors are created by linking fluorescent compounds, termed labels, to peptide chains. The fluorescent labels are then used to detect chemical or biological reactions by monitoring for emitted light. Interest in quantum dot optical and surface properties were evaluated in several application studies (43-48).

Quantum dots coupled with the luminescence event of fluorescence resonance energy transfer, FRET, were studied as contenders for biosensors monitoring enzyme activity (43-45). FRET is the

occurance when two fluorescent species come within close proximity of each other (49). When the primary fluorescing agent is excited it donates its excess energy to the nearby secondary fluorescing agent without light emission. The transferred energy when absorbed is released as the acceptor's characteristic wavelength of light, red-shifted from the donor's characteristic's emission wavelength.

Rhodamine was used as a FRET acceptor from CdSe/ZnS quantum dot donors by Shi et al. (43). Peptide chains modified with the rhodamine were linked to the surface of the quantum dot using cysteine. The intensity of the modified quantum dots decreased by four-fold following peptide addition. An optimal ratio for rhodamine molecules per quantum dot was determined as 48:1 that yielded acceptable FRET efficiency for probe application. Cleavage of the peptide chains by trypsin simultaneously decreased the rhodamine emission and increased the quantum dot emission. Fifteen minute reaction times provided 1 ppm detection limits. Extending the reaction time to 2 hours improved detection by one order of magnitude.

More quantum dot-peptide configurations were examined for early cancerous, disease detection (44-45) to replace radioactive biomarkers. Phosphorylation by protein-kinase activity was monitored by the increase of the FRET-acceptor intensity, AlexaFluor 647 (44). Water-soluble CdSe/ZnS quantum dots were synthesized to emit near 600 nm. Using quantum dots with tunable emission presented the ability to keep observed emission separate from cellular fluorescence. Tyrosine activity was dependent on adenosine triphosphate concentration. Tested kinases Src and AbI allowed up to 75% efficiency in FRET and sub-nanomolar detection comparable to previously reported sensor capabilities (44).

Lowe et al. (45) exploited enzyme-binding specificity with pre-modified, purchased quantum dots. Two different emitting quantum dots, 525 nm and 655 nm, were linked to different peptide chains. The 525-nm emissive quantum dots were linked to peptides with gold nanoparticles. The peptide chains of the 655-nm emissive quantum dots were available for phosphorylation to attract FRET acceptors.

Both peptide-configured quantum dots were combined in the same solution to detect a kinase activator, uPA, and kinase receptor, Her2. Early breast cancer detection has relied on monitoring Her2 onset levels (45). The neat solution prior to enzyme addition displayed emission at 520 nm for the FRET with the gold nanoparticle, and 655 nm for the unphosphorylated quantum dot-peptide configuration. Addition of uPA cleaved the gold nanoparticle peptide diminishing the FRET intensity and increasing the 525-nm quantum dot intensity. Simultaneously, Her2 addition catalyzed the phosphorylation of the 655-nm quantum dot-peptide configuration by phosphate removal from adenosine triphosphate, causing intensity growth at 695 nm. Detection of each enzyme by activity was not affected by the other in the same assay. Limits of detection were found to be 50 ng/mL for uPA and 7.5 nM for Her2 (45). These limits were improved to 25% and 50% of previously stated values, respectively.

Portable and on-demand devices were conceptualized using quantum dot biosensors (46,47). Detection of pesticide, 2, 4-dichlorophenoxyacetic acid, was of particular interest by Long et al. (46) for its role in human toxicity. A microfluidic device less than 0.02 m^3 was constructed to excite volumes of 35 µL and measure the FRET emission. The emission intensity was shown to be inversely proportional to the pesticide's concentration. A dynamic range was produced between 10 and 1000 nM that exhibited a linear regression of 0.9829. The technique was found to be completely recoverable within experimental error, and be sensitive down to 0.5 nM. Additionally, the device flushing and sample analysis times combined only required a total of six minutes. The device described by Long et al. (46) provided a rapid and simple task for determining a toxin at trace levels.

Fluorescent CdSe/ZnS quantum dots were applied to immunochromatographic strip assays by Zou et al. (47) for environmental testing of pesticides. Immunochromatographic strips allow for separation of important analytes from the matrix or environment they reside. Trichloropyridinol was selected as the analyte for evaluating the on-demand testing device. Competitive binding activity between free TCP and TCP-quantum dot conjugates provided the mode of analyte detection. As free TCP competition increased against the TCP-quantum dot conjugates binding, less bounded conjugates resulted

in a fluorescent intensity decrease. The integrity of the on-demand device was comparable to existing capabilities (47). A detection limit of 1 ng/mL was determined with exceptional linearity, $R^2 = 0.9935$, up to 50 ng/mL. Recovery of the analyte was 102% with variability less than 13%.

Quantum dots as fluorescent bioprobes have not only been investigated for trace molecular detection, but also for medical imaging purposes. Bioconjugated quantum dots were illuminated to induce "blueing" (48) of the dots' fluorescence emission. Photooxidation was stated as the culprit to the emission shifting to higher-energy wavelengths as oxygen diffused beneath the ZnS shell of the quantum dots. As previously mentioned (32) the mismatch between CdSe and ZnS geometries compromised photostability. The quantum dot application to nanoscopy reported by Hoyer et al. (48) produced cellular images of microtubular structure patterns. Brilliant emission intensities of the quantum dots yielded resolution on the nanoscale comparable to the size of a quantum dot.

<center>Quantum Dot Immobilization</center>

The optical properties of quantum dots make them intriguing to many optical and electronic applications discussed in previous sections. Application of the quantum dots, however, is inhibited by their dynamic and mobile environments. To overcome this inhibition, methods to bond or immobilize the quantum dots have introduced a sector of research related to quantum dot chemistry. Common substrates used to immobilize quantum dots have been polymers (50-52), gels (53,54), and silica (55,56).

Immobilizing quantum dots with trans-polyisoprene was evaluated for producing biocompatible biosensors (50). Inorganic CdSe quantum dots alone pose a toxic effect to biological entities. Preparation of biocompatible quantum dots have typically diminished the above-average quantum efficiency (50) demonstrated by the core quantum dots in non-aqueous media. Yin et al. immobilized CdSe/ZnS in polyisoprene via emulsification in a surfactant. The encapsulated quantum dots were prepared through polymer and quantum dot dissolution in a compatible solvent followed by transfer to the surfactant. The surfactant acted as an inhibitor against agglomeration of the polymer-coated CdSe dots.

<center>27</center>

The encapsulated CdSe/ZnS quantum dots proved to be resistant to defective surface chemistry for several weeks yet, the emission color and intensity changed. Photooxidation of the quantum dots was stated (50) as the reason for the change of emission. Yin's group also reported that the quantum dots were not completely shielded from external factors such as oxygen. A second round of polyisoprene-quantum dot composites was prepared with emphasis on cross-linking of the polymer. Results proved an oxygen-resistant barrier had been constructed as the emission color did not change. The stability of the cross-linked composites far extended those non-cross-linked lasting for at least eight months (50).

Application of the polyisoprene-quantum dot composites was tested for biosensing. The composites were modified with streptavidin. The streptavidin when in proximity to biotin would cause the CdSe/ZnS quantum dots to fluoresce. Biotin was attached to polystyrene particles for use in controlled experiments with the streptavidin-modified composites (50). Microscopy images were taken to observe streptavidin-biotin interactions. It was observed that the quantum dots emitted light on the circumference of the polystyrene particles. Streptavidin-free composites did not fluoresce when reacting with the biotin on polystyrene. This guaranteed that quantum dot emission was only initiated by streptavidin-biotion reactions.

Another polymer of interest for immobilizing quantum dots has been polystyrene (51,52). Polystyrene surfaces were modified with sulfur-linkage groups known as thiol groups (51). The thiols were supplied through addition of polythiourethane. Other sources of thiols were substituted with results showing larger molecular weight thiols ineffective for modification to immobilize quantum dots. The group tested polyurethane without thiols, and saw no retention (51). This proved retention relied on the sulfur linkage provided with thiol groups. To improve the effectiveness of retention, free-radical polymerization to cross-link the polystyrene was tested. Intriguingly, the emission of the quantum dots was quenched. The loss of emission was mentioned that the free-radical polymerization created an environment friendly to agglomeration of the quantum dots forming bulk materials (51). Yin et al. (50) observed an opposing effect; however, their quantum dots were encapsulated rather than adsorbed.

28

Microgel formation of polystyrene was evaluated for immobilizing CdSe quantum dots (52). Solvent optimization was the key factor studied. It was observed that a co-solvent system provided immobilization of the quantum dots into the pores of the polystyrene particles as they swelled. A mixture of 60% chloroform and 40% propanol by volume provided the optimum immobilization (52). At this solvent ratio it was observed that the quantum dots could be immobilized in approximately 40% of the polystyrene particles.

Additional examination with gels for immobilization of quantum dots has been performed. Peptides forming organogels were used to retain CdSeS core-mixed shell quantum dots (53). The gel was formed via self-assembly of monomers of the peptide, diphenylalanine. Emission of the quantum dots was unaltered after immobilization. A disadvantage of the immobilized quantum dots for application falls on the gel substrate. Fluorescence of the gel was observed when excitation light was below 400 nm (53). Advantageously, quantum dots can be excited above 400 nm without drastic decrease in emission intensity or efficiency.

Polyethylene glycol gels immobilized CdSe and CdTe for application to drug delivery monitoring (54). Similar to polyisoprene (50) polyethylene glycol is a biocompatible material. The two quantum dots chosen were selected for observing the differences in particle size. Cross-linking of the glycol gel did not retain the CdSe dots when submerged in chloroform solvent. The CdTe dots were well immobilized, thus quantum dot size was isolated as the reason for unacceptable retention of the CdSe dots. The research group increased the diameter of the CdSe dots, and the retention was improved (54). When testing the glycol-CdSe gels in aqueous solvents the immobilization was also acceptable. Solvent interaction between the hydrophobic quantum dots and water was found to keep the CdSe dots in the gel.

Silica has also been another means of immobilizing quantum dots for their optical properties. Tetraethyl orthosilicate, TEOS, created a silica coating on gold nanoparticles (55). The silica coating required ethanol:water:propanol mixture of 9.8:0.2:90.0 volume percentages. Thickness of the silica was

approximately 60 nm on average with a stability of at least one year. A red-shift in the original quantum

dot emission was observed though, and expected to be an effect of ligand interaction with the core

quantum dot surface.

Jeong et al. used silica films to immobilize CdSe quantum dots (56). The silica films with

quantum dots were prepared using a spin-casting technique. As a glass substrate was spun at a high

speed, the silica and quantum dot precursors were dispensed on the glass. The resulting film was baked in

an oven, where both quantum dot growth and film strengthening occurred. Jeong and colleagues were

able to obtain different emitting films by increasing the bake time, or quantum dot growth time. The

quantum dots on the films expressed quantum efficiencies up to 35% (56). Loading, or saturation, of the

film with quantum dots reached a maximum of 13% not previously reported (56). Dissolution of the

CdSe dots in melted glass was considered as an alternate approach, but glass requires extremely hot

temperatures to melt. The alternate would probably quench the fluorescence through agglomeration of

the quantum dots to form bulk material. With the ease of processing and "tuning" the silica films of

quantum dots on glass, application to optoelectronics is very promising.

CHAPTER 2

LUMINESCENCE AND FLOW INJECTION ANALYSIS

Introduction

Luminescence is a unique portion of chemistry involving electronic transitions. The ability of a species to absorb and emit energy in the form of light has attracted many researchers. Explorations and discoveries in luminescence have provided numerous analytical applications. Several types of luminescence including fluorescence and chemiluminescence have opened the door for sensitive and selective detections. Analytical applications have matured in the recent decades from reagent streams using luminol to using immobilized fluorophores.

History of Luminescence

Luminescence is a phenomenon that has been observed for many centuries, dating all the way back to the ending centuries of the B.C. era (57). The term "luminescence" refers to any molecule or species that is emitting light as a "cold light," which is not the same as light produced by incandescence. The luminescence stems from an initial excitation that can be from a variety of energy sources. Some of the initial observations of luminescence were made by famous Greek and Chinese philosophers. The historical observations were of many common luminescent occurrences still seen by many today, such as firefly and marine life (58).

Over time luminescence was seen more as a supernatural effect rather than an effect that could be explained by scientific investigations. As the sixteenth and seventeenth centuries arose, so did the attempts of divulging these "cold light" observations noted over the previous two millennia. From the accounts of Francis Bacon, Kircher, Gesner, and many more; luminescence began to be investigated deeper to understand why it occurs. These investigations were accounted for in several known works of literature, including the first book written on luminescence by Conrad Gesner (57).

Eventually, these independent researchers began to congregate and discuss their observations. These meetings of similar interests led to the formation of scientific societies. One of those societies was the Academy of Experiments, or also known as "Academia del Cimento". It was formed in 1657 and existed into the mid-twentieth century. A parallel society, residing in France, was responsible for publishing the first article on luminescence. It was published in the "Journal des Scavans" in April 1666, discussing luminous worms found in oysters (57).

As the twentieth century approached, many more discoveries and principles of luminescence evolved. Sir George Stokes in 1852 had a realization about fluorescence through a simple experiment. The experiment used a setup of prisms, where the emission of quinine sulfate increased as the solution was illuminated with an "invisible light", later referred to as ultraviolet light (58). Sir Stokes noted that excitation frequency was greater than the emission frequency, thus the excitation wavelength is less than that of the emission ($\lambda_{ex} < \lambda_{em}$). This separation between the excitation and emission wavelengths would later be termed as "Stokes Shift" in his honor. It would also help in the introduction of the concept of fluorescence (58).

Sir George Stokes continued his research to observe that the intensity of luminescence is related to the concentration of the luminescent species under study. He noted that as the concentration of the of the luminescent compound increased, or if it was in the presence of known foreign materials, the intensity would reach a maximum or diminish, respectively. Sir George Stokes also contributed to luminescence by proposing to apply the fluorescence technique for analytical demands (58).

A few years after Stokes's experimental discoveries, another major discovery in luminescence was made by Edmond Becquerel. His research introduced the technique of phosphorescence. He tested several known phosphors by varying the temperature, and recording the lifetimes of those phosphors. These experiments led to his development of the first phosphoroscope in 1858. The instrument was capable of measuring lifetimes down to a tenth of a millisecond (58).

Into the twentieth century, some of the largest contributions from luminescence to analytical chemistry were made. The application of luminescence to analytical chemistry provided an extra benefit for quantitative and qualitative measurements alike. Photoluminescence observations became better understood after the introduction of the Jablonski diagram in 1935, illustrating the electronic transitions needed for absorption, emission, and other electronic pathways (59). Closer to the mid-1900s the adaptation of the photomultiplier tube to existing luminescent-detecting instrumentation yielded higher sensitivities. Now trace amounts of luminescent compounds could be detected with ease.

In the recent centuries, luminescent discoveries were laying the ground work for the basic concepts familiar today. Luminescence had been divided into different classifications based on the source of excitation employed for observance of emission. A few of the classifications were labeled as photoluminescence, chemiluminescence, and triboluminescence. Within the first two classifications just mentioned, lie the more commonly known and practiced techniques of fluorescence, phosphorescence, chemiluminescence, and bioluminescence (58,59).

Photoluminescence

When discussing luminescent techniques, photoluminescence is the most common among the several types that exist (59-62). Photoluminescence is comprised of fluorescent and phosphorescent emission pathways that are initiated by the luminescent molecule's excitation with an external light source. The process of a given molecule to undergo excitation, and follow immediately with either a radiative or non-radiative relaxation back to the ground state is best detailed by the Jablonski diagram shown below in Figure 2.
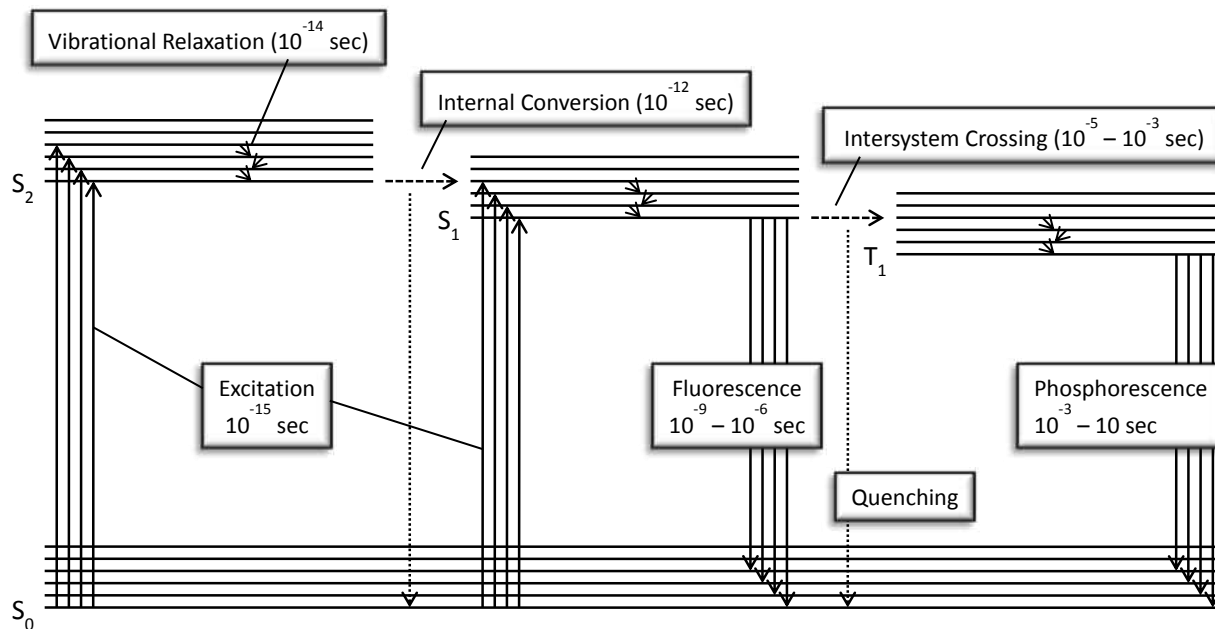
Figure 2. Jablonski Diagram Illustrating the Excitation and Emission Processes of Luminescence

Photoluminescence Excitation Process

The more desired, radiative and luminescent pathways begin in the ground singlet state of $S_0\nu_0$. The excitation process to an excited singlet state, $S_1\nu_n$ or $S_2\nu_n$, occurs quite rapidly with a lifetime of 10^{-15} second. Following excitation several possible pathways can relieve the excited molecule back to the ground state $S_0\nu_n$. These pathways are as follows in order of favorability and shortest lifetimes: vibrational relaxation, internal conversion, fluorescence, intersystem crossing, quenching, and phosphorescence. In order to create the analytically desired pathways that end in fluorescence or phosphorescence; the electronic structure along with molecular and environmental factors must be considered and controlled if required.

To understand why luminescence occurs, a luminescent molecule's electronic structure needs to be studied. There are five kinds of orbitals that the electrons in the structure can reside in: sigma (σ), pi (π), and non-bonding (n). The σ and π orbitals also have corresponding anti-bonding states, σ^* and π^*.

A general diagram is portrayed below in Figure 3 with a reference to the energy of each level in respect to the others.

$$E = h\nu$$
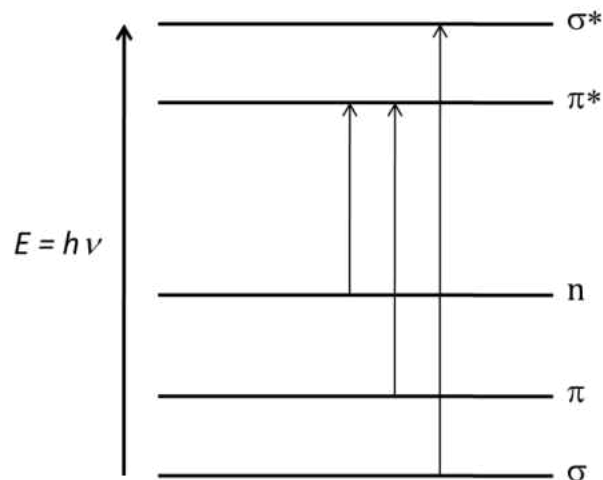
Figure 3. Depiction of the general orbital diagram and electronic transitions between the states

In the bonding of atoms to create molecules, electrons are used as the bonding source. Considering the luminescent molecule as an aromatic hydrocarbon for example, σ-bonds are the most stable. These bonds make the backbone of the molecule acting as single bonds between atoms. The next stable bonding possible is the π-bond that is formed from electrons in overlapping π-orbitals. These are seen as double bonds, and when evenly alternated among σ bonds participate in conjugation. Lastly, any valence electrons not involved in bonding are termed as non-bonding and reside at the highest energy level of the ground states.

Among the possible transitions upon excitation, the n $\rightarrow$ π* and π $\rightarrow$ π* transitions are the ones that lead to luminescence. The σ $\rightarrow$ σ* transition can occur with sufficient energy; however, luminescence is not probable because of the bond dissociation following that leads to a molecular breakdown and non-radiative relaxation. This breakdown of a molecule post excitation is better known as photodecomposition (59). Because of the increase in probability of photodecomposition occurring with

high excitation energies, analytical practice in measuring photoluminescence prefers to use the lowest allowed excitation energy, or wavelength.

Photoluminescence Emission Process

Once the molecule arrives in an upper singlet state upon excitation, the excited molecule can undergo one of the six listed processes on its journey to quantifiable light emission. The fastest process to occur will be vibrational relaxation at a time range just short of excitation, 10^{-14} to 10^{-12} seconds. This will allow the molecule to relax from $S_2\nu_n$ to $S_2\nu_0$ before the next process becomes competitive as seen in Figure 2.

With the molecule reaching the $S_2\nu_0$ state, it can either fall back to the ground state, $S_0\nu_n$, or skip over to a $S_1\nu_n$ state that is of similar energy to the $S_2\nu_0$ state. This "skip" is termed internal conversion, and allows the excited molecule to continue relaxing through vibrations down to the $S_1\nu_0$ state. Here, fluorescence is now more competitive given that favoring conditions are set for the system. If fluorescence occurs, a rapid light emission takes place with nanosecond to microsecond lifetimes.

Fluorescence is commonly seen at wavelengths of lower energy than that of the excitation wavelength. This is due to the loss of energy through all of the processes discussed above before the molecule can fluoresce. The displacement of the emission wavelength from the excitation wavelength is also known as the Stokes Shift, and was discovered as mentioned earlier.

If molecular or environmental conditions are not favorable for fluorescence, the three remaining processes or electronic transitions can be experienced (59). If the excited molecule reaches the $S_1\nu_0$ state, but fluorescence is not favored, the molecule can undergo quenching or intersystem crossing (ISC). Quenching occurs when the molecule or environment contains species that absorb the extra energy sustained by the excited molecule, allowing it to relax back to $S_0\nu_n$ without luminescence. The same species that can absorb the extra energy of the excited molecule can also aid in ISC of the molecule. By

36

ISC an electron in the molecule will change its spin-state and thus the multiplicity from singlet to triplet as seen by using Equation 1, where S represents the total spin value of paired electrons (59). This process is considered as "spin-forbidden", however, can occur with the correct conditions. Because ISC has slow lifetimes compared to fluorescence, the conditions required are typically low temperatures and substituents or solvents promoting spin-state change.

$$2S + 1 = \text{multiplicity} \hspace{4cm} \text{Equation 1}$$

As the molecule surpasses ISC, it is now able to participate in phosphorescence. The emission of phosphorescence requires low temperatures as well in order to reduce other transitions that are more favorable because of their much shorter lifetimes than 10^{-3} to 10 seconds. With the long lifetime of phosphorescence, it is commonly observed as an afterglow upon removal of the excitation source.

Structural Effects on Photoluminescence

For fluorescence or phosphorescence to occur, there must be sufficient energy absorbed and a favorable pathway for it to end in light emission. This relates to the definition of quantum efficiency, Φ. The efficiencies, Φ_f for fluorescence and Φ_p for phosphorescence, are based on the rates of internal conversion (k_{IC}), intersystem crossing (k_{ISC}), fluorescence (k_f), phosphorescence (k_p), quenching (k_q), and the amount of quencher (Q) if present (59, 62). A change in one of these rates or quencher concentration can have a major impact on the respective quantum efficiency. This can be seen in Equations 2 and 3.

$$\Phi_f = k_f / (k_f + k_{IC} + k_{ISC} + k_q[Q]) \hspace{3cm} \text{Equation 2}$$

$$\Phi p = \Phi_{ISC}k_p / (k_p + k_{IC} + k_{ISC} + k_q[Q]) \hspace{3cm} \text{Equation 3}$$

By applying the equations above, the efficiencies can be increased easily be diminishing or eliminating the non-radiative rates. The same can be done with the quencher concentration; however, the rates can also be increased easily through changes in the molecular and environmental conditions (59, 60). These changes can include structure shape, geometry, and substitution or addition of substituents for

the molecular factors. Because most measurements for photoluminescence, with the exception of phosphorescence, are taken in dynamic media, environmental changes cover solvent polarity, pH, temperature, and quenching (60).

Looking on the molecular level, the ability to lower rotational and vibrational movement is an important factor in increasing the quantum efficiency. This can be achieved with a molecule whose structure is planar and linear. If the molecule cannot twist or bend within itself energy will not be lost, and the lowest singlet, S_1, or triplet, T_1, state has a better probability of population increasing the efficiency. The planar and linear arrangement also leads to better delocalization of π-electrons when a molecule is conjugated.

The second factor lies in what is attached to the molecule. When the substituent attached is a functional group, it can affect the parent molecule's efficiency positively or negatively. To better understand how these contribute, the electronic structure must be considered. If the functional group is known as electron-donating, it can have a lone-pair or non-bonding electrons that will be promoted to the π^* orbital under excitation. These electronic transitions, $n \rightarrow \pi^*$, are typically weak (60). The participating non-bonding electrons can also lead to ISC, which decreases Φ_f and increases Φ_p.

Following with the traits of electron-donating functional groups, halide substituents can have major impacts on the Φ_f. The impact is primarily negative and more impressive as the atomic number of the halide increases (59, 60). With this said the effective strength of halides on decreasing Φ_f generally follow this order: $I^- > Br^- > Cl^- > F^-$. The iodide ion has the greatest effect due to its size. The ion size causes bond dissociation, which creates a pathway back to the ground state from an excited state sufficiently decreasing Φ_f.

On the other hand, if the substituent exhibits electron-withdrawing properties, the Φ_f can be increased. The positive effect on fluorescent measurements is due to the lowering of energy related to the $\pi \rightarrow \pi^*$ transition. A general portrayal of this shifting in orbital energies is seen in Figure 4.
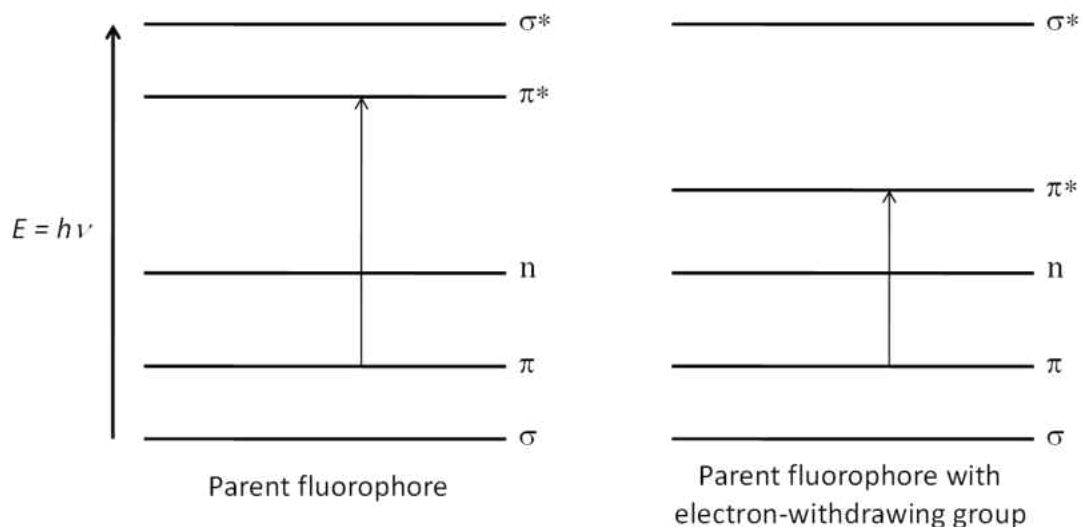
Figure 4. Effect of electron-withdrawing substituent on orbital energies of a fluorophore

<u>Environmental Effects on Photoluminescence</u>

Switching gears to discuss environmental factors, the same can be mentioned about controlling the dynamics of the system as was on the molecular level. The first and probably most important environmental factor is solvent polarity. The polarity, or dipole, of the solvent differs between the ground and excited states and is explained by the Frank-Condon Principle (63). As the principle states, upon absorption of energy the surrounding solvent molecules do not have time to re-orientate in respect to the new dipole experienced in the excited state. After arrival in the excited state, the solvent molecules now have time to adjust to the new dipole and do so by releasing some energy. As the molecule proceeds through the motions and reaches the $S_1 v_0$ state, emission occurs. Though the molecule and corresponding solvent cage has returned to the ground state, the current orientation of the solvent molecules does not agree with the dipole experienced in the ground state. For this reason the solvent cage must adjust once again lowering the remaining excessive energy held by the molecule bringing it back to the original ground state. This is well depicted in Figure 5.
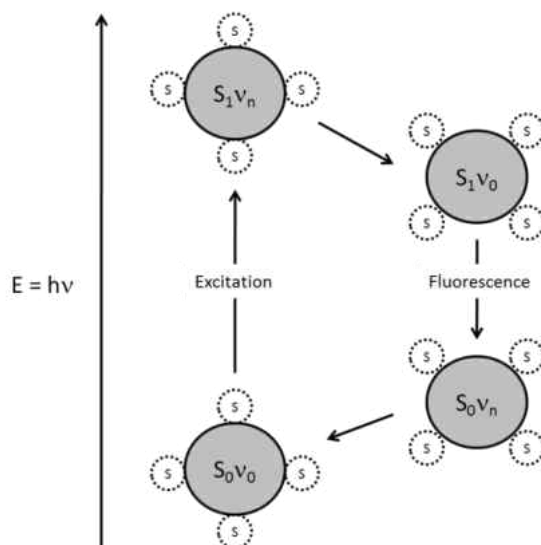
Figure 5. Depiction of how solvent molecules alter fluorescence of molecules per the Frank-Condon Principle

Solvents can also impact the efficiency of photoluminescence through pH and quenching. The effects of pH are observed in three regions; acidic, basic, and neutral. Emission wavelengths and intensities can be altered by changes in the pH (62). Electronic ground and excited states express differences in acidity and basicity. Most carbonyl functional groups such as ketones and carboxylic acids increase in basicity in the excited state (59). Increased electronic density surrounding the oxygen of the carbonyl can explain the increased basicity. On the other hand, alcohols and amines display increased acidity in the excited state. Again, an increase in electron density on the oxygen is the suspected culprit, stretching the O-H bond because of the dipole.

Photoluminescence emission intensities are affected negatively when heavy-atom solvents are employed. These drops in intensities are considered a quenching effect. In this case the heavy-atom is usually a high molecular weight halide such as chlorine, bromine, or iodine. These atoms in the vicinity of a fluorescent molecule allow for spin-forbidden, or intersystem crossing transitions to proceed. This quenches the fluorescence of the molecule by promoting phosphorescence through population of the lowest triplet excited state.

Solvent viscosity and temperature effects can be discussed together. Both factors affect photoluminescence through increased molecular collisions. A decrease in solvent viscosity leads to an increase in molecular movement. A rise in molecular collisions favors excited state relaxation through non-radiative pathways resulting minimal or no luminescence. An increase in viscosity enhances photoluminescence intensities by diminishing vibrational relaxation and internal conversion rates making fluorescence rates more competitive by using the previous, Equation 3. In some instances the solvent viscosity can be increased to a point, where intersystem crossing and phosphorescence becomes competitive with fluorescence (62).

Temperature affects photoluminescence intensities in an inverse fashion with regards to viscosity. As temperature is increased, so do molecular collisions increasing the favorability of vibrational relaxation and internal conversion. Sample chilling is commonly practiced to enhance the intensity by reducing the number of molecular collisions. Phosphorescence analyses typically require temperatures below freezing with solvents of high viscosity (59).

<center>Chemiluminescence</center>

Chemiluminescence is the oldest form of luminescence observed (57,58). It is another light-emitting phenomenon similar to fluorescence. Chemiluminescence, however, has a different source of excitation energy. Fluorescence requires an excitation source external to the system under study, such as a xenon-arc lamp (64). The energy for excitation in chemiluminescence is provided from within the system by a specific chemical reaction. Chemical reactions producing between 40 and 70 kilocalories per mole (58) are sufficient for observing a spectrum of emission colors from blue to red. Energies greater than the range just mentioned may lead to molecular decomposition through bond dissociation.

The efficiency of chemiluminescence tends to be of concern for analytical applications. Efficiencies below one percent (65, 66) create sensitivity barriers for trace analyses. Chemiluminescence efficiency, ϕ_{CL}, is defined as the quantity of photons emitting per molecule of reactant consumed by the

<center>41</center>

chemiluminescence-generating reaction (65). This statement is summarized into Equation 4. Efficiency values can be presented in percent or numerical form. The most efficient reactions have values of 100% or 1.

$$\emptyset_{CL} = \frac{\#\ photons\ participating\ in\ luminescence}{\#\ moles\ of\ reactant\ consumed}$$

Equation 4

Over the recent decades, research has provided reactions and systems capable of chemiluminescence efficiencies greater than 1%. Peroxyoxalate reactions have been introduced that can achieve efficiencies up to 50% (67). Studies of chemiluminescence in biological entities, bioluminescence, presented exceptional efficiencies (68, 69). One of the most studied (65, 70-72) bioluminescent reactions is that of firefly luciferin-luciferase. Ongoing research in bioluminescence has aided mechanistic insight for intermediate formation (68, 69) and application for trace analyses (65).

Chemiluminescence intensities are also of importance for analytical measurements. For analytical purposes the chemiluminescence signal is compared among analyses based on its integrated area, or more commonly by peak intensity. The intensity, I_{CL}, is relative to the system's efficiency coupled with the formation rate, dP/dt of the excited-state product (58,65). Equation 5 presents the relationship between intensity, efficiency, and reaction rate.

$$I_{CL} = \emptyset_{CL} \frac{dP}{dt} \ where\ A + B \rightarrow P$$

Equation 5

Chemiluminescence occurs through one of two possible pathways (58). Both pathways begin with reactants producing an excited-state species. The first pathway is considered "direct". The "direct" pathway occurs when the exicted-state species is the emissive component. A second pathway follows an "indirect" approach to producing luminescence. The "indirect" pathway produces a non-emitting intermediate. The intermediate can, however, transfer energy through electron transfer, or molecular decomposition to an added fluorophore. If the energy transferred is sufficient to promote the fluorophore

to an excited singlet state, luminescence will follow. Both "direct" and "indirect" pathways are presented

in Figure 5.

$$A + B \rightarrow P^*, \; P^* \rightarrow P + light \qquad \qquad \text{Direct Pathway}$$

$$G + H \rightarrow I^*; \; I^* + \; F \rightarrow I + F^*; \; F^* \rightarrow F + light \qquad \text{Indirect Pathway}$$
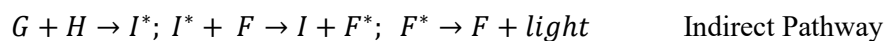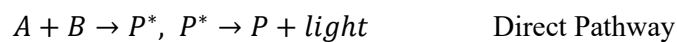
Figure 6. Direct and indirect pathways of chemical reactions to produce chemiluminescence.

Peroxyoxalate Chemiluminescence

      Peroxyoxalate chemiluminescence, POCL, is considered a subset of all chemiluminescent

reactions. POCL is observed as the emission of light when adding hydrogen peroxide to a solution of

oxalate ester and fluorophore in the presence of imidazole catalyst (73). The reaction scheme is presented

in Figure 7. Chandross (74,75) was the first to observe the mild-bluish emission after solely mixing

oxalyl chloride with hydrogen peroxide.

      Since 1963 the POCL mechanism has been extensively investigated. Research groups have

studied and documented how the mechanism proceeds, (66, 75-77) oxalate ester chemistry (78, 79) and

determination of reaction intermediates (67,80-82).

Figure 7. Reaction scheme of TCPO with hydrogen peroxide in presence of imidazole catalyst for

peroxyoxalate chemiluminescence

Rauhut and colleagues expanded on the understanding on Chandross's initial report (74) of POCL. Studies were performed with focus on kinetic data to provide insight into the POCL mechanism. Oxalyl chloride (77), aryl oxalate esters (66), and aryl oxalic anhydrides (76) on oxalyl chloride concentration were evaluated. Oxalyl chloride was found (66) to be a quencher of emission at high concentrations. Increasing hydrogen peroxide and fluorophore concentrations both increased the system's quantum yield; however, the quantum yield plateaued with high concentrations of the fluorophore due to concentration quenching (77).

Substituting aryl oxalate esters (66) for oxalyl chloride (77) improved the quantum efficiency approximately three-fold. A contributing factor to the increased efficiency was the stability of the esters compared to oxalyl chloride. The ester stability, however, can be degraded in basic and polar solvent conditions. This is likely due to the ester hydrolyzing before it can react to begin the chemiluminescent process. Ester depletion was found to be complete within 5 minutes after initiating a POCL reaction (66), where interestingly about 50% of the emission curve remained before the signal returned to baseline.

A classroom demonstration of POCL was used by Hadd et al. (78) to help explain the mechanism through ester hydrolysis. Nucleophilic substitution of the oxalate ester by hydrogen peroxide proceeds similar to ester hydrolysis by water (78,79). Imidazole when used as the catalyst was found to first undergo deprotonation by a second imidazole before nucleophilic attack on the oxalate ester (79). Bases were added to the system to improve deprotonation increasing signal intensities. Lastly the leaving group post nucleophilic attack contributed to the efficiency, where pKa's of the leaving groups aided these observations (78,79).

Aryl oxalate esters commonly employed in POCL are *bis* (2,4,6-trichlorophenyl) oxalate, TCPO, and *bis* (2,4-dinitrophenyl) oxalate, DNPO. Preference lies with TCPO due to its exceptional stability even though DNPO has better reactivity (81). TCPO when prepared and stored properly can remain

stable for several months (73). Studies of non-catalyzed and base-catalyzed POCL reactions using TCPO have led to elucidating mechanistic intermediates.
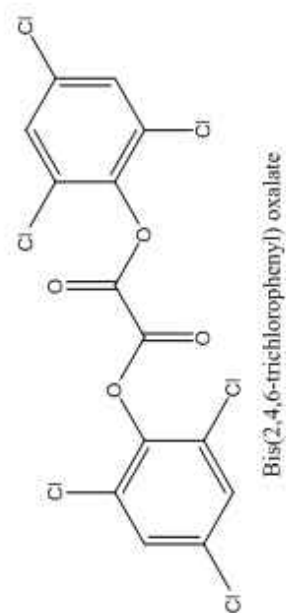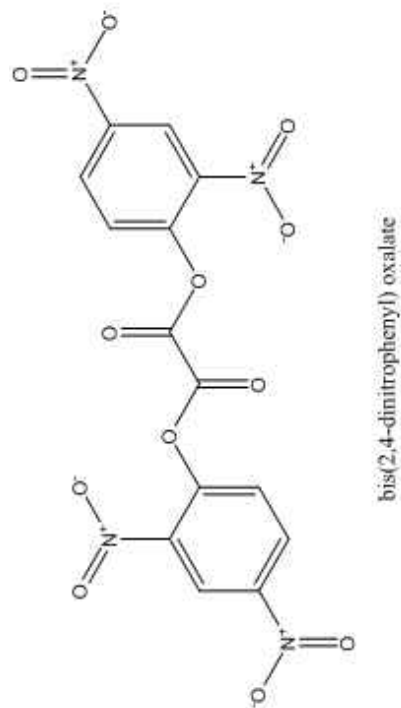
Figure 8. Molecular structures for TCPO and DNPO

Several research groups (80-83) have directed their attention towards exposing the intermediates formed in the POCL mechanism. Two intermediates, Figure 9, have been proposed since Rauhut and colleagues began their inquiry almost 5 decades ago. The first proposed structure (77) was 1, 2-dioxetanedione, a cyclic peroxide that releases an abundance of energy when decomposing into two molecules of carbon dioxide. The energy released is absorbed by an adjacent fluorophore that undergoes light emission.

1,2-dioxetanedione   1,1-oxalyldiimidazole
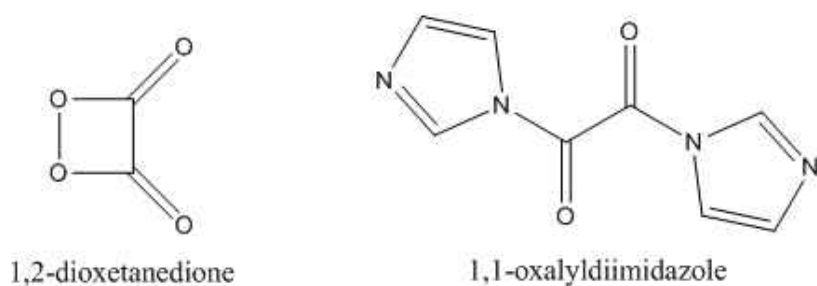
Figure 9. Molecular structures of 1,2-dioxetanedione and 1,1-oxalylimidazole POCL intermediates

An integral intermediate in POCL when using aryl oxalate esters is 1, 1-oxalylimidazole, better known as ODI. This intermediate does not participate in the chemi-exictation leading to chemiluminescence observations (81,83). Instead the role of ODI is to create favorable conditions for producing CL. Reacting hydrogen peroxide with TCPO has been stated to produce CL, but with low reactivity (81). Imidazole as catalyst addition to the reaction improves yields and signal response time (79). Emteborg et al. (81) evaluated POCL using ODI directly as the reagent rather than TCPO and imidazole. Kinetic data reported by Orlovic et al. (82) revealed that excess imidazole had a negative effect on the quantum yield. The observation of excess imidazole was later explained (81) through the reaction of imidazole with ODI. Formation of the intermediate soon follows with nucleophilic attack by the peroxide anion (83) leading to proposed formation of 1, 2-dioxetanedione.

Research groups have labeled 1, 2-dioxetanedione as the intermediate responsible for producing chemiluminescence (80, 82, 83). This intermediate has been the focus of exhaustive study by many

research groups. Confirmation of the intermediate was made after four decades using ^{13}C NMR spectroscopy (80). Since confirmation, Ciscato et al. (67) have refuted that the intermediate responsible for chemiluminescence cannot be a cyclic peroxide. Activation energy data suggested the accumulated molecule had a stability lower than 1, 2-dioxetanedione.

Observations of CL are claimed to stem from the decomposition of 1, 2-dioxetanedione (67, 73). Electron transfer between the intermediate and fluorophore initiates the chemiexcitation step. The application of semiconductor quantum dots suggests electron transfer for luminescence. Semiconductor quantum dot luminescence requires excitation to produce electron-hole separation. A proposed mechanism using quantum dots supports 1, 2-dioxetanedione as the intermediate.
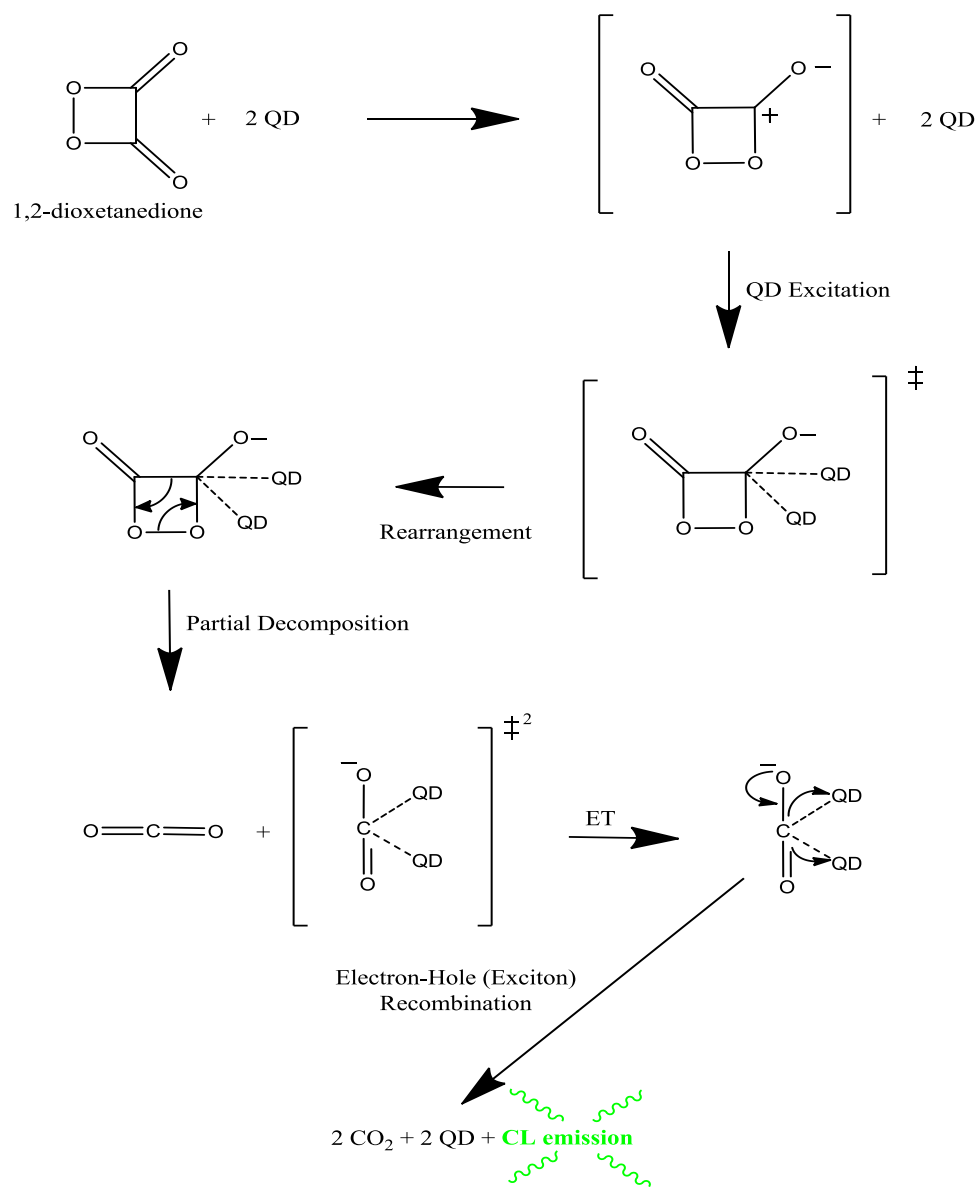
Figure 10. Proposed mechanism by thesis author of quantum dot reaction with 1,2-dioxetanedione producing chemiluminescence

Analytical Instrumentation in Luminescence

The use of chemistry to quantitate species has been practiced since I.M. Koltoff established analytical chemistry (84). Instrumentation is a crucial organ of analytical chemistry. The introduction of luminescence spectrometers has expanded the capability to perform analyses requiring sensitive detection. Photoluminescence instrumentation includes spectrofluorometers and phosphorimeters. Chemiluminescence instrumentation, however, is available in a variety of configurations.

Fluorescence of a species is measured using a spectrofluorometer. A basic diagram of the instrument can be found in Figure 11. A xenon-arc lamp with stable power supply (60,85) is typically used to provide excitation energy for molecular absorption and promotion from the ground electronic state to an excited state. Light-emitting diodes, LEDs, are beginning to see application as excitation sources. LEDs consume less energy and operate over a wider frequency range (85). Sources lamps are not required in chemiluminescence instrumentation because the excitation source is a chemical reaction. The absence of a source lamp improves the sensitivity because emission is collected from a light-free background.
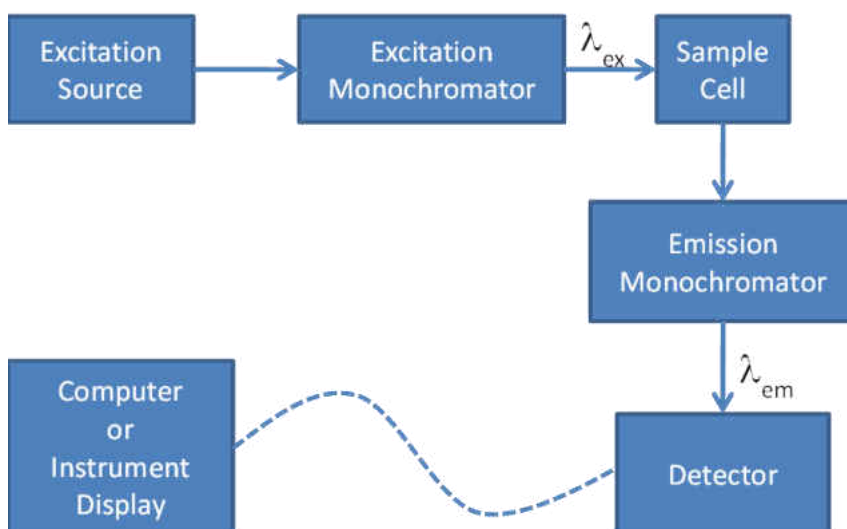
Figure 11. Schematic of basic fluorescence instrument

The polychromatic excitation beam, is broken down into component wavelengths using a monochromator. Monochromators of choice are prisms and diffraction gratings (62). Current instrumentation allows for component wavelength selection with the monochromator installed. Diffraction gratings in instruments are replicates of a master grating containing 1200 to 1400 grooves per millimeter (62). Again, chemiluminescence is exempt from another part of fluorescence instrumentation. The energy produced by a chemiluminescence reaction is related to a specific wavelength . The chemical reaction in this case is its own monochromator.

The state of the sample under study provides an array of sample cells or holders (86,87). Fluorescence is commonly a measurement performed on a dynamic medium, such as liquid. Cuvettes of precisely constructed dimensions are used to contain a sample at the intersection between the excitation and emission pathways. Solid samples can also be measured for fluorescence, but only at the surface (86). This technique is referred to as front-face fluorescence (60). Some sample cells may also be equipped with cooling features (88).

Sample holders for chemiluminescence may be similar to those used in fluorescence when solutions are used. The simplest and most common setup is a cuvette in a spectrofluorometer. Reagent addition to the cuvette produces emission observed by the detector allowing chemiluminesce observation. More complex sample cells for chemiluminescence measurements involve flow cells. Techniques such as high-performance liquid chromatography and flow-injection analysis using liquid carrier streams use flow cells. The flow cell is positioned adjacent to the detector, or fiber optics can be used between the flow cell and detector. Flow cells are also used in instrumentation with gaseous carrier streams (89,90). Figure 12 displays static and dynamic configurations for measuring chemiluminescnce.
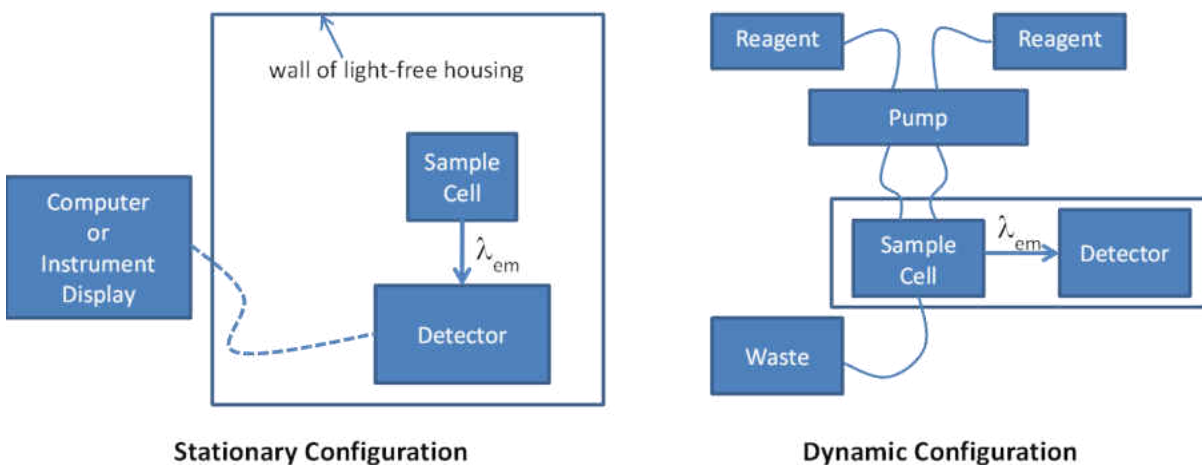
Figure 12. Schematics for basic stationary and dynamic configurations of chemilumenscence instrumentation

The detector is ubiquitous for both fluorescence and chemiluminescene measurements. A photomultiplier tube, PMT, provides sensitive light detection spanning several orders of magnitude of linearity (58). Dynodes in the construction of PMTs make this possible. As electrons reach the PMT, collision with a dynode releases a larger amount of electrons that collide with the next dynode in series. Each dynode has a higher cathodic charge than the previous. When the last dynode is struck, an amplified signal exists for conversion readout response.

Several commercial instruments are available. Most fluorescence instruments are stationary units (89-91). Ocean Optics (92) offers a portable spectrofluorometer, where fiber optics participate as the light carrier to and from the sample cell. For flow-type analyses, Agilent (93) offers a spectrofluorometer adaptable to their liquid chromatography instruments. Chemiluminescence options are not quite as easily available. Simple chemiluminescence measurements can be performed using spectrofluorometers as previously mentioned. Complex chemiluminescence measurements involving flow typically do not have universal configurations. For this reason complex flow instruments for chemiluminescence are laboratory-built for specific use.

53

Applications of Peroxyoxalate Chemiluminescence

Peroxyoxalate chemiluminescence has found a niche in analytical applications since its discovery by Chandross. Chemiluminescence alone has been a preferred choice over other techniques due to its reduced background noise. The chemistry behind POCL provides the efficiency desired by many to reach detection limits below that of other techniques. Selectivity also plays a role for related applications. Though hydrogen peroxide is a primary determination resulting from POCL, the reaction can be manipulated to expand on the multitude of analytes possible for detection.

Several applications have found liquid chromatography as a platform. Sigvardson and Birks (94) demonstrated the detection of polycyclic aromatic hydrocarbons. Perylene, tetracene, and 9,10-diphenylanthracene yielded picogram detection limits of 0.77, 10, and 20, respectively. These limits were found to be better than both UV absorption and fluorescence detections in liquid chromatography. Fluorescence by liquid chromatography had the best detection limits for most of the aromatic hydrocarbons surveyed. Improvements to the POCL detection method was recommended by removing background emission (94,95). Hanaoka et al. (95) evaluated POCL kinetics in liquid chromatography to determine the optimum relationship among reagent concentrations, temperature, pH, and solvent matrix.

A review of hydrogen peroxide determinations was made by Tsunoda and Imai (96). Direct hydrogen peroxide determination is the most fundamental analysis performed by POCL. A step up from hydrogen peroxide is the use of immobilized enzymes to produce the hydrogen peroxide. The light intensity due to created peroxide by enzymatic reaction can be used to stoichiometrically calculate the original analyte. Tsunoda and Imai (96) also made mention of the advantage of POCL over luminol-based systems for enzymatic reactions.

Immobilized enzyme reactors, IMER, coupled with POCL were investigated for glucose, choline, and acetylcholine (97). The reagent stream was found to affect the enzyme activity based on water content. Reversing the ratios of water and acetonitrile from 80:20 to 20:80 saw no major change in

sensitivity when comparing calibration slopes. Glucose standards were tested on the configured setup using the IMER, and complete recovery was determined once corrected for β-glucose content. Reproducibility of the recovery data had a relative standard deviation of 2% for four determinations. The use of a separation column before the IMER, produced nanomolar detection limits for the analytes previously mentioned.

Quenching of POCL by salts and anilines was studied using liquid chromatography (98). The species of interest tested for quenching were reductants, or electron donors. The effect of quenching was found to not alter the POCL linearity in the micro- to millimolar range. More than 10 analytes were found to have detection limits less than 10 nanograms for flow injection analysis. When extended to high performance liquid chromatography, three of four analytes yielded detection limits between 2.4 nanograms and 5.6 nanograms. Reproducibility was determined as 2.5% RSD when tested at concentrations one order above the respective detection limits. Linearity up to three orders was also determined.

Laboratory-specific instruments have been used to apply POCL for analytical determinations. Flow injection analysis instruments are modular with various configurations, built for the task at hand. The addition of cupric ions to an aqueous reagent solvent revealed increased sensitivity (75). Applying this observation to liquid chromatography was considered. Steiger et al. used computational chemistry to explain why cupric increased the emission signal much better than ferric and other transition metals. Data suggested that a balance existed between the cupric ions and imidazole. Unpublished research by the thesis author involved the decomposition of hydrogen peroxide using substituted imidazoles with a binuclear copper catalyst. The imidazole ligands were coordinated to the copper catalyst to improve its efficiency. Observation of increased decomposition rates were observed when a methyl substituent was bonded between the nitrogen atoms in the ring structure. This observation aided the author's input that the cupric ion with imidazole created a complex that participates easily in electron transfer.

Other adaptations to flow injection analysis for POCL involve in-situ polymerized supports (99) and a gas diffusion scrubber (100). Studies of in-situ polymerized supports, ISPS, were carried out to provide an alternative to packed bed reactors (99). The ISPS were polymerized using photoinitiation. The efficiency of ISPS were in correlation with the degree of functionalized sites using 3-aminofluoranthene as the fluorophore. Various methacrylate-based polymers were tested with 6% RSD and nanomolar detection limits.

Hydrogen peroxide was selectively determined with the use of a diffusion scrubber (100). Atmospheric gases contain mixtures of organic peroxides with hydrogen peroxide. Rauhut et al. (66) demonstrated that POCL is selective for hydrogen peroxide over organic peroxides. Sterically hindered organic peroxides exhibit the worst reactivity. Separation of hydrogen peroxide from the organic peroxides was carried out by passing the gaseous peroxide mixtures against an acetic acid buffer. Without separation all peroxides were detected as the same chemiluminescence signal. Excess methyl hydroperoxide over hydrogen peroxide decreased the signal by 25.7%. Recovery using the scrubber configuration was demonstrated to be 95% after four replicates at 270 ppbv. Optimizing scrubber flowrates provided sampling frequencies up to 120 injections per hour, and detection limits of 30 pptv and below. A calibration of the gas diffusion separation flow injection analysis apparatus had a correlation coefficient of 0.999 between 0.6 ppbv and 3.4 ppbv hydrogen peroxide with a flowrate of 0.5 mL/min (100).

<u>Flow Injection Analysis</u>

In the profession and practice of analytical chemistry, sample preparation prior to analysis is a necessity. Sample preparation involves dissolution, reaction, separation, and possibly much more depending on the samples and analyses to be performed. Most sample preparations are performed across multiple steps or operations. Typically sample preparations are carried out on the macro-scale.

A factor affecting sample preparation for analysis is the reproducibility of the procedure. If the sample preparation is performed over a long period of time, a day-to-day variability of the analytical environment can affect reproducibility as well. Considering these factors along with the ability to minimize chemical consumption, increase sample frequency, and improve sensitivities; flow-injection analysis was developed with an optimistic future (101-103).

Dispersion in Flow Injection Analysis

Flow injection analysis, FIA, is an analytical technique that performs sample preparation and analysis in one complete unit. The technique thrives on the principles of dispersion and the factors influencing them. Understanding the dispersion of an injected sample into the carrier/reagent stream allows one to optimize the desired analysis configuration. Focusing exclusively on sample dispersion, however, can be an inhibition to the overall system design. This is evident when not considering reagent dispersion because many variables affect dispersion.

Dispersion is related to sample or reagent dilution when a volume of sample is injected into the carrier stream, of concentration, S_0, the sample travels with the carrier stream to the window of detection, and divides the carrier stream creating a gradient as time progresses (104). This process is shown in Figure 13. The gradient formed is due to dispersion between the sample and carrier or reagent stream.

Figure 13. Representation of a dispersed sample gradient within flow injection analyzer.

As time passes the original sample concentration, S_0, disperses into the carrier/reagent at an original concentration, R_0. The formation of the gradient creates a variance of sample concentrations,

where a finite concentration exists at a specific time. The concentration of sample in the gradient at a specified time is noted as, S_t. Dividing S_0 with S_t provides a ratio that is equal to the dispersion coefficient, D_S, at the given time in the given FIA configuration (104).

$$D_s = S_0/S_t \qquad \text{Equation 6}$$

The diffusion coefficient, D_S, just mentioned can be used to generally characterize FIA configurations. When the coefficient is found to be less than 10, the dispersion is said to be slight to average (101-104). As the dispersion becomes more vigorous, S_t falls in magnitude increasing the coefficient to values commonly above 10. For a variety of required FIA conditions, minimal or excessive dispersion can be beneficial or detrimental.

Several factors as mentioned can affect the dispersion taking place in a given FIA unit. These factors include sample residence time, sample volume, reactor design, flow rate, and the diameter of the flow path.

Effects of Analysis Time and Flowrate on Dispersion

Dispersion increases with time. The residence time is commonly defined as time taken for sample upon injection to reach the detector. The relation is seen in the following equation (104).

$$D_{max} = 2\pi^{3/2}R^2D_f^{1/2}T^{1/2} / S_v \qquad \text{Equation 7}$$

Dispersion is also affected by flow rate. The flow rate primarily affects the axial, or linear, dispersion of the sample region. Axial dispersion of the region grows with increasing flow rates. On the other hand, when the flow rate is halted the axial dispersion is disrupted leaving radial dispersion as the main event. Flow rate, Q, is inversely proportional to residence time. Therefore, increasing flow rate decreases the residence time as the reactor volume, V_R, is held constant.

$$T = V_R / Q \qquad \text{Equation 8}$$

<u>Effect of Sample Volume on Dispersion</u>

A third factor on dispersion is the sample volume injected into the carrier stream. The amount of sample injected affects the overall dispersion instead of the dispersion process itself. By monitoring the output signal the affect can be observed. As the sample volume is increased, the resulting peak intensity will increase in height and width. When the injected volume reaches an allowable maximum for the employed FIA unit; the peak height flattens as the peak widens. One other observation of increasing sample volume is to see a double-peak response. These are illustrated in Figure 14.
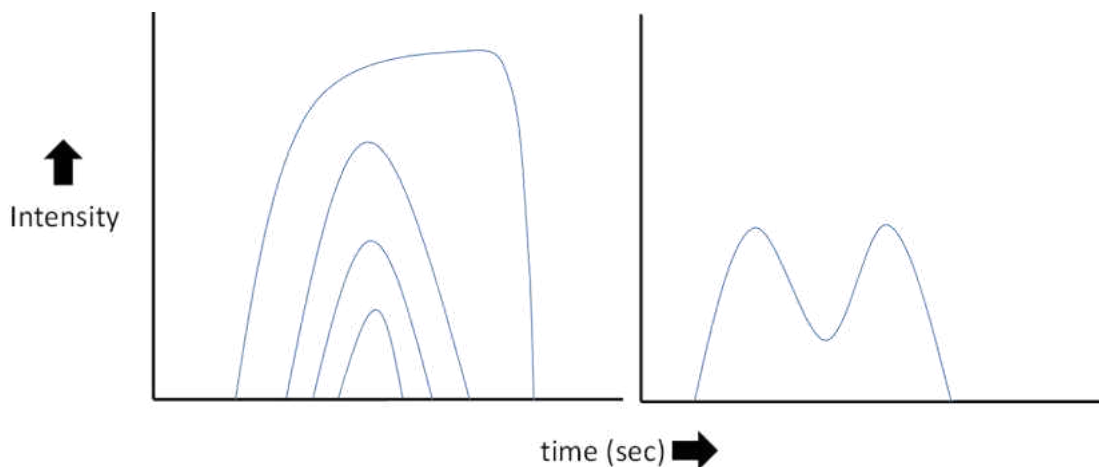
Figure14. Representation of changes in peak intensity due to increasing sample volume and flow path diameter

The other aspect of sample volume effect lies with the initial concentration of the injected sample. Dispersion in FIA can be used in favor of sample preparation prior to detection. Depending on the concentration of the sample, the volume injected can be used as a form of dilution. The volume can also be figured such that the FIA system itself can be used to dilute the sample prior to other operations needing to be performed before detection.

<u>Effects of the Flow Path and Instrument Design on Dispersion</u>

Another factor affecting dispersion is the diameter of the flow path. The diameter is important to dispersion in a similar manner as sample volume is. If say, a fixed sample volume was injected into two different systems using different flow path diameters, the length that the volume occupies will differ. For tubing of smaller inner diameters this creates a need for higher dispersion in order to be equivalent to that of a larger diameter. This relation is seen in Figure 15, where "n" is a multiple of the original tubing diameter. If the dispersion is not higher for the smaller diameter, then the double-peak formation as mentioned before is commonly observed (103,104).
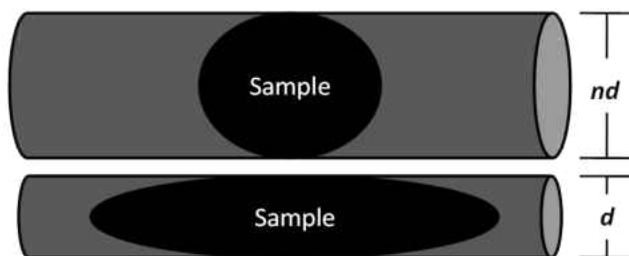
Figure 15. Representation of expanding the sample zone by decreasing flow path diameter

With flow path diameter, it is important to keep in mind the practicality of the operating requirements. When minimizing the tubing diameter a limit is eventually reached. If the diameter becomes too small back-pressure on the tubing is created when the flow rate is not simultaneously reduced. Other possible limitations include small particles blocking flow and poor optical conditions during detection.

The design of the reactor has the greatest importance on dispersion (101). The reactor of a FIA unit is designed accordingly to the dispersion needed. Three primary designs have been characterized as coiled, knotted, and knitted. Each design is fashioned such that the axial dispersion is minimized and radial dispersion is increased. Greater dispersions provided are beneficial to certain experimental requirements. The other benefit of these reactor designs is it allows the shrinking of the overall instrument design, giving rise to economical savings as well.

Effect of Chemical Reactions on Dispersion

In certain FIA units chemical reactions are required. Just like sample dispersion, reagents must also disperse in order for chemical reactions to take place in situ. This leads to effects on sampling frequency. As reagent dispersion decreases, sampling frequency decreases. Eventually the ratio of reagent-to-sample concentration becomes important, which is said to be optimal at a five-to-one ratio (104).

Reviewing all of the effects on sample and reagent dispersion, one sees that they also affect each other. In general there is a balance among the affects for every individual FIA instrument created. By understanding these effects in detail, an optimal FIA configuration can constructed.

Instrumentation of Flow Injection Analysis

To understand flow injection analysis one needs to become familiar with the primary components and the factors affecting dispersion in the construction and optimization of instrumentation. Though many components can be pieced together in a flow injection analyzer, only a few parts are always required. These required parts are pumps, injectors, reactors, detectors, and the tubing connecting them all.

Following the flow through an injection analyzer, the tubing is the component that comes in contact with all solutions employed. For this reason chemical inertness of the tubing is a highly desired

quality. Structural integrity and flexibility of tubing is important when discussing the repeatability of analysis. This is inherent with reactor design.

Pumps in Flow Injection Analysis

Pumps used in FIA can be considered the heart of the analyzer propelling solution through the system. Several pumps have been considered for use in flow injection analyses. The most practical pump is the peristaltic pump. The peristaltic pump has several advantages as well as a few disadvantages (104). A couple of advantages are low costs and no chemical contact. A disadvantage of the peristaltic pump is a flow pulsation. This disadvantage can be overcome using higher flow rates or more cylinder rollers that will decrease the pulsation intensity.

Other pumps employed are piston displacement, syringe, and pressurized reservoirs (104). The piston displacement pump is commonly coupled with gradient techniques because of the precise timing required. Syringe pumps are also used for high precision; however, these need periodic refilling halting analyses. For simple flow injection analyzers, reservoirs with a pressurized head space can be used. These pressurized reservoirs are the most economical, but fall short in multi-channel analyzers.

Injectors in Flow Injection Analysis

The injection of the sample has several requirements for FIA to be useful in analyses. The most important are reproducible injections and a consistent frequency. In the early days, manual injections were done with a syringe through the tubing wall into the flow path (104). This method was later replaced by rotary-valve injectors. These injectors contain a fixed-volume sample loop for more precise volume injections. They can also be automated to improve the injection reproducibility and timing.

Reactors in Flow Injection Analysis

Between injection and detection, the sample zone must undergo sufficient dispersion. If chemical reactions are also required, they need to occur within the reactor. The reactor can take on different

geometries. Three common geometries are coiled, knotted, and knitted. Coiled reactors are common throughout flow injection analyzers. The reactor is formed by coiling tubing around a cylindrical center.

The knitted and knotted geometries undergo simple and elaborate bending, respectively. To bend the tubing without creating flow restrictions involves careful technique with specific tubing characteristics. Because the tubing is flexible enough to create the geometry desired, slight flexibility from flow during analysis can create irreproducible results (104). Securing the tubing to fixed supports helps to overcome the flexibility from flow.

Packed reactors and integrated micro-conduits make up the remainder of possible reactors. The packed reactor works well in situations using immobilized reagents. These reactors are typically only a few centimeters in length (104). Coated silica particles increase the surface area and efficiency of the reactor. Progress in micro-conduit reactors further shrinks the overall reactor design using fixed flow channels. These channels have charted pathways mimicking the appearance of an integrated circuit board (105).

Detectors in Flow Injection Analysis

Lastly, the detector is where applications are evolving. A variety of detectors can be used with flow injection analysis under given circumstances. Possible detectors can be classified into one of two groups, spectrophotometric or electrochemical (101,103,104). Each detector classification comes with its limitations. Spectrophotometric detectors have possible peak broadening concerns while electrochemical detectors are only surface-contacting measurements. A wide range of detectors are available such as; absorption, luminescence, and ion-selective.

Coupling these detectors with the other components necessary to flow injection analysis; manufacturers have produced a variety of commercial instruments. The instruments provided are for quantifying common analytes with high sample throughput (101-104). The downside to commercializing

flow injection analyzers is that one instrument configuration does not work for all cases. It is still customary to see laboratory-built analyzers for most research and development needs.

<u>Applications of Flow Injection Analysis</u>

Many articles and publications have surfaced over the recent decades on applications of flow injection analysis in analytical chemistry. Areas of interest or application of flow injection analysis include agriculture, biological assays, and fundamental/exploratory research (105-111). The main advantages for its use in all fields are relative inexpensive costs, high sample throughputs, and trace levels of detection possible.

The food and agriculture sector uses flow injection analysis in a couple of unique ways. First, Kotorman et al (106) used flow injection analysis coupled with an immobilized enzyme reactor. This configuration along with a spectrophotometer was used to monitor levels of lactic acid in various wines. Their approach resulted in a micro-molar detection limit with high reproducibility of approximately 2% RSD.

Nanita et al (107) developed a flow injection analyzer using tandem mass spectrometry for detection. Automation capabilities of flow injection analysis with the selectivity of mass spectrometry led to a sample frequency of up to 60 samples per hour. Repeatability at this rate was fair with 20% RSD. The technique was developed to perform a multi-component analysis of insecticides and herbicides. A detection limit in aqueous samples was found to be 30 ppt. Liquid chromatography methods have sampling frequencies about half of the flow injection method proposed (107). This provides an advantage of the flow injection method; however, there still exists a disadvantage in its complexity.

Flow injection analyzers have been applied for faster and more repeatable immunoassays. Chemiluminescence detection and immobilized enzymes were paired for measuring oxidized amino acids (108). Analytes of interest were L-Glutamate and L-Lysine. Previous work to co-immobilize enzymes showed activity decrease as enzyme population increased. To overcome the activity concern, Kiba's

64

group immobilized the enzymes on polymeric beads. These beads were then packed into a flexible tube coiled in front of a photomultiplier tube. Detection of the analytes to 50 nanomolar per oxidized acid was possible. A sampling frequency of 11 samples per hour was also achieved. The group also elaborated on the interference of luminol-chemiluminescence in the presence of reductants.

Though several more areas employ flow injection analyzers or combination thereof; fundamental and exploratory research provides some of the best approaches to applying flow injection analysis currently and beyond. Research in the later twentieth century on flow injection analysis investigated possibilities for peroxyoxalate chemiluminescence (109,110).

Substitution of *bis*-2, 4-dintroperoxyoxalate for *bis*-2, 4, 6-trichloroperoxyoxalate was evaluated because of its greater quantum efficiency by Honda et al. (109). The group also determined the affects of halides, water, and respective phenols of each oxalate ester system. The halides as expected showed fair to complete quenching of chemiluminescence. Increasing concentrations of chloride diminished the chemiluminescence intensity; however, bromide and iodide quenched all intensity.

In the peroxyoxalate chemiluminescence system, *bis*-2, 4-dinitroperoxyoxalate experienced more detrimental effects from water than *bis*-2, 4, 6-trichloroperoxyoxalate, a 40% difference. Lastly, the respective phenols of 2, 4-dinitrophenol and 2, 4, 6-trichlorphenol were found to also lower the chemiluminescence intensity. *Bis*-2,4,6-trichloroperoxyoxalate was affected more by its conjugate phenol than *bis*-2, 4-dinitroperoxyoxalate. This observation causes concern for users of *bis*-2, 4, 6-trichloroperoxyoxalate regarding the purity of the chemiluminescence reagent.

Milofsky and Birks researched into the initiation of peroxyoxalate chemiluminescence with light instead of hydrogen peroxide (110). They termed the chemistry involving light initiation as "photo ionization chemiluminescence". The detection limits were found to be acceptable, but not as optimal as found in previous peroxyoxalate chemiluminescence methods. It was found that certain matrix requirements must be met for emission to be observed. The requirements were the availability of

65

dissolved oxygen, fluorophore, and an alcohol or carbonyl that can release a hydrogen atom. The hydrogen atom is absorbed by the oxalate ester during a reduction step. This was also seen in electrochemical induced peroxyoxalate chemiluminescence by Bard (110).

Other approaches in fundamental and exploratory work include the investigations of new detectors due to improved electronics and miniaturized devices (105,111). An electrochemical detector similar to an ion-selective electrode can be coupled to a flow injection analyzer. This technique used the ability to produce a liquid-gel micro interface (111). The interface allowed for ion transport, specifically anions. Employing high-resistance or pure water as an eluent, halides were carried to the electrochemical detector. At the detector, a pulse of applied potential was used to help measure the current due to ion transport across the liquid-gel interface. Lee and his colleagues (111) found that increasing the pulsed, applied potential increased the sensitivity of the detector to ppb detection limits.

Miniaturization of devices has been an area of interest for analytical chemistry in the recent years. Scaling down in instrumentation allows decreasing amounts of chemicals required, and lessens the amount of waste. Flow injection analysis was miniaturized with fluorescence detection by Leach et al. of Stanford University (105). Their work produced a durable and disposable unit with a goal of being economical. The flow injection analyzer was constructed of micron-size flow channels. When pressure was placed on and off the channels, a pumping action was created. The pressure was applied using electrical pulses and the characteristics of the poly-dimethylsiloxane tubing collapsed upon the pulses.

Repeatability excelled for the miniature flow injection apparatus. Reproducibility was found to be less than 3% RSD. Samples of nanoliter volumes per injection can be injected as the unit occupies only the palm of an adult's hand (105). Also impressive were the detection limits proving to be in the zeptomolar range.

CHAPTER 3

EXPERIMENTAL PROCEDURES

Purpose of Research

As discussed in Chapter One, nanoparticles and quantum dots possess optical properties that can be tailored by changing their size and surface chemistry. This has the attention of many research groups evaluating nanoparticle applications for electronic technology and medical imaging. Proposed applications of nanoparticles have used their ability to be immobilized with a variety of substrates.

The luminescent properties of quantum dots make them ideal substitutes for organic fluorescent dyes. Luminol is one of the most common organic fluorophores employed in chemiluminescence analyses. Assays involving enzyme-generated hydrogen peroxide are included. The use of immobilized enzymes has provided improvements for chemiluminescence analyses coupled to flow injection.

Interest was taken in colloidal CdSe quantum dots as sources of luminescence in peroxyoxalate chemiluminescence analyses. Immobilizing these semiconductor nanoparticles makes luminescence measurements more appealing and applicable. Fluorophores immobilized in a flow injection system simplify the construction and reduce materials consumption. The ability to successfully immobilize non-passivated CdSe quantum dots for chemiluminescence measurements offers future improvement opportunities in analytical chemistry to increase sensitivities, stabilities, and additional applications.

Goals were set to study the application of immobilized quantum dots in POCL-FIA and have been listed immediately following this paragraph. The remainder of the chapter was constructed to describe how the luminescent quantum dots were immobilized in selected polymers. Experimental details for optimizing the flow injection analyzer used, characterizing the quantum dots prepared, and testing the application based on linearity, robustness, stability, and variability were also recorded.

- Synthesize two quantum dot sizes in batch quantities for later immobilization and size comparisons.

- Immobilize quantum dots with trans-polyisoprene, polymethylmethacrylate, and low-density polyethylene polymer substrates

- Develop and construct a flow cell for multi-use with immobilized quantum dot preparations

- Optimize FIA configuration for evaluation of immobilized quantum dot preparations

- Use POCL-FIA to evaluate each immobilized quantum dot preparation for the following:

    o Determine linearity of each immobilized quantum dot preparation

    o Determine robustness of immobilized quantum dot preparation by number of sequential samples injected at a given analyte concentration

    o Determine shelf-life stability of each immobilized quantum dot preparation

    o Determine variability within a single immobilized quantum dot preparation and across multiple preparations of the same immobilized quantum dots

- Consider application of technique for measuring H_2O_2 in non-aqueous matrices

Reagents

Cadmium selenide, CdSe, quantum dots were synthesized per the procedures described by Boatman, Lisensky, and Nordell (13). The following chemicals were obtained for synthesizing the CdSe quantum dots. Cadmium oxide (98.9%), selenium powder (99%), oleic acid (99%) was purchased from Alfa-Aesar (Ward Hill, MA). Technical-grade trioctylphosphine (90%) was supplied by Sigma-Aldrich (St. Louis, MO). The coordinating solvent, 1-octadecene, was technical grade (90%) and manufactured by Acros Organics, a division of Thermo-Fisher Scientific (Pittsburgh, PA). Triethylamine (sequenal grade) was purchased from Pierce Chemicals (Rockford, IL) then distilled prior to use.

Immobilization of the CdSe quantum dots was based from procedures discussed in Yin et al. (50) article. Modifications were made as needed due to solvent compatibility with the selected polymers.

Polymethylmethacrylate powder, PMMA, and low-density polyethylene, LDPE, (500 micron) was used as substrates in addition to trans-polyisoprene, PI. The PMMA and LDPE were purchased from Alfa-Aesar (Ward Hill, MA), and the PI was obtained from Sigma-Aldrich (St. Louis, MO). High-purity grade chloroform solvent was from Burdick & Jackson (Muskegon, MI), and ACS reagent grade acetone was purchased from Fisher Chemicals (Pittsburgh, PA). The surfactant solution for encapsulation used lauric acid from Acros Organics (Pittsburgh, PA), sodium hydroxide pellets from Fisher Chemicals (Pittsburgh, PA). Deionized water was supplied from a purification kit purchased from US Filters (Pittsburgh, PA).

Bis-(2,4,6-trichlorophenyl) oxalate, TCPO, was synthesized following Mohan and Turro's article (73). 2,4,6-trichlorophenol (98%) and oxalyl chloride (98%) was a purchased from Alfa-Aesar (Ward Hill, MA). It is important to note that trichlorophenol is a known carcinogen! Anhydrous magnesium sulfate powder and ACS reagent grade benzene and petroleum ether were purchased from Fisher Chemicals (Pittsburgh, PA). The TCPO was dissolved for flow measurements in ACS reagent grade acetonitrile also purchased from Fisher Chemicals (Pittsburgh, PA). Imidazole (99%) from Sigma-Aldrcih (St. Louis, MO) was used as a catalyst.

Hydrogen peroxide (30%) from Fisher Chemicals (Pittsburgh, PA) and hydrogen peroxide (3%) from a local retailer were used to create standards used for initiating the peroxyoxalate chemiluminescence. Additional solvents of cyclohexane, isopropanol, and glacial acetic acid were ACS reagent grade.

<div align="center">Stock Solutions</div>

Selenium Precursor Solution

A 30-mL solution of selenium precursor was prepared for bulk CdSe syntheses with the procedure detailed by Boatman et al. (13). Weights and volumes per the procedure by Boatman et al. were adjusted accordingly to accommodate the bulk syntheses performed. The stock was made by weighing 183.2 mg of selenium powder in a 100-mL beaker. A stir bar and 30 mL of 1-octadecene were

added to the selenium powder in the beaker. The mixture was stirred with gentle heat while 2.5 mL of tri-octylphosphine were added to induce the dissolution of the selenium powder. The resulting solution was stored at room temperature in an amber jar until required for use in the CdSe syntheses.

"Yellow" CdSe Solution (QD$_{520}$)

To synthesize the batch of "yellow" CdSe quantum dots for immobilizing in selected polymers, the procedure detailed by Boatman et al. (13) was followed with minor alterations. First, 131 mg of cadmium oxide were weighed into a 250-mL round-bottom flask. Next a stir bar, 6 mL of oleic acid, and 100 mL of 1-octadecene were added to the flask in the order listed. The flask and contents were then placed on a 250-mL soft-shell heating mantle controlled by a rheostat with a setting of "70". The mantle sat above a stir plate to allow for stirring before and after the addition of the selenium precursor solution.

Using a 260°C thermometer, the cadmium oxide solution temperature was monitored as it calmly rose to 225°C. At 225°C while stirring, 10 mL of the previously prepared selenium precursor solution was added using a 10-mL gas-tight syringe and needle. After the selenium precursor solution was added, the flask containing the mixture was immediately transferred to an ice-water bath. The reaction time was about 5 seconds from selenium precursor injection till flask emersion in the ice-water bath halting the colloidal growth of the quantum dots.

"Red" CdSe Solution (QD$_{555}$)

The procedure for the synthesis of the "yellow" CdSe solution (QD$_{520}$) was followed in similar motions for the "red" CdSe solution (QD$_{555}$) except for the following details. The preparation of the "red" CdSe solution used 136 mg of cadmium oxide, and was allowed to react with the selenium precursor solution on heat while stirring for about 60 seconds before halting the colloidal growth.

Imidazole Solution

An imidazole, catalyst solution was prepared for POCL-FIA measurements. A 1 M solution of imidazole for later dilutions was made by dissolving 1.7326 g of imidazole in 25 mL of de-ionized water using a 25-mL volumetric flask. The solution was shaken till completely dissolved then stored in a refrigerator between uses.

Encapsulation Surfactant Solution

A surfactant solution was prepared in bulk for use in immobilization-by-encapsulation preparations. The surfactant solution was made by weighing 2.5327 g of NaOH pellets and 8.5392 g of lauric acid flakes into a plastic weighing boat. The NaOH and lauric acid was then placed in a 4-L amber jar together. De-ionized water was added using a 1-L graduated cylinder, bringing the final volume to 2.5 L. A stir bar was added to the 4-L jar, and the jar set on a stir/hot plate to help dissolve the lauric acid. Once completely dissolved, the surfactant solution was allowed to cool to room temperature, and remained in the 4-L jar for storage at room temperature until needed for use in immobilizations.

Hydrogen Peroxide Solution

A solution of 30% hydrogen peroxide was purchased from Fisher Chemicals (Pittsburgh, PA) for use in preparing working solutions used in all POCL-FIA measurements. The solution was stored in a refrigerator between uses.

Working Solutions

Preparation of CdSe Solutions for Characterization by Fluorescence Emission

The prepared CdSe quantum dot solutions were diluted to 5% for fluorescence emission characterizations. Aliquots of 500 µL of each CdSe solution were diluted in a 10-mL volumetric flask

with cyclohexane. The flask was shaken in hand to mix the CdSe solution and cyclohexane efficiently prior to use in fluorescence emission measurements.

Preparation of TCPO Solution for Imidazole Optimization

A solution of TCPO in acetonitrile for use in POCL-FIA measurements to find the optimum concentration of imidazole catalyst was prepared in the following manner. Synthesized TCPO (details of TCPO synthesis to follow later) was weighed in a plastic weighing boat to 2.7 g. The TCPO was transferred to a 500-mL beaker. Next, 360 mL of acetonitrile was added to the beaker. The beaker with contents was then placed in a soniccator bath for 60 minutes at $35^{\circ}C$ to increase the rate of dissolution. The preparation was also carried out in minimal light, and the soniccator was covered loosely with aluminum foil.

Preparation of Imidazole Standards in TCPO for Catalyst Optimization (1×10^{-6} M – 1.0×10^{-1}M)

Standards of imidazole in TCPO were prepared by diluting aliquots of the previously prepared imidazole stock solution, 1 M, into separate 50-mL volumetric flasks. Serially diluting the 1 M stock imidazole; 1.0×10^{-1}, 1.0×10^{-2}, 1.0×10^{-3}, 1.0×10^{-4}, 1.0×10^{-5}, and 1.0×10^{-6} M concentrations were achieved beginning with 5 mL of the stock 1 M imidazole brought to the 50-mL volume with previously prepared TCPO solution. Each subsequent concentration was made by repeating the preparation of the previous standard. The imidazole standards were gently shaken to ensure efficient mixing of imidazole throughout the solution prior to their immediate use.

Preparation of Imidazole Standards in TCPO for Catalyst Optimization (10 μM – 500 μM)

Standards of imidazole in TCPO were prepared by initially diluting a 2.5 mL-aliquot of the previously prepared imidazole stock solution, 1 M, into a 50-mL volumetric flask to produce a concentration of 5.0×10^{-2} M. Diluting the temporary stock of imidazole; 5.0×10^{-4}, 2.5×10^{-4}, 1.5×10^{-4}, 1.0×10^{-4}, 5.0×10^{-5}, and 1.0×10^{-5} M concentrations were achieved by diluting aliquots of 500 μL, 250

μL, 150 μL, 100 μL, 50 μL, and 10 μL to the 50-mL volume with previously prepared TCPO solution per flask, respectively. The imidazole standards were gently shaken to ensure efficient mixing of imidazole throughout the solution prior to their immediate use.

Preparation of TCPO Solutions for Remaining POCL-FIA Measurements

The remaining POCL-FIA measurements pertaining to instrument flowrate optimization, immobilized-quantum dot preparation characterizations, and technique applicability required multiple preparations of TCPO solution with the optimized imidazole concentration included. Each preparation of TCPO solution was made by weighing approximately 0.75 g of synthesized TCPO per 100 mL of acetonitrile. The TCPO solids were weighed then placed in the appropriate volumetric flask, where acetonitrile was added till the volume was about one-half inch from the volumetric mark on the flask. Here the correct amount of 1 M imidazole stock solution (10 μL/100 mL TCPO solution) was added to achieve the previously determined optimum concentration of imidazole at 100 μM. Acetonitrile was used to bring the volume to the mark on the flask prior to soniccation for 60 minutes at 35°C. The TCPO solids were allowed to continue to reach complete dissolution during this time while covered with aluminum foil. Minimal light was used while preparing the solution; and its use was immediate after preparation. No solutions were prepared and stored for later use.

Preparation of Hydrogen Peroxide Standards for Linearity Studies

Seven hydrogen peroxide standards were prepared by first diluting a 568-μL aliquot of stock 30% hydrogen peroxide solution to 1.0×10^{-1} M in a 50-mL volumetric flask with de-ionized water. The 1.0×10^{-1} M standard was then diluted serially to concentrations of 5.0×10^{-2}, 1.0×10^{-2}, 5.0×10^{-3}, 1.0×10^{-3}, 5.0×10^{-4}, and 1.0×10^{-4} M in 50-mL volumetric flasks with de-ionized water. The standards were prepared fresh from stock each day of testing.

Preparation of Hydrogen Peroxide Standards for Robustness Studies

A hydrogen peroxide standard of 1.0×10^{-2} M was prepared by diluting a 57-µL aliquot of stock 30% hydrogen peroxide solution in a 50-mL volumetric flask with de-ionized water. The standard was prepared fresh from stock each day of testing.

Preparation of Hydrogen Peroxide Standards for Stability Studies

A hydrogen peroxide standard of 1.0×10^{-2} M was prepared by diluting a 57-µL aliquot of stock 30% hydrogen peroxide solution in a 50-mL volumetric flask with de-ionized water. The standard was prepared fresh from stock each day of testing.

Preparation of Hydrogen Peroxide Standards for Variability Studies

A hydrogen peroxide standard of 1.0×10^{-2} M was prepared by diluting a 57-µL aliquot of stock 30% hydrogen peroxide solution in a 50-mL volumetric flask with de-ionized water. The standard was prepared fresh from stock each day of testing.

Calibration of POCL-FIA Instrument Configuration

Seven hydrogen peroxide standards were prepared by first diluting a 568-µL aliquot of stock 30% hydrogen peroxide solution to 1.0×10^{-1} M in a 50-mL volumetric flask with de-ionized water. The 1.0×10^{-1} M standard was then diluted serially to concentrations of 5.0×10^{-2}, 1.0×10^{-2}, 5.0×10^{-3}, 1.0×10^{-3}, 5.0×10^{-4}, and 1.0×10^{-4} M in 50-mL volumetric flasks with de-ionized water.

Preparation of Hydrogen Peroxide in Non-Aqueous Solvents

Two hydrogen peroxides standards were prepared in each isopropanol and glacial acetic acid. The first standard in each solvent was made by diluting 57-µL aliquots of stock hydrogen peroxide solution in 10-mL volumetric flasks with the appropriate solvent. The resulting concentration of the first standard was 5.0×10^{-2} M. The second standard for each solvent was prepared using a 100-µL aliquot of

the respective 5.0 x 10^{-2} M standard. The aliquot was diluted in a 10-mL volumetric flask with the respective solvent. The concentration of the second standard of each solvent was 5.0 x 10^{-4} M.

Instrumentation

A Perkin-Elmer 650-10S series spectrofluorometer was used to determine the emission spectra of the two different quantum dots synthesized. The excitation beam was produced with a xenon flash-lamp using a Perkin-Elmer 150 Xenon flash-lamp external power source. The emission was detected at a perpendicular path from the excitation beam path with the sample under analysis in a quartz cuvette. Pathways for the excitation and emission beams passed through 2 nm slits. Spectra for the emission of all samples were recorded by scanning from 240 nm up to 820 nm at intervals of 5 nm. Intensities were viewed with a digital readout, while the sensitivity setting was a "1". A basic diagram of the instrument configuration is seen in Chapter 2 as Figure 11.

The other instrument used to perform the research at hand was a laboratory-built FIA instrument. The instrument was configured using a Cole-Parmer (Chicago, IL) Masterflex peristaltic pump (7013-20) with a controller box (7520-25) set at "350". The pump propelled the prepared TCPO reaction solution through Masterflex 6409-13 tubing with a 1.6 mm inner-diameter and max capacitiy flowrate of 36 mL/min. The operating flowrate was approximately 5 mL/min.

As the TCPO solution was pumped through the system, the solution passed through a Rheodyne 7125 series injector. The injector was comprised of a 50-μL loop, and a two-position valve for loading or injecting the standards of hydrogen peroxide prepared for the research. The injected sample plus solution reacted as it flowed to the custom-built, glass flow-cell where the immobilized-quantum dot preparation under current study was held. A picture of the flow-cell is seen in Figure 16, where it contains one of the several immobilized-quantum dot preparations. The design of the flow-cell was considered to allow for quick and easy change of preparations. It also allowed for reducing the possibility of plugging by the preparations.

Figure 16. Photo of custom glass flowcell for POCL-FIA with immobilized-quantum dot preparation

With the flow-cell containing the immobilized-quantum dots positioned in front of a Hamatsu photomultiplier tube, the chemiluminescence signal intensity was relayed to an analog output with multiple choices of sensitivities. The analog output was displayed on a control box salvaged from an American Instruments Company (Silver Springs, MD), AMINCO, spectrofluorometer. A schematic of the configuration is sketched in Figure 17, while an actual photograph of the instrument is shown in Figure 18.
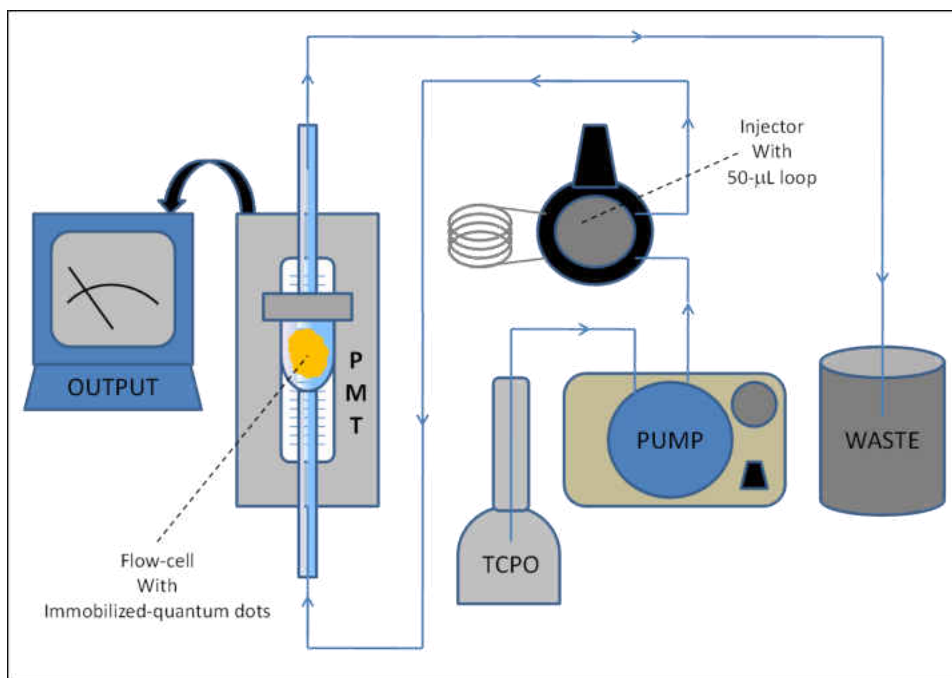
Figure 17. Schematic of laboratory built of FIA configuration used in POCL-FIA analyses

Figure 18. Photo of laboratory built FIA instrument for POCL-FIA measurements with immobilized quantum dots

Characterization of CdSe Solutions Using Fluorescence Emission Spectra

The prepared CdSe quantum dots were evaluated for emission spectra upon excitation by light at a wavelength of 400 nm. The emission spectra were produced by first diluting 500 μM of each CdSe solution to 5% in a 10-mL volumetric flask with cyclohexane. A Perkin-Elmer 650-10S spectrofluorometer was used to produce the spectra of the cyclohexane solvent and each prepared CdSe solution. The observed emission wavelength of maximum peak intensity was used in part to characterize the prepared quantum dots.

Synthesis of *bis*-(2,4,6-trichlorophenyl) oxalate (TCPO)

In order to perform the POCL-FIA analyses required to study and in-part characterize the immobilized-quantum dot preparations, a chemiluminescence reagent needed to be synthesized. The required material of *bis* (2,4,6-trichlorophenyl) oxalate, TCPO, was synthesized for this research work following the method described per the article by Mohan and Turro (73). Depending on the amount of TCPO required at a given time, multiples of the original procedure were synthesized. This was done by distilling 15 mL of sequenal-grade triethylamine into a 250-mL round-bottom flask. Once the majority of the triethylamine distillate had collected in the round-bottom flask, approximately 10-12 g, the flask was removed from the distillation apparatus.

Next, 19.75 g of 2,4,6- trichlorophenol were weighed into a plastic weighing boat then transferred to the round-bottom flask containing the freshly-distilled triethylamine. After drying 300 mL of benzene with 5 g of anhydrous magnesium sulfate salt, the benzene was filtered of the salt prior to adding 250 mL of the dried benzene to the 250-mL round-bottom flask containing the triethylamine and 2, 4, 6 – trichlorophenol. The resulting mixture was placed into an ice-water bath to reduce the contents temperature to below 10°C. This was a requirement along with minimal lighting during the addition of the oxalyl chloride.

The addition of the oxalyl chloride was carried out patiently by slowly dropping 5 mL of the light-sensitive chemical to the round-bottom flask containing the previously mentioned contents. As the oxalyl chloride was added, fumes were released from the chemical reaction taking place forming the dark-orange, crude product of TCPO. After the complete addition of the oxalyl chloride, the flask was loosely stoppered and secured with a Keck clamp. The flask was set aside overnight away from heat and light to allow additional formation of crude TCPO.

Following the synthesis of the crude TCPO, the material was removed from the round-bottom flask the next day with petroleum ether as it was collected, washed, and air-dried using vacuum filtration. The washing with petroleum ether and air-drying in a Buchner funnel was also carried out in minimal light and heat. Once the product was washed, beige to light-brown in color, it was transferred to an amber jar with the lid loosely fixed to allow residual volatiles to vent as the product continued to dry. The product was ready to use for creating the TCPO solutions required for the POCL-FIA analyses. Recrystallization of the TCPO was not performed, and the purity was not tested.

A spare batch of TCPO was also produced by the same method, but magnetic stirring was applied during the addition of oxalyl chloride. The spare batch material had a fine crystalline appearance and white in color. This TCPO was not used for any experimental work due to injector plugging issues when adding the imidazole catalyst to the TCPO solution. The plugging was a result insoluble 1, 1-oxalylimidazole in acetonitrile (81).

<center>Determining the Optimum Imidazole Concentration for POCL-FIA Measurements</center>

Wide Range Determination

The optimum amount of imidazole catalyst for the POCL-FIA analyses was determined using the setup requiring its determination. A solution of TCPO in acetonitrile was prepared by dissolving 2.7 g of synthesized TCPO into 360 mL of acetonitrile while soniccating for 60 minutes at 35°C. The TCPO solution was used to dilute 5 mL of stock 1 M imidazole solution to 1.0×10^{-1} M in a 50-mL volumetric

<center>79</center>

flask. Five subsequent standards were made serially diluting from the first following the same procedure using 5 mL of previous standard to 50 mL with TCPO solution. The resulting set of standards of imidazole in TCPO solution ranged from 1.0×10^{-6} M to 1.0×10^{-1} M, where each standard concentration changed by a factor of ten.

Using the custom POCL-FIA instrument, the standards of imidazole prepared in TCPO solution were drawn through the configuration using the peristaltic pump set at "350", or approximately 5 mL/min flowrate. The standard was allowed to rinse the configuration for approximately one minute prior to any data being collected. To create the chemiluminescence required for making the measurements, a preliminary product of immobilized quantum dots with polyisoprene was placed in the flowcell. Once the configuration was ready for measurements per standard, triplicate injections of neat 3% hydrogen peroxide were made. The flow was stopped between injections within seconds of the maximum signal being observed. The intensities of the chemiluminescence produced were observed on the analog output of the POCL-FIA instrument, where the sensitivity setting was at "3".

The recorded data set from this experiment was plotted with the chemiluminescence-intensity averages dependent on the imidazole concentration applied to a logarithmic scale.

Narrow Range Determination

After determining the range that the optimum imidazole concentration existed in from the experiment previously mentioned, a second set of imidazole standards in TCPO solution was prepared. This set narrowed the range of possible concentrations that could be the optimum concentration. Following similar procedures from the "Wide Range Determination" experiment, this experiment only differed in the preparation of the required concentrations. The range of choice here was chosen to be 1.0 $\times 10^{-5}$ M to 5.0×10^{-4} M (10 μM – 500 μM) imidazole in 50-mL volumes. These were prepared by making a temporary stock of imidazole at 5.0×10^{-2} M, then diluted aliquots of 500, 250, 150, 100, 50, and 10 μL into 50 mL volumes.

Again each standard was drawn through the custom POCL-FIA instrument, where neat 3% hydrogen peroxide was injected in triplicates. The chemiluminescence-intensity averages were plotted dependent on the true concentration of the imidazole per standard to find the optimum concentration of imidazole that produced the maximum intensity for the upcoming POCL-FIA analyses used to characterize the immobilized-quantum dot preparations under study.

Determining the Optimum Flowrate for POCL-FIA Measurements

Before performing any measurements to characterize the preparations of immobilized-quantum dots, the optimum flowrate for the instrument configuration must be determined. Considerations for the optimum flowrate were peak height, peak shape, reaction solvent consumption, and configurational pressure capacity. To determine the optimum flowrate, the flowrate was increased stepwise using the dial-selector on the peristaltic pump module. Each time the flowrate was increased; triplicate injections of neat, 3% hydrogen peroxide were injected. The corresponding chemiluminescence intensity averages were recoreded for plotting against the flowrate.

Immobilization of CdSe Quantum Dots for Linearity, Robustness, Stability, and Variability Studies

The following preparations of immobilized quantum dots were performed to create material for all analyses related to linearity, robustness, shelf-life stability, and variability. The first set of immobilized-quantum dot preparations was made to provide sufficient amounts of material for the first three analyses listed. The second set of immobilized-quantum dot preparations was made the same as the first, but only for the variability study. The variability study required triplicates of each immobilized-quantum dot preparation to be prepared. There were 12 immobilized-quantum dot preparations in total stemming from the combinations of 2 different CdSe quantum dot sizes, three different polymers, and two different immobilization techniques. Each immobilized-quantum dot preparation is described below.

PI-QD$_{520}$-Melt / PI-QD$_{555}$-Melt Preparations

This preparation of immobilized-quantum dots, both sizes, in polyisoprene was done by simply melting the polymer in an oven at high temperature for a short time then mixing in the quantum dots. In detail, 2 g of polyisoprene were placed into a 250-mL beaker followed by placement of the beaker into an oven at a temperature of approximately 250°C. The polyisoprene was allowed to sit in the oven for 10 minutes to melt becoming goop-like.

Here the beaker was removed from the oven carefully while still very hot, and 2.5 mL of the desired quantum dots were added. Immediate stirring with a glass rod followed prior to replacement in the oven for another 3 minutes. After the 3 minutes, the preparation was pulled from the oven and stirring with a glass rod continued while the polymer cooled to near room temperature to mix in the quantum dots as best possible. The cooled preparation was stored in a glass, amber jar till used for characterization.

PI-QD$_{520}$-Encapsulation / PI-QD$_{555}$-Encapsulation Preparations

This preparation of immobilized-quantum dots, both sizes, in polyisoprene was done following a slight modification of the encapsulation method described by Yin et al (50). In detail, 2 g of polyisoprene were placed into a 250-mL beaker. Next, 40 mL of chloroform solvent was added along with a stir bar. The beaker with materials was placed on a heat/stir plate to dissolve the polymer for addition of the designated quantum dots.

Once the polyisoprene was dissolved, 2.5 mL of the designated quantum dots were added and mixed in efficiently. The mixture was then transferred to a 50-mL solution of previously prepared surfactant. The polymer-quantum dot mixture was allowed to stir in the surfactant solution for 5 minutes. The immobilized-quantum dot preparation was produced by heating the surfactant to remove residual organic solvent. Resulting product was collected through vacuum filtration then transferred to an amber jar for storage.

<u>PMMA-QD$_{520}$-Melt / PMMA-QD$_{555}$-Melt Preparations</u>

This preparation of immobilized-quantum dots, both sizes, in polymethylmethacrylate was done by simply melting the polymer in an oven at high temperature for a short time with the designated quantum dots. In detail, 2 g of polyisoprene were placed into a 250-mL beaker. Next, 35 mL of acetone was added to the beaker plus 2.5 mL of designated quantum dots solution. The beaker and contents were then placed in an oven at a temperature of approximately 250°C. The polymethylmethacrylate mixture was allowed to sit in the oven for 5 minutes.

After the 5 minutes in the oven, the preparation was pulled and allowed to cool. The immobilized-quantum dot product was transferred to an amber jar for storage.

<u>PMMA-QD$_{520}$-Encapsulation / PMMA-QD$_{555}$-Encapsulation Preparations</u>

This preparation of immobilized quantum dots, both sizes, in polymethylmethacrylate was done following a slight modification of the encapsulation method described by Yin et al (50). In detail, 2 g of polymethylmethacrylate were placed into a 250-mL beaker. Next, 25 mL of acetone solvent was added along with a stir bar. The beaker with materials was placed on a heat/stir plate to dissolve the polymer for addition of the designated quantum dots.

Once the polymethylmethacrylate was dissolved, 2.5 mL of the designated quantum dots were added and mixed in efficiently. The mixture was then transferred to a 50-mL solution of previously prepared surfactant. The polymer-quantum dot mixture was allowed to stir in the surfactant solution for 5 minutes. The immobilized-quantum dot preparation was immediately produced upon addition to the surfactant. The preparation was removed from the surfactant solution by draining some of the liquid, and using forceps to transfer to an amber storage vial.

<u>LDPE-QD$_{520}$-Melt / LDPE-QD$_{555}$-Melt Preparations</u>

This preparation of immobilized quantum dots, both sizes, in low-density polyethylene was done by simply melting the polymer in an oven at high temperature for a short time then mixing in the quantum dots. In detail, 2 g of low-density polyethylene powder were placed into a 250-mL beaker followed by placement of the beaker into an oven at a temperature of approximately 250°C. The low-density polyethylene was allowed to sit in the oven for 3 minutes to melt becoming goop-like.

Here the beaker was removed from the oven carefully while still very hot, and 2.5 mL of the desired quantum dots were added. Immediate stirring with a glass rod followed while the polymer cooled to near room temperature to mix in the quantum dots as best possible. The cooled preparation was stored in a glass, amber jar till used for characterization.

<u>LDPE-QD$_{520}$-Encapsulation / LDPE-QD$_{555}$-Encapsulation Preparations</u>

This preparation of immobilized-quantum dots, both sizes, in low-density polyethylene was done following a slight modification of the encapsulation method described by Yin et al (50). In detail, 2 g of low-density polyethylene were placed into a 250-mL beaker. Next, 25 mL of hexane solvent was added along with a stir bar. The beaker with materials was placed on a heat/stir plate to dissolve the polymer for addition of the designated quantum dots.

Once the low-density polyethylene was dissolved, 2.5 mL of the designated quantum dots were added and mixed in efficiently. The mixture was then transferred to a 50-mL solution of previously prepared surfactant. The polymer-quantum dot mixture was allowed to stir in the surfactant solution for 5 minutes. The resulting liquid was allowed to sit with no stir on mild heat to evaporate the hexane solvent leaving the immobilized-quantum dot product insoluble in the surfactant. The immobilized-quantum dot preparation was collected through vacuum filtration. The product was placed in an amber jar for storage.

Determining the Linearity of Immobilized Quantum Dot Preparations

The first characterization of the immobilized quantum dots was the dynamic range, or linearity, of each preparation. This was done by analyzing each preparation with seven hydrogen peroxide standards spanning three orders of magnitude. The range chosen was 1.0×10^{-4} M to 1.0×10^{-1} M for hydrogen peroxide concentrations to be injected. The standards were prepared by diluting stock 30% hydrogen peroxide, 568-µL up to 50 mL with deionized water in a 50-mL volumetric flask. The 1.0×10^{-1} M standard was diluted serially down to 1.0×10^{-4} M by alternating between diluting 25 mL and 12.5 mL of the existing standard to create the next. The standards made in the series of seven were 1.0×10^{-4}, 5.0×10^{-4}, 1.0×10^{-3}, 5.0×10^{-3}, 1.0×10^{-2}, 5.0×10^{-2}, and 1.0×10^{-1} M.

For the hydrogen peroxide to react and create the energy-sustaining intermediate, TCPO reaction solution with the optimum amount of imidazole was prepared by weighing 0.75 g of synthesized TCPO per 100 mL of acetonitrile. The imidazole was added at a ratio of 10 µL per 100 mL of solution preparation. The solution was soniccated for 60 minutes at 35°C to obtain complete dissolution prior to use in the custom POCL-FIA instrument. Once the solution was ready it was pumped through the instrument to flush the system prior to any measurements. The flowrate was approximately 5 mL/min at the setting of "350" on the peristaltic pump.

With the TCPO/imidazole reaction solution, immobilized-quantum dot preparation, and hydrogen peroxide standards ready; the instrument was turned on after covering from residual lighting. The sensivity setting was set to the lowest initially then increased as needed with increasing hydrogen peroxide concentrations. For each standard measurement, five replicates were performed by injecting 50 mL of sample into a Rheodyne injector loop of equal volume. Regular practice was followed by injecting three amounts of the sample loop size prior to any measurements with the current standard for rinsing the sample loop.

After injection of the standard into the Rheodyne injector module, the pump was turned on. The flow was allowed to come to a stable rate, about 5 seconds after starting. With a stable output being observed on the analog readout, the injection valve on the Rheodyne was moved from the "LOAD" position to the "INJECT" position. When done the hydrogen peroxide was pushed through the sample loop via the TCPO/imidazole reaction solvent. On its path towards the flow cell containing the immobilized-quantum dot preparation of choice, the intermediate was formed where its transfer of energy to the immobilized quantum dots was observed by the adjacent photomultiplier tube.

The resulting chemiluminescence intensities were recorded along with the sensitivities at which the signals were observed. The intensity results were averaged for the five replicate injections per hydrogen peroxide standard, and then plotted versus of the concentration of the standard to determine the linear range of the immobilized-quantum dot preparation currently under study. The linear-regression values were also obtained using a trendline function found in Excel spreadsheets.

Determining the Robustness of Immobilized Quantum Dot Preparations

The immobilized quantum-dot preparations were tested for robustness, or ability to withstand a number of sequential analyses. To do this fresh TCPO/imidazole solution was prepared along with a fresh hydrogen peroxide standard of 1.0×10^{-2} M. The TCPO/imidazole solution was passed through the POCL-FIA instrument at approximately 5 mL/min. The hydrogen peroxide standard was injected in 50-µL increments with a 50-µL loop.

Each immobilized-quantum dot preparation was exposed to 20 consecutive injections of the hydrogen peroxide standard at 1.0×10^{-2} M with 50-µL injections. To determine each preparation's robustness, the signals per consecutive injections were plotted. The difference between the average signal intensities of the first five injections and the final five injections were used to set a value of robustness to each preparation.

Determining the Stability of Immobilized Quantum Dot Preparations

The shelf-life of each immobilized-quantum dot preparation was determined by measuring the resulting POCL signal using material from the same preparation over the course or 30 days. Each preparation was analyzed on four separate days of the 30-day period. Those days were 1, 10, 20, and 30. Each day all preparations were tested with fresh TCPO/imidazole solution and 1.0×10^{-2} M hydrogen peroxide. The hydrogen peroxide standard was injected at 50-μL volumes.

The immobilized-quantum dot preparations were analyzed using five replicate injections. The average signal of each preparation was plotted versus day tested. Also, to conserve reagents, chemicals, and preparations the data obtained for the shelf-life stability on Day 1 was also data obtained in the "Linearity" experiment. Also, for Day 10, the first five injection signals of the robustness experiment were used for this experiment. Days 20 and 30 had no overlap with any other experiment.

Determining the Variability in a Single Preparation of Immobilized Quantum Dots

The variability, or reproducibility, of making each immobilized-quantum dot preparations was analyzed using a fresh TCPO/imidazole solution with injections of 1.0×10^{-2} M hydrogen peroxide. The variability within each single preparation was determined by sampling three portions of the preparation of choice for testing.

Each of the three sampled locations per immobilized-quantum dot preparation was analyzed with the POCL-FIA instrument and five replicate injections of the hydrogen peroxide standard in 50-μL volumes. The signals of the replicate injections were averaged, had standard deviations determined, and their respective relative standard deviation calculated. The results of each preparation were tabulated into a column graph for easy comparisons.

<u>Determining the Variability Among Multiple Preparations of Immobilized Quantum Dots</u>

The variability, or reproducibility, of making multiple immobilized-quantum dot preparations was analyzed using a fresh TCPO/imidazole solution with injections of 1.0×10^{-2} M hydrogen peroxide. The variability among multiple preparations was determined by sampling each of the multiple preparations only once.

Each of the multiple immobilized-quantum dot preparations was analyzed with the POCL-FIA instrument and five replicate injections of the hydrogen peroxide standard in 50-μL volumes. The signals of the replicate injections were averaged, had standard deviations determined, and their respective relative standard deviation calculated. The results of each preparation were tabulated into a column graph for easy comparisons.

<u>Determining Technique Applicability to Non-Aqueous Solvents</u>

The POCL-FIA technique was tested for applicability by measuring known hydrogen peroxide concentrations in isopropanol and glacial acetic acid. To do this the POCL-FIA instrument was calibrated using fresh preparations of the hydrogen peroxide in water standards at concentrations of 1.0×10^{-1}, 5.0×10^{-2}, 1.0×10^{-2}, 5.0×10^{-3}, 1.0×10^{-3}, 5.0×10^{-4}, and 1.0×10^{-4} M.

With the instrument configuration calibrated, hydrogen peroxide standards in isopropanol and glacial acetic acid were prepared. Standards of 5.0×10^{-2} M hydrogen peroxide in each solvent were prepared by diluting 57 μL of the 30% stock hydrogen peroxide to 10 mL per solvent. The 5.0×10^{-2} M standards were then used to create a second standard per solvent. The second standard was made by diluting 100 μL of the 5.0×10^{-2} M standard to 10 mL. The concentration for the second standard was 5.0×10^{-4} M.

The four standards prepared, two concentrations and two solvents, were injected in 50-μL volumes to obtain respective POCL volumes. The average of five replicate injections per standard-

solvent combination was applied to the recently constructed calibration curve. The back-calculated

concentration of hydrogen peroxide was compared to that of the known concentration to produce a value

of recovery per solvent per concentration level.

CHAPTER 4

RESULTS AND DISCUSSION

The experimental results of the procedures described in the previous chapter are discussed here. The preparations of CdSe quantum dots immobilized in the selected polymers were evaluated for analytical application in peroxyoxalate chemiluminescence (POCL) coupled with flow injection analysis (FIA). Optimization of the constructed flow injection apparatus was conducted to be able to produce and report data on the immobilized-quantum dot preparations.

Quantum Dot Batch Preparation

Synthesis of the quantum dot batch solutions proved successful. Several early attempts of producing the selenium precursor failed due to the insolubility of selenium powder in the 1-octadecene solvent. The use of fresh of tri-n-octylphosphine oxide provided immediate dissolution of the selenium powder. This demonstrated that reagent purity is of high importance during quantum dot synthesis.

The smaller size quantum dots were produced first, QD_{520}. The nomenclature for naming the quantum dots synthesized stemmed from "QD" for quantum dot and the peak emission wavelength in subscript. After injection of the selenium precursor, the reaction was carried out for approximately 5 seconds between 270° and 275° Celsius. The colloidal solution immediately became bright yellow throughout. The flask containing the quantum dots was carefully placed into an ice-water bath to halt the reaction, and thus colloidal growth of the quantum dots. Removing the chilled solution of quantum dots from the bath, the bright yellow had changed to a darkened and golden tint. The change in color is suggested to be continued colloidal growth occurring in the center of the flask, where a temperature gradient had been formed.

The larger quantum dots, QD_{555}, were synthesized by the same procedures as QD_{520}, but were allowed to react for 60 seconds. As reaction time continued, the color of the quantum dot solution

changed from bright yellow to golden yellow to burnt-orange and finally red. The color shift from bright

yellow to red could be described as following an exponential trend with red being observed for the

longest time. No color change was observed when placing the batch solution in the ice-water bath as seen

with in the QD_{520} solution. Both QD_{520} and QD_{555} solutions are displayed under white- and UV-light

illumination in Figures 19 and 20, respectively.

Figure 19. Photos of synthesized yellow quantum dots with fluorescence emission at 520 nm

Figure 20. Photos of synthesized red quantum dots with fluorescence emission at 555 nm

Characterization of CdSe Solutions Using Fluorescence Emission Spectra

The prepared CdSe quantum dots were diluted in cyclohexane to 5% of their synthesized concentrations. The diluted quantum dot solutions were then each transferred to a quartz cuvette for fluorescence emission characterization. The emission spectra were used to provide size comparison between the CdSe dots due to the lack of transmission electron microscopy, TEM. Several providers of colloidal CdSe quantum dots have labeled sizes by emission wavelengths.

The emission spectra were to also ensure that the size dispersity of the quantum dots did not overlap. No overlap would distinguish size as a factor if results in the immobilized-quantum dot preparations had trending differences. Fluorescence characterization was also performed on a portion of quantum dot solution extracted from both melt preparations in polymethylmetharcylate, PMMA. These extracted solutions were also diluted to the same 5% as the original quantum dots prior to immobilization.

Holding the $\lambda_{ex} = 400$ nm, the emission spectra of all CdSe solutions were scanned by recording the emission intensities at 5-nm intervals between the full instrument range of 200 nm to 800 nm. Figure 21 presents an overlay spectrum of all four solutions tested. Peak intensities for the CdSe quantum dots

observed as yellow and red in visible light was at 520 nm and 555 nm, respectively. It was observed for the extracted solutions that the peak wavelengths did not shift when exposed to high temperatures and a mixed acetone-octadecene solvent. Spectral bandwidths were noted to change, however, providing insight to a change in the size dispersity. Differences between the intensities were minimally suggestive that the environment during immobilization was not harsh on the non-passivated CdSe dots.

Sizes of the quantum dots were determined by applying the respective emission wavelengths to the polynomial equation presented by Dai et al. (112). The sizes calculated were 2.6 nm and 3.2 nm for the quantum dots emitting at $\lambda=520$ nm and $\lambda=555$ nm, respectively. These calculated sizes when compared with commercially produced CdSe are very agreeable (113).
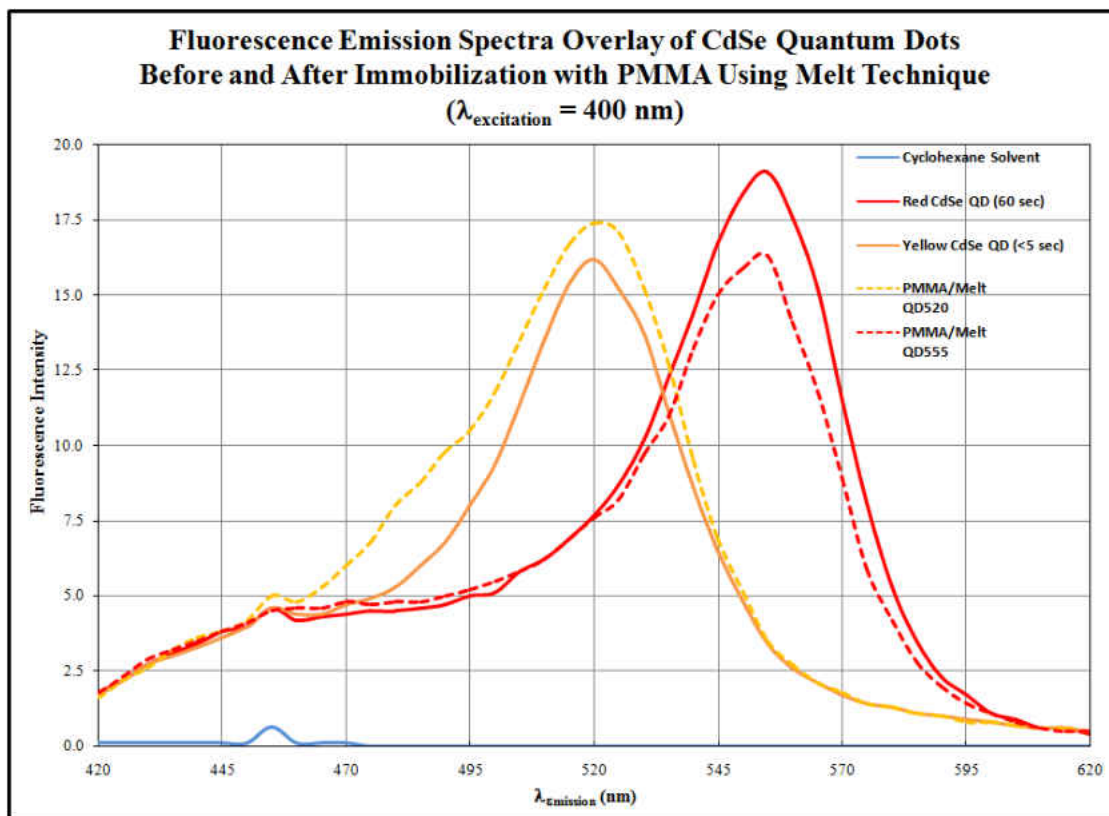
Figure 21. Fluorescence spectra of CdSe quantum dots before and after immobilization

Review of the fluorescence spectra overlay in Figure 21 presented observations that can be explained through quantum dot growth. The differences between the solid and hashed lines for the QD_{520} sample suggested additional growth during the immobilization procedure with applied heat. Confirmation can be made by the widening of the emission band, which is characteristic of increasing size dispersity of the colloidal quantum dots.

In reverse fashion, however, the QD_{555} dots exhibited a narrowing effect from the immobilization process with applied heat. Statements (12) regarding Ostwald ripening coincide with the observation in Figure 21. As the emission band narrowed, the size dispersity of the QD_{555} dots decreased through agglomeration creating larger quantum dots with smaller variation in size.

It was noticed that no significant shifts in the peak emission wavelengths were apparent. Therefore, dramatic changes in the average quantum dot size were irrelevant as a change in the band gap due to dot size would have shifted the emission. Also, stability of the quantum dots during exposure to high heat, near synthesis temperature, did not degrade. The changes in emission intensity were suspected to be due to differences in the amounts of quantum dots immobilized with the PMMA substrate creating a concentration or dilution effect of the extracted portions tested.

<u>Optimization of Imidazole Concentration for POCL-FIA Measurements</u>

Two series of solutions were prepared for determining the optimal concentration of imidazole for the POCL-flow system employed. The solutions contained serially-diluted concentrations of imidazole in acetonitrile with 20 mM TCPO. The first range of imidazole was wide covering five orders of magnitude, 1.0×10^{-6} M to 1.0×10^{-1} M. After review of the first series data, a second and narrower range was analyzed. The second range was 1.0×10^{-5} M up to 5.0×10^{-4} M.

Prior to analyzing each standard, the flow system was flushed with approximately 10 mL of the respective standard. Peak intensities plotted dependent of the imidazole concentrations were averages from triplicate injections of locally purchased 3% hydrogen peroxide. Because the initial series covered a

wide range of concentrations, the imidazole concentrations were converted to a logarithmic scale for ease in plotting. The average peak intensity for the 1.0×10^{-4} M, or -4 by log scale, was the highest intensity. Figure 22 is a depiction of the initial range of imidazole standards.
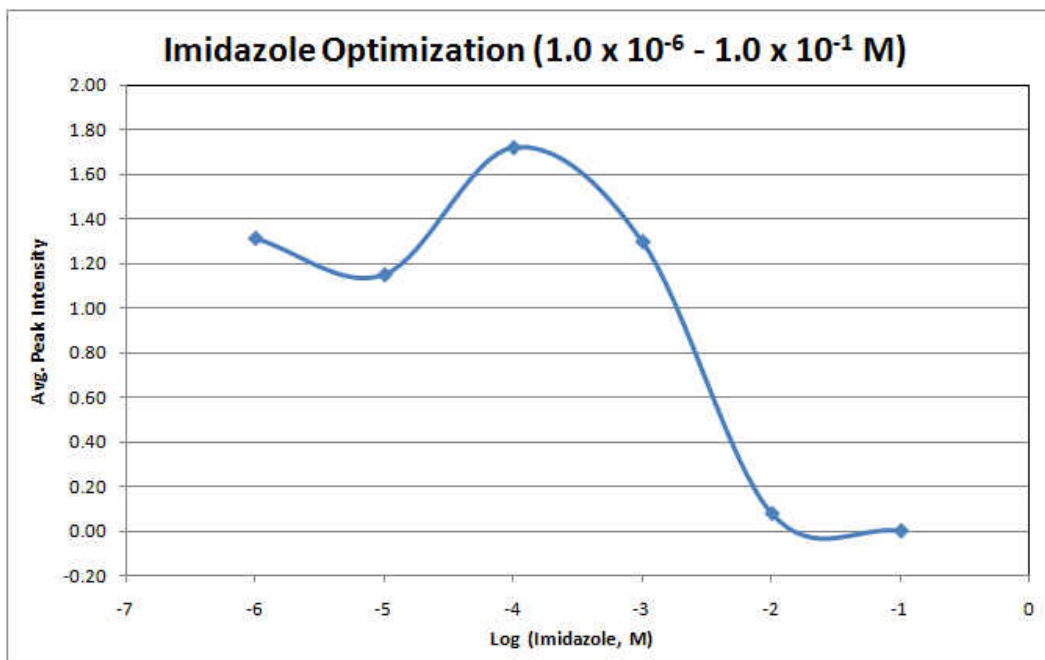
Figure 22. Determination of optimal POCL-FIA catalyst concentration with wide range of imidazole standards

The data in Figure 23 showed a concentration range to bracket for pinpointing the optimal imidazole catalyst concentration. A range from 1.0×10^{-5} M to 5.0×10^{-4} M, 10-500 µM, was analyzed in identical fashion to the wide-range standards. The results from the narrow range suggested that the optimal concentration was 50 µM. Figure 23 represents the narrow range of imidazole concentrations and respective average intensities. With a minimal difference in average peak intensities between 50 µM and 100 µM, the optimal concentration of imidazole for remaining analyses was chosen to be 100 µM to simplify the FIA reaction solution preparation. In regards to the 150 µM standard's low intensity, the FIA flow was reversed by mistakenly switching the peristaltic pump in reverse dispensing an unknown

volume from the analyzer into the standard prior to analysis. As the higher concentration standards yielded a linear decrease of intensity with increasing concentration, the 150 μM standard was ignored.
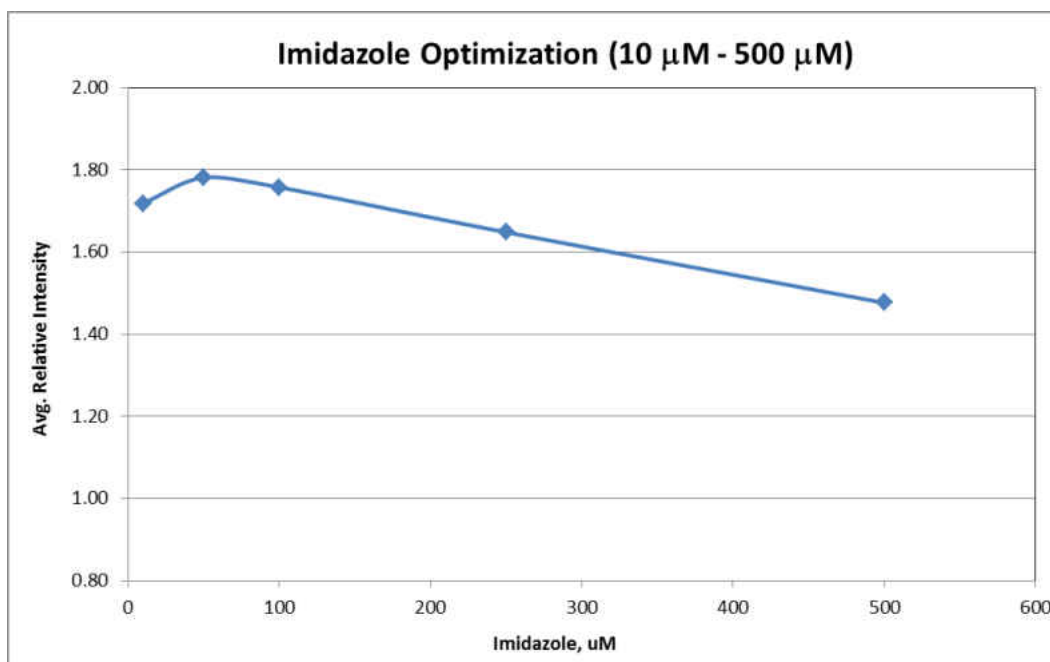
Figure 23. Determination of optimal POCL-FIA catalyst concentration with narrow range of imidazole standards

Flowrate Optimization for POCL-FIA Measurements

The preparations of immobilized CdSe quantum dots in this study were subjected to FIA. Flowrates of the FIA configuration were taken into consideration due to the affects upon the injected sample's diffusion into the reaction solvent, and thus the reaction kinetics. This is one factor of many that influence the POCL-QD emission intensity that can be easily controlled.

The flowrate was determined through performing a series of injections of locally purchased, 3%, hydrogen peroxide into the optimal reaction solvent recipe. The reaction solvent was a combination of 20 mM TCPO and 100 mM imidazole in acetonitrile. A portion of preliminary QDs immobilized with PI was used to create a POCL signal.

Beginning with the lowest pump speed, reaction solvent was introduced to flush the system prior to the first standard and between subsequent standards. The peak intensity and peak life time was recorded per each injection of hydrogen peroxide. The intensities recorded were plotted versus of the peristaltic pump's flowrate per speed setting. The data in Figure 24 presents the maximum CL intensities per flowrate. Flowrates based on the pump's speed settings were determined in preliminary experimental work. Data in Figure 25 displays the peak shape and lifetime characteristics associated with the increasing flowrates. The data in both Figures 24 and 25 were collected from the same experiment, however, the two highest flowrates were difficult of monitoring CL intensity as a function of time. The CL signal was immediate upon injection.
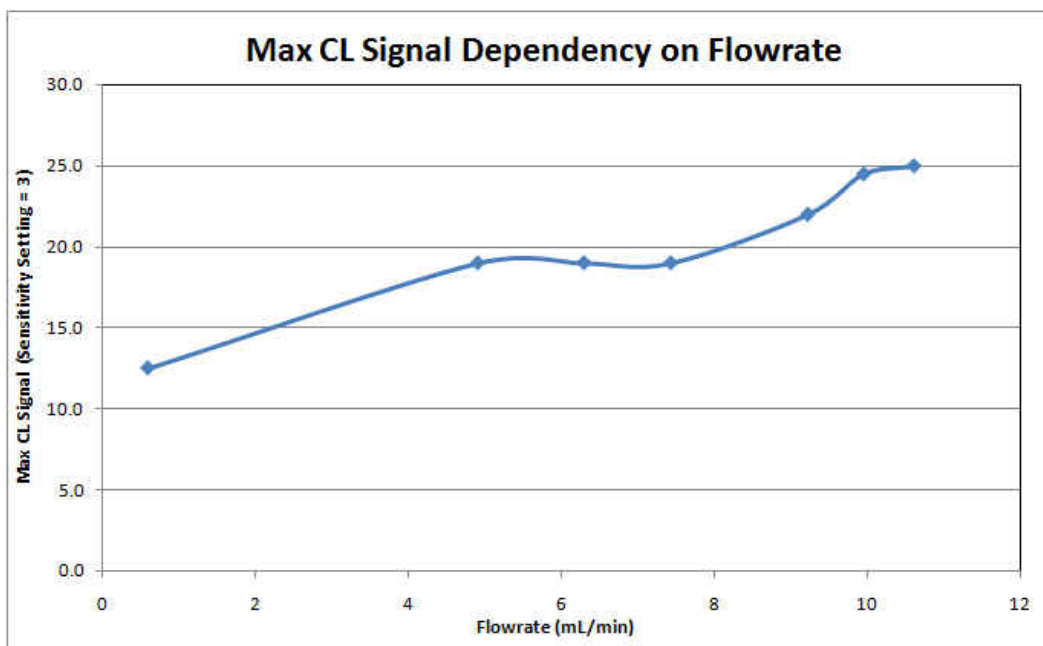
Figure 24. Determination of optimal flowrate for POCL-FIA configuration

Table 1. Preliminary experimental data relating peristaltic pump speed setting to flowrates

Flowrates per Peristaltic Pump Speed						
Pump Speed	100	200	250	300	400	450	500
Flowrate (mL/min)	0.583	4.896	6.285	7.419	9.209	9.942	10.597
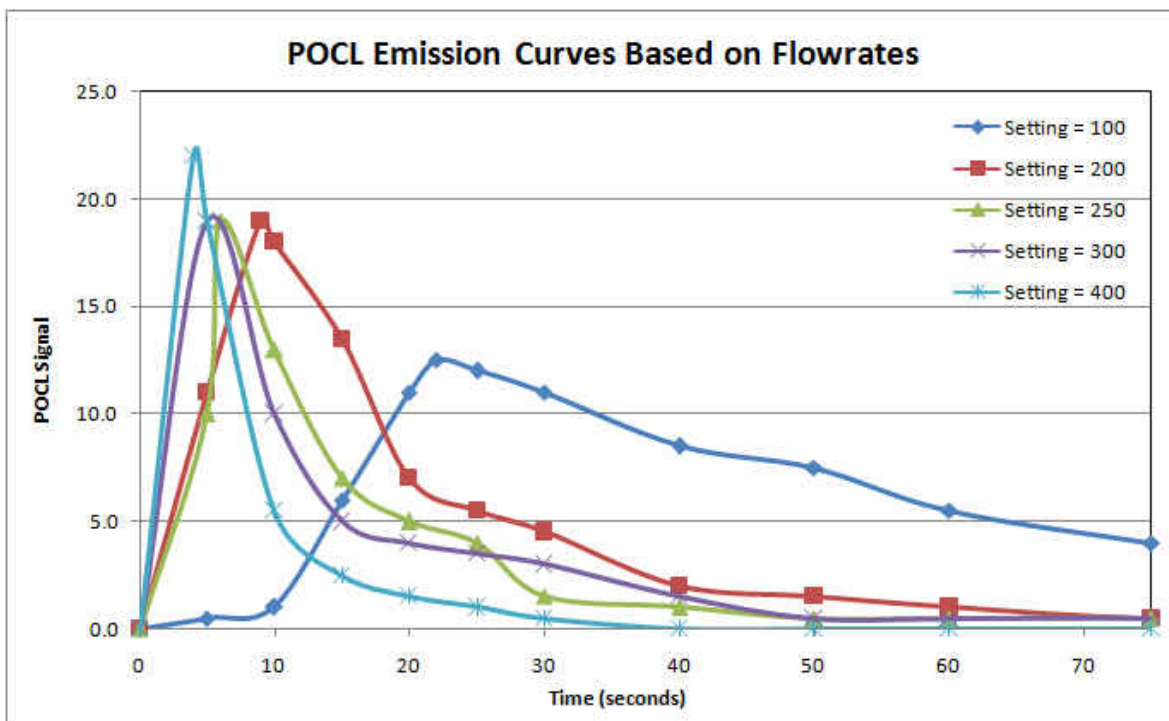
Figure 25. Shapes of POCL emission curves based on the flowrate of the FIA configuration

Based on the flowrate data and emission curve shape, the peristaltic pump speed was set at 250. The relative flowrate produced at this setting was approximately 6.3 mL/min. This moderately high flowrate was selected for two reasons. The first was its corresponding emission curve shape reaching its peak emission within 5 seconds, and returning to below 5% of the peak emission intensity. Secondly, variations in the flowrate would not drastically affect the peak emission as seen by Figure 24. If variation of the flowrate occurred by ± 1 mL/min, the peak emission would not differ by more than a few percent.

Data plotted in Figure 24 that peak intensity continued to increase with increasing flowrates. Flowrates above 6.3 mL/min were not used. As the flowrate was increased to 10 mL/min and above the tubing of the FIA configuration began to fail. Failure by tubing leaks and ruptures were observed, however, a 25% increase in peak emission intensity was noted.

Linearity of Immobilized Quantum Dot Preparations

The immobilized quantum dot preparations were evaluated for linear response to the concentration of aqueous hydrogen peroxide. Concentrations ranging from 1.0 x 10^{-4} M to 1.0 x 10^{-1} M were injected into the flowing reaction solvent of 20 mM TCPO and 100 μM imidazole. Each immobilized quantum dot preparation was inserted into the flowcell then rinsed with the reaction solvent. The rinsing was performed to remove any residual 1-octadecene solvent from the preparation that may have remained. A control of PI preparation without quantum dots was tested here with no CL signal resulting. No controls for PMMA or LDPE were tested for such, and assumed to not contribute to CL in the absence of quantum dots.

With the preparation readied in the flowcell, each individual hydrogen peroxide standard was injected in five replicates. The POCL emission of one injection was allowed to deplete prior to the following injection was introduced. Aliquots of 150 μL were injected into the Rheodyne injector's 50 μL loop to rinse and remove the TCPO reaction solvent. The final 50 μL injected remained in the loop awaiting introduction to the flow path and reaction with TCPO to produce POCL.

Resulting regression values for each immobilized quantum dot preparation were exceptionally linear. Regression values, R^2, were above 0.9750 for 10 of the 12 preparations. The two preparations failing the linearity test were both quantum dot sizes encapsulated in PMMA. Integrity of the quantum dots encapsulated was compromised by the solubility of the preparation in the acetonitrile-based reaction solvent. Upon the second injection of the lowest hydrogen peroxide standard, the emission intensity had diminished completely. This suggested that the quantum dots were leaching from the entrained polymer matrix.
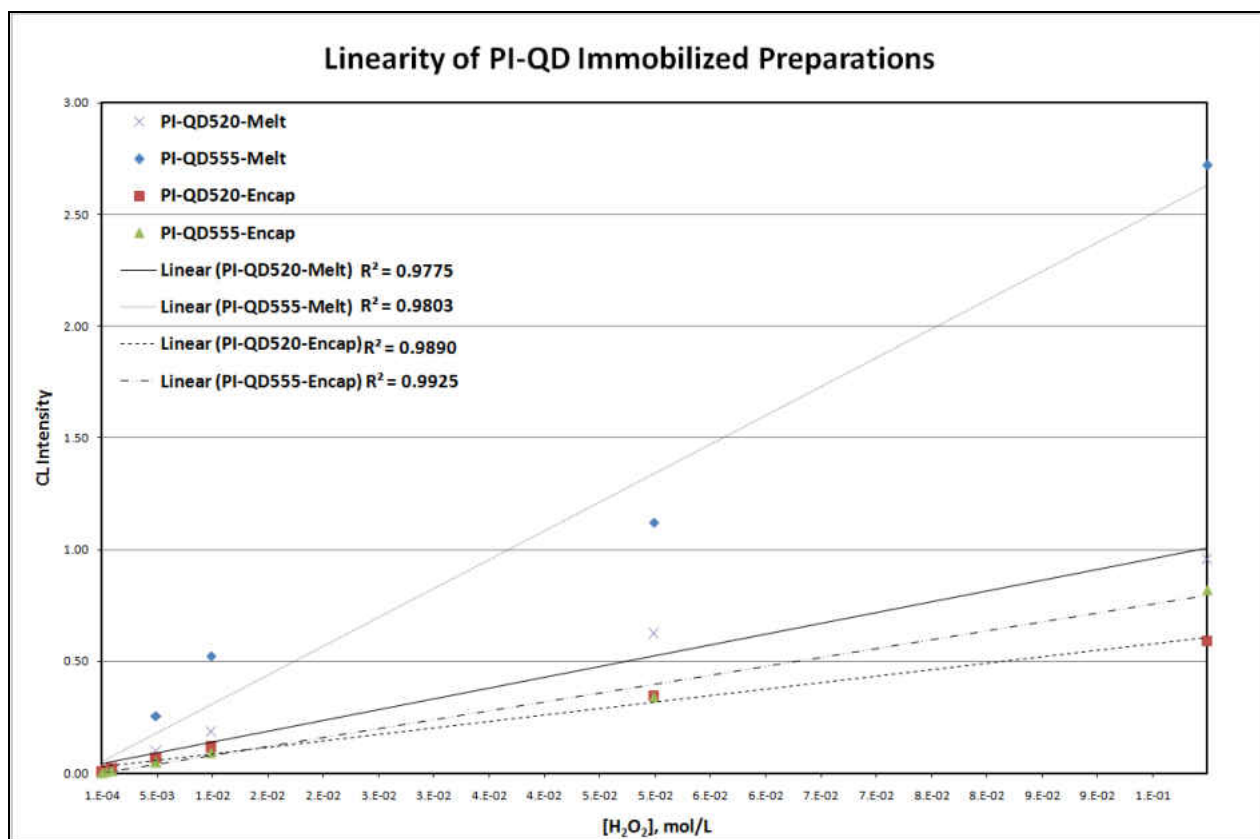
Figure 26. Linear plot of POCL emission dependent of hydrogen peroxide concentration with PI-QD

melt and encapsulated immobilizations
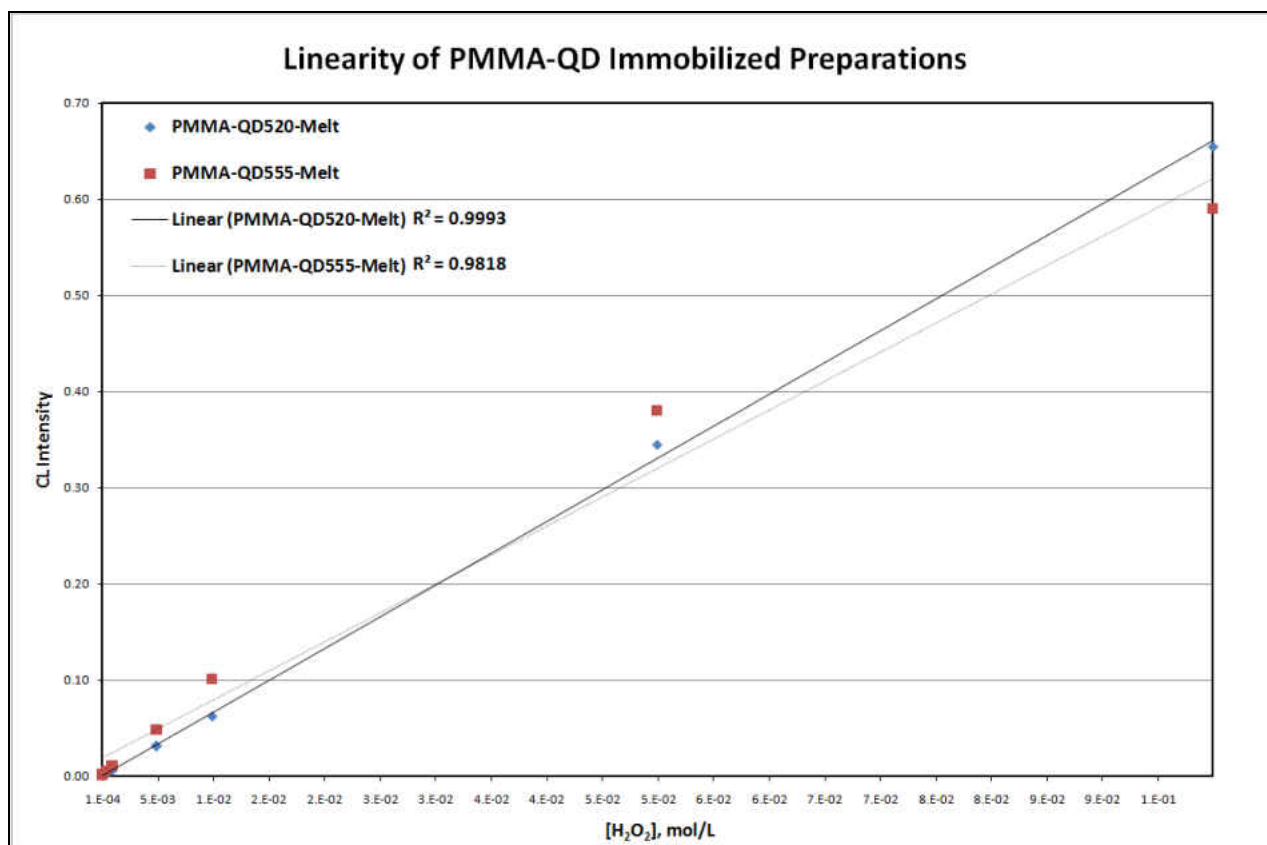
Figure 27. Linear plot of POCL emission dependent of hydrogen peroxide concentration with PMMA-QD melt and encapsulated immobilizations
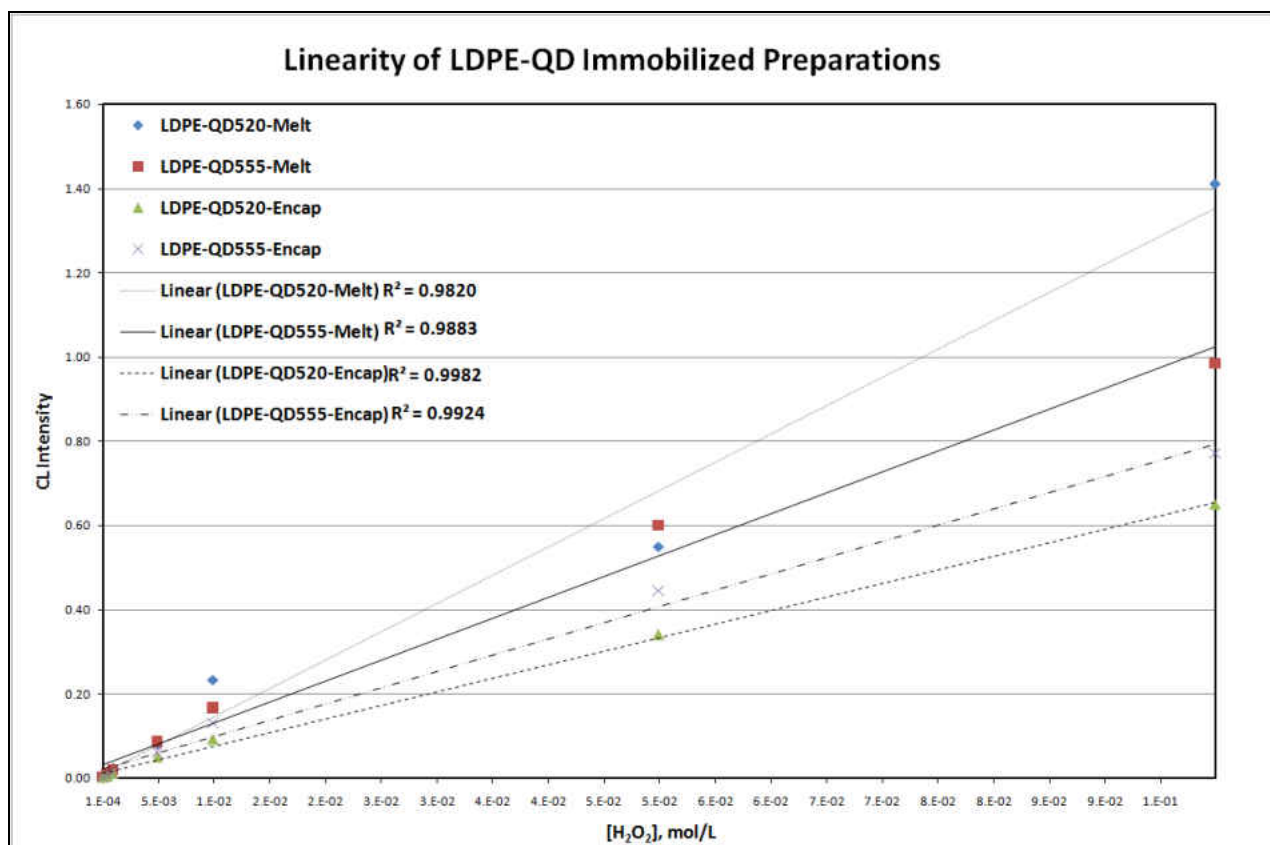
Figure 28. Linear plot of POCL emission dependent of hydrogen peroxide concentration with LDPE-QD melt and encapsulated immobilizations

The remaining 10 preparations exhibited linearity across three orders of magnitude. Improved linearity above $R^2 = 0.9900$ was observed by bracketing the concentration range between 5.0×10^{-4} M to 5.0×10^{-2} M. This concentration range of aqueous hydrogen peroxide relates to 17 ppm to 1700 ppm. This is a decent range for trace measurements, however, increased sensitivity has been observed for other POCL applications (47, 65, 96, 100). The PI-QD520-E and LDPE-QD520-M immobilized preparations, however, decreased in linear response when bracketing the concentration to $R^2 = 0.9194$ and $R^2 = 0.9506$, respectively. This decrease in linearity displayed the effect of the 1.0×10^{-1} M standard influencing the linearity of the trendline. Table 2 presents a summarized layout of the linear regression values to their respective hydrogen peroxide concentration ranges and immobilized quantum dot preparations.

The regression values remaining above $R^2 = 0.9000$ as increasing concentrations of hydrogen peroxide are injected were promising. This suggested two points of interest; one being that hydrogen peroxide did not attack the polymer substrates leaching quantum dots. The second point was that numerous consecutive injections could be made on a single preparation. Additional data on the second point were produced by determining the robustness of each preparation, which is discussed later.

Table 2. Summarized comparison of linear regression values for immobilized quantum dot preparations

Summary of Linear Regression Values for Immobilized-QD Preparations		
Immobilized-QD Preparation	10^{-4} M - 10^{-1} M	5×10^{-4} M - 5×10^{-2} M
PI-QD520-M	0.9775	0.9913
PI-QD555-M	0.9803	0.9832
PI-QD520-E	0.9890	0.9194
PI-QD555-E	0.9925	0.9961
PMMA-QD520-M	0.9993	0.9997
PMMA-QD555-M	0.9818	0.9960
LDPE-QD520-M	0.9820	0.9506
LDPE-QD555-M	0.9883	0.9943
LDPE-QD520-E	0.9982	0.9948
LDPE-QD555-E	0.9924	0.9917

In regards to the sensitivity, the detection limit was determined to be between the lowest standards of hydrogen peroxide, 1.0×10^{-4} M and 5.0×10^{-4} M. Standards down to 1.0×10^{-8} M, 0.34 ppb, were also prepared by serially diluting the 1.0×10^{-4} M standard. Injections of these ultra-trace standards did not produce any observable emission as read by the analog output of the FIA instrument. A response was not observed until the 1.0×10^{-4} M, 3.4 ppm, standard was injected. For all acceptable preparations the response of the 3.4 ppm standard provided an emission signal value of three or lower. In the case of the FIA instrument configuration used for the experimental studies, the noise was considered to be less than three on the most sensitive setting. This provided a signal-to-noise ratio of 3/N, and thus a LOD for all preparations at approximately 5 ppm to15 ppm.

Robustness of Immobilized Quantum Dot Preparations

An important analytical characteristic of immobilized reagents in a flow system is the number of sample injections it can withstand. This is the definition as to how robust the immobilized reagent is in its respective configuration. Design and results of the linear range evaluations provided insight that consecutive injections of the analyte, aqueous hydrogen peroxide, could be made with slight change in emission intensity.

The robustness of each immobilized quantum dot preparation was measured as a decrease of the intensity over 20 injections. Twenty was chosen as it is one-fifth of 100, allowing an easily extrapolated value to be calculated. Hydrogen peroxide, 1.0×10^{-2} M, was injected producing a signal centered in the sensitivity range selected. After 20 injections were made, the first three and final three injections were averaged separately. This was done to reduce any injection-to-injection variability. The difference between the two averages was calculated. Dividing the difference by the larger average yielded the percentage drop in emission intensity. The immobilized quantum dot preparations along with their experimental and extrapolated percentage drops are presented in Table 3.

Table 3. Summary of the robustness values of the immobilized quantum dot preparations

Summary of the Robustness of Immobilized QD Preparations by Percentage of POCL Emission Decrease		
Immobilized-QD Preparation	After 20 Injections	Extrapolated to 100 Injections
PI-QD520-M	7.30	36.52
PI-QD555-M	6.37	31.87
PI-QD520-E	15.84	79.18
PI-QD555-E	4.50	22.52
PMMA-QD520-M	7.88	39.41
PMMA-QD555-M	16.15	80.76
LDPE-QD520-M	0.00	0.00
LDPE-QD555-M	11.90	59.52
LDPE-QD520-E	12.40	61.98
LDPE-QD555-E	14.02	70.09

The extrapolated injection values suggested that with a linear assumption over 100 consecutive injections can be made on a single portion of the preparation. Unfortunately, no significant correlation could be made between the intensity loss and quantum dot size or polymer substrate. It was observed that the smaller quantum dots in melted preparations for each polymer substrate exhibited better robustness than others. If size of the quantum dot was a factor, the larger QD_{555} dots would be better retained and not as easily leached as the smaller QD_{520} dots.

The non-correlated values could simply be variation of the orientation of the portions of immobilized quantum dot preparations in the flowcell. The flowcell's primary consideration for construction was to be reusable through the course of the study. The design proved well in that consideration; however, holding the portion in a fixed position relative to the photomultiplier tube window was not accurately controlled. The portion if disturbed by the flow of reaction solvent could be twisted or tilted from its original orientation during the experiment. The flowcell's compartment was small enough to make this a negligible factor for this study. In more strenuous studies, location of the portion with respect to the detector would need to be fixed.

<u>Stability of Immobilized Quantum Dot Preparations</u>

Oxidation is an inevitable effect of the surrounding atmosphere. Unpassivated quantum dots are known to undergo optical changes when oxidized (30,35). The quantum dots prepared for this study were not passivated prior to immobilization. Thus for acceptable application to FIA and other analyses, the immobilized quantum dots need to be stable over a period of time. Stable immobilized quantum dots would involve less materials and time preparing for analyses.

The immobilized CdSe quantum dots were subjected to a 30-day stability study. Once every 10 days, fresh portions of each immobilized preparation were placed in the FIA instrument for POCL intensity measurements. Day zero intensity measurements were taken within hours of preparing all immobilized quantum dot preparations. The plots in Figures 29-31 show an offset from zero that

accounts for the time between preparation and analysis. Each intensity measurement used to plot the stability over time was an average from five replicate injections. Aqueous hydrogen peroxide at 1.0×10^{-2} M, 340 ppm, was used as the standard.

Figures 29-31 show the time plots of the stability for the quantum dots immobilized in PI, PMMA, and LDPE, respectively. The average POCL intensities increased by 35% to 417% of the Day 0 intensity averages by Day 10. The overall intensity increase was suggestive of residual quantum dot solvent, 1-octadecene, present during Day 0. Quantum dots remaining in the residual solvent were possibly rinsed from the preparations in the FIA instrument. Following 10 days of sitting in a storage vial, presence of residual solvent was non-existent. This observation alluded to the intensity increasing as a result of the dried residual solvent. The CdSe quantum dots remaining in the solvent were considered to be adsorbed on the polymer surface. Further evidence of the adsorption to the polymer surface is the similar intensities following on days 20 and 30.

In respect to the stability exclusively, the immobilized quantum dots were very stable for a one-month period. This proved that quantum dots could be immobilized with any of the three selected polymers and be used for multi-day analyses. This decreased the need to immobilize the quantum dots prior to every experiment. Stability of the quantum dots was not compromised either. Though fluorescence measurements were not performed on the preparations individually for changes in wavelengths; ultraviolet light illuminations did not show any dramatic color shift. No color changes were indicative of alterations in the surface chemistry of the CdSe quantum dots.

The preparation PI-QD555-M showed a decrease in POCL intensity rather than increase. The decrease was suspected to be related to the portioning of the preparation used on Day 0. It was noticed that the quantum dots were not uniformly mixed into the polymer matrix of the melted preparations. Use of ultraviolet light proved that concentrated areas of quantum dots existed. No change was observed for

LDPE-QD520-M. Because this preparation was made by the polymer melting technique, the residual

quantum dot solvent must have been completely dried before any POCL-FIA measurements.

Table 4. Summary of average POCL intensity changes during one-month stability study

Average POCL Intensity Change During One Month Time Stability Study						
Immobilzied QD Preparation	Day 0 Avg Intensity	Day 10 Avg Intensity	Day 30 Avg Intensity	(Day 10 - Day 0)	(Day 30 - Day 0)	(Day 10 - Day 0)%	(Day 30 - Day 0)%
PI-QD520-M	0.19	0.33	0.26	0.14	0.07	74	37
PI-QD555-M	0.52	0.27	0.26	-0.25	-0.26	-48	-50
PI-QD520-E	0.12	0.24	0.21	0.12	0.09	100	75
PI-QD555-E	0.09	0.24	0.21	0.15	0.12	167	133
PMMA-QD520-M	0.06	0.31	0.23	0.25	0.17	417	283
PMMA-QD555-M	0.10	0.24	0.24	0.14	0.14	140	140
LDPE-QD520-M	0.23	0.23	0.26	0.00	0.03	0	13
LDPE-QD555-M	0.17	0.23	0.24	0.06	0.07	35	41
LDPE-QD520-E	0.09	0.26	0.23	0.17	0.14	189	156
LDPE-QD555-E	0.13	0.23	0.24	0.10	0.11	77	85
Overall Average						115	91
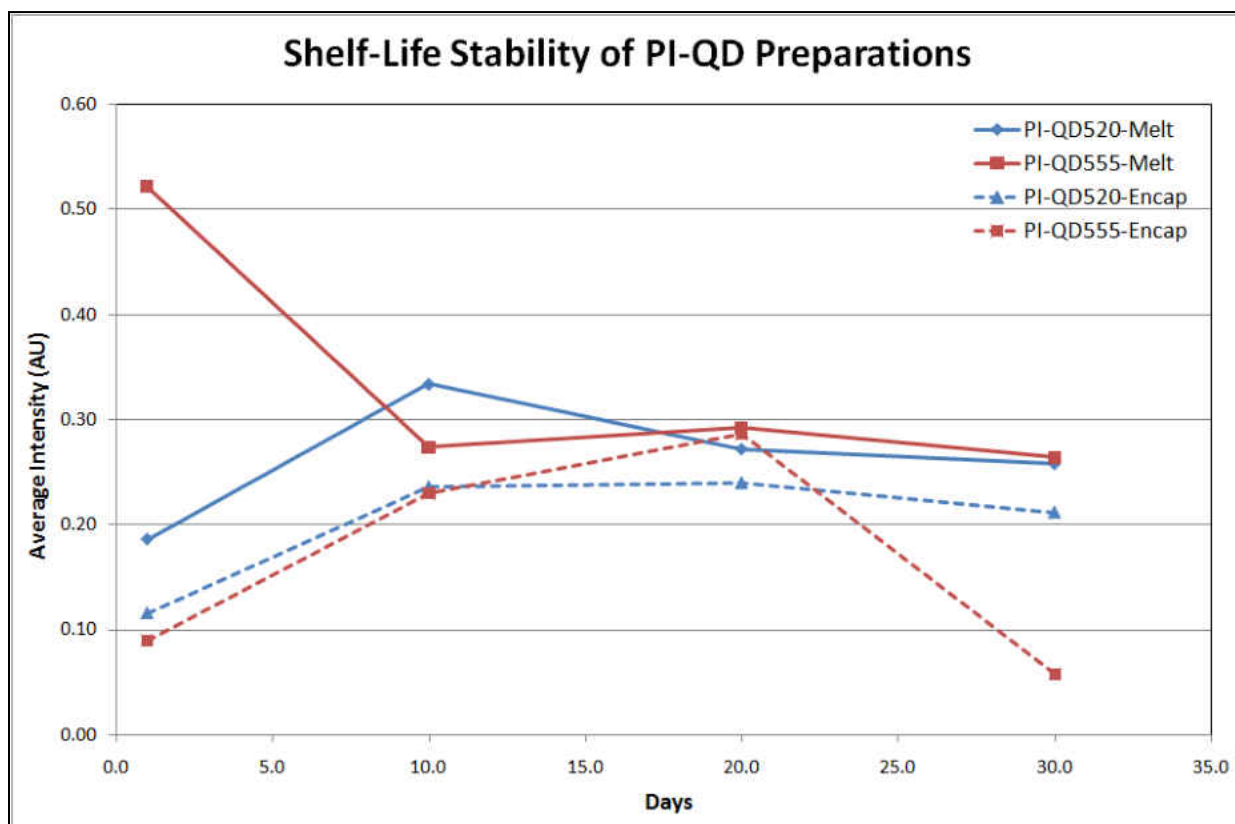
Figure 29. Stability of PI-QD preparations during one-month period based on POCL intensity
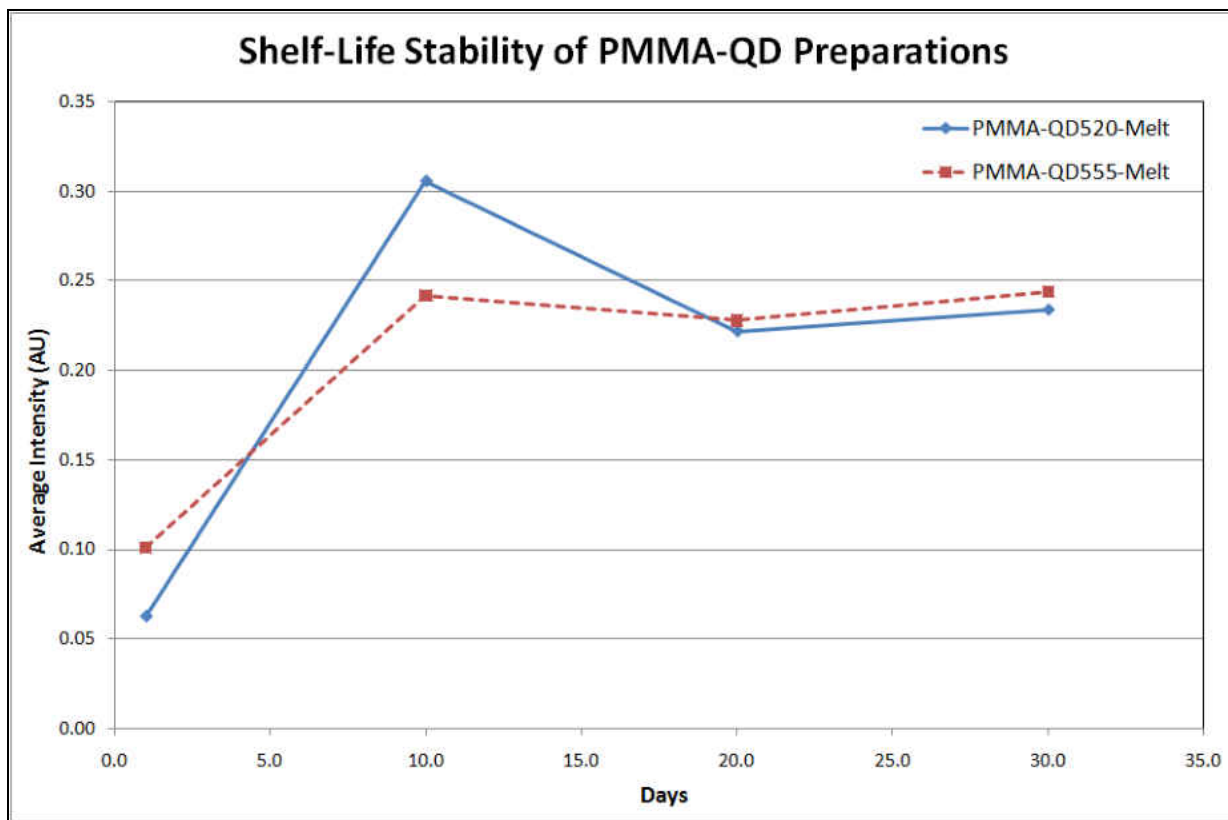
Figure 30. Stability of PMMA-QD preparations during one-month period based on POCL intensity
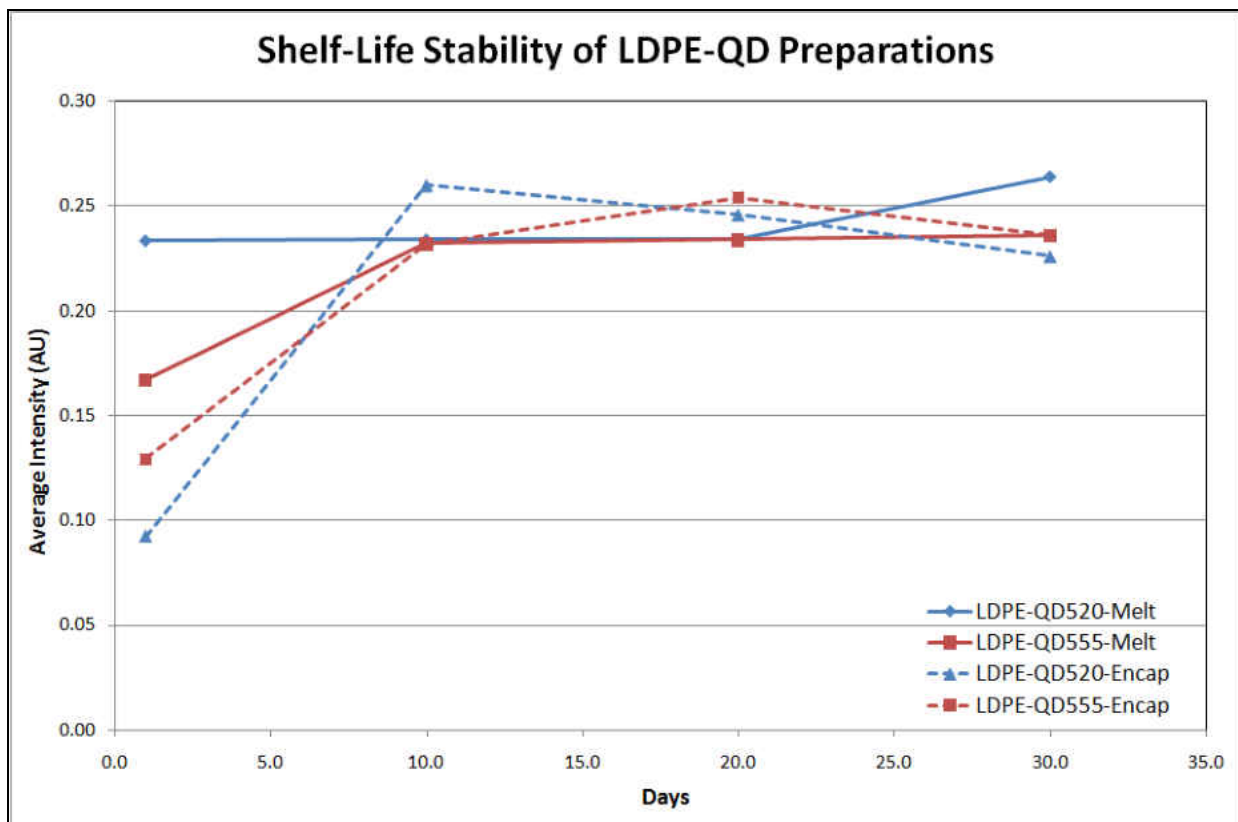
Figure 31. Stability of LDPE-QD preparations during one-month period based on POCL intensity

<u>Variability of Immobilized Quantum Dot Preparations</u>

Analytical methods or techniques that are fit-for-use must have low variability in analyte response. For trace analyses variability must be minimal. If a sample was to normally exhibit 5 ± 6 ppm with upper and lower specification limits of 0 ppm and 10 ppm, the sample would fail to meet acceptable specifications. This creates confusion in the true result, and the method is unacceptable for use.

The study performed evaluated the variability in each immobilized quantum dot preparation. Three replicate preparations were made for each polymer, quantum dot size, and immobilization technique combination. The variability was tested within a single replicate, and also across the three replicates. Five replicate injections of 1.0×10^{-2} M, 340 ppm, aqueous hydrogen peroxide were made into the FIA instrument containing a portion of each immobilized quantum dot preparation. The resulting

POCL signals were recorded and statistical analysis on them followed. The variability data were summarized into Tables 5 and 6.

Table 5. Variability of Immobilized Quantum Dot Preparations within Single Batch Preparation

Variability of Immobilized Quantum Dot Preparations Within Single Batch Prepared									
Immobilized QD Preparation	Portion # of Single Batch	Injection 1	Injection 2	Injection 3	Injection 4	Injection 5	Avg	SD	%RSD
PI-QD520-M	1	11	13	15	14	14	13	1.5	11.3
	2	11	15	16	16	15	15	2.1	14.2
	3	14	17	16	16	15	16	1.1	7.3
	Combined						15	1.8	12.2
PMMA-QD520-M	1	11	12	12	11	12	12	0.5	4.7
	2	10	11	11	11	11	11	0.4	4.1
	3	10	11	11	10	11	11	0.5	5.2
	Combined						11	0.7	6.0
LDPE-QD520-M	1	23	22	22	21	22	22	0.7	3.2
	2	16	14	15	15	15	15	0.7	4.7
	3	12	12	13	12	11	12	0.7	5.9
	Combined						16	4.4	26.9
LDPE-QD520-E	1	12	14	13	14	14	13	0.9	6.7
	2	9	10	11	11	11	10	0.9	8.6
	3	11	12	12	13	12	12	0.7	5.9
	Combined						12	1.5	12.5

Table 6. Variability of Immobilized Quantum Dot Preparations across Multiple Batch Preparations

| Variability of Immobilized Quantum Dot Preparations Across Multiple Batches Prepared | | | | | | | | | |
Immobilized QD Preparation	Batch #	Injection 1	Injection 2	Injection 3	Injection 4	Injection 5	Avg	SD	%RSD
PI-QD520-M	1	10	13	13	13	13	12	1.3	10.8
	2	9	13	13	13	12	12	1.7	14.4
	3	11	13	15	14	14	13	1.5	11.3
	Combined						13	1.5	12.3
PMMA-QD520-M	1	11	12	12	11	12	12	0.5	4.7
	2	10	12	13	13	12	12	1.2	10.2
	3	11	12	13	13	13	12	0.9	7.2
	Combined						12	0.9	7.7
LDPE-QD520-M	1	23	22	22	21	22	22	0.7	3.2
	2	17	15	15	15	15	15	0.9	5.8
	3	18	17	16	14	14	16	1.8	11.3
	Combined						18	3.3	18.8
LDPE-QD520-E	1	12	14	13	14	14	13	0.9	6.7
	2	9	10	10	10	10	10	0.4	4.6
	3	9	10	11	10	11	10	0.8	8.2
	Combined						11	1.8	16.2

Only four immobilized quantum dot preparations were tested. Stock TCPO solids used for preparing the FIA reaction solvent was in diminishing supply. Another batch of TCPO was synthesized; however, the FIA instrument injector began developing plugging issues from its use. This plugging required many injector rebuilds and cleanings. Observations during the repetitive troubleshooting revealed white crystalline material that was insoluble in the FIA reaction solvent acetonitrile. The crystals though were soluble in distilled water used to rinse the injector parts. Crystalline matter was also found in the flask containing the reaction solvent. Literature (81) states similar observations leading to the insolubility of the 1,1-oxalylimidazole intermediate in acetonitrile. Because imidazole was added to the TCPO in acetonitrile, this was suspected to cause the injector plugging.

The four immobilized preparations tested all contained the QD_{520} size quantum dots. Design in polymer selection and immobilization technique was such that comparison could be made. Review of Table 5 shows that variability within the portions of single batches was acceptable. The variability was

3.2% RSD to 8.6% RSD for all portions except those associated with PI-QD520-M. Combined statistics of each single batch preparation showed that variability ranged from 6.2% RSD to 26.9% RSD. This suggested that concentrated areas of immobilized quantum dots existed in the polymer matrices. The difference between portions of the LDPE-QD520-M preparation supported the previous statement. Low variability of the PMMA-QD520-M preparation was considered a result of the immobilization technique. Because the acetone co-solvent was required to mediate the quantum dots to the polymer; the polymer likely soaked in the quantum dots evenly as their solvent evaporated.

Variability was also tested across multiple batches of immobilized quantum dot preparations. The results displayed in Table 6 show similar character and response as with the single batch variabilities. Portions individually from multiple batches yielded 3.2% RSD to 11.3% RSD that are acceptable for analytical procedures. The overall variabilities ranged from 7.7% RSD to 26.9% RSD. The PI-QD520-M preparation exhibited this highest individual batch variability between 10.8% RSD and 14.4% RSD. This preparation was made by melting chips of PI, which took longer to liquefy and mix into solution with the quantum dot solvent. As for the LDPE-QD520-M preparation, the large % RSD value of 18.8% was another suggestive set of data related to concentrated areas of quantum dot population.

Comparisons of the polymers selected for immobilizing the CdSe quantum dots did show a difference between PI and the other two polymers. No significant difference in variability was observed between PMMA and LDPE when looking at individual portions. As mentioned previously the melt technique to immobilize quantum dots with PI required melting chips of the polymer. The polymers PMMA and LDPE were in powder and flake forms that made liquification easier than seen with the PI chips. Better mixing with the respective quantum dot solvents provided better color uniformity in the PMMA and LDPE preparations. This was not the case observed when mixing melted PI chips. Minor swirling was observed if the PI chips were not completely melted.

Immobilization technique comparison did not show any significant difference. These data are evidence that the melt preparation is equally acceptable as the encapsulated preparations. The comparable variabilities mean that less labor and materials are required to immobilize CdSe quantum dots in LDPE. Ignoring the data from the first batch of LDPE-QD520-M due to a concentration of quantum dots; reduces the variability to approximately 13% RSD. This corrected combined variability was then comparable to the encapsulated preparation of immobilized quantum dots.

Recovery of Hydrogen Peroxide in Non-Aqueous Solvents

Most applications of POCL coupled with FIA lie in the aqueous realm for immunoassays due to biological compatibility. The POCL-FIA configuration in this study was tested for application with non-aqueous solvents. The solvents of choice were isopropanol and glacial acetic acid. These are common organic solvents with multiple uses.

The FIA instrument was first calibrated using aqueous standards of hydrogen peroxide ranging from 1.0×10^{-4} M to 1.0×10^{-1} M, 3.4 – 3400 ppm. Following the calibration standards of 17 ppm and 1700 ppm hydrogen peroxide were prepared in each non-aqueous solvent. Each non-aqueous standard was injected in five replicates. The resulting POCL signals were recorded and compared against the aqueous calibration curve. Signals by both non-aqueous solvent systems provided intriguing observations.

Standards of hydrogen peroxide in glacial acetic acid did not produce any POCL signals. Both concentrations of hydrogen peroxide had no observable POCL emission. The sensitivity of the instrument was increased, however, emission remained undetectable. Standards in isopropanol on the other hand produced POCL signals above the selected sensitivity ranges. Blank isopropanol injections were recorded to produce POCL signals equivalent to the aqueous 5.0×10^{-4} M hydrogen peroxide standard. It was determined that non-aqueous POCL reactions cannot be compared to an aqueous calibration curve for recovery studies.

Consideration of the chemistry behind the POCL reaction proposed that glacial acetic acid may inhibit the cyclization of the peroxyoxalate following the release of imidazole from 1,1-oxalylimidazole. Sterics and electron repulsion by the acid's carbonyls could be the inhibiting factors. Isopropanol, however, undergoing nucleophillic attack on the peroxyoxalate does not create a steric effect. The cyclization of the peroxyoxalate compound is essential to create the proposed high-energy intermediate, 1,2-dioxetanedione. A final mention regarding the isopropanol solvent is that the observation of its intense signal compared to those of aqueous injections may provide means of increasing the POCL-FIA system's sensitivity to reach sub-ppm detection limits.

CHAPTER 5

CONCLUSIONS

Synthesis of batch quantities of CdSe quantum dots yielded two moderately disperse sizes of quantum dots. The colors of the quantum dots were an indicator to the size differences. Fluorescence spectra for both batches isolated emission peaks at wavelengths of 520 nm and 555 nm. Their immobilization with polymers such as polyisoprene, polymethylmethacrylate, and low-density polyethylene proved promising for application to peroxyoxalate chemiluminescence coupled with flow injection analysis. Comparisons between the immobilization techniques of melting and encapsulating exhibited minimal differences. This suggested that the quicker and less expensive route of melting the polymer was as reliable as the encapsulated quantum dots.

During the immobilization of quantum dots in polymethylmethacrylate, excess quantum dot solvent were available for extraction. The quantum dots when diluted in cyclohexane retained fluorescence at the wavelengths, 520 nm and 555 nm. Changes in the size dispersity were evident by the spectra. It was observed that quantum dot growth could be halted then restarted, while Ostwald ripening was occurring during the melt immobilization process.

Preparations of the immobilized quantum dots showed exceptional linear response to concentrations of aqueous hydrogen peroxide standards. Linear regressions over three orders of magnitude were 0.9775 and above. The range of concentrations was 1.0×10^{-4} M to 1.0×10^{-1} M, or 3.4 ppm to 3400 ppm. A few immobilized preparations had $R^2 > 0.9900$, such as PI-QD555-E, PMMA-QD520-M, and LDPE-QD520-E.

Consecutive injections on each immobilized quantum dot preparation revealed that they were robust through 20 injections. Based on POCL intensity decreases, an efficiency decrease up to 16.2% was calculated. The loss in efficiency was assumed to be the leaching of CdSe quantum dots from the

polymer substrate into the reaction solvent. By also assuming that efficiency loss was a linear function, 100 consecutive injections of aqueous hydrogen peroxide are possible. The degrading efficiency over injections, however, would require controls to be randomly injected for intensity correction. A promising observation for application was with the LDPE-QD520-M showing no efficiency loss over the 20 consecutive injections made.

Stability also provided promising results. Ten days after preparing the immobilized quantum dots, the stability for most preparations increased between 35% and 417% from their initial intensities. These increased intensities were consistent through the remaining 20 days of testing. The PMMA-QD520-M preparation displayed the 417% increase. This was suspected to be a result of residual quantum dot solvent on the surface of the polymethylmethacrylate substrate drying over time. Quantum dots under this circumstance would be expected to adsorb to the polymer surface and possibly form a thin film to protect them.

The variability in the preparations was acceptable for analytical application. Several preparations had less than 10% RSD. Within a single batch and across multiple batches of immobilized quantum dots, PMMA-QD520-M showed the least variability at 6.0% RSD and 7.2% RSD, respectively. The largest variability was seen in the LDPE-QD520-E preparation. Single, 19% RSD, and multiple, 27% RSD, batches provide insight that the quantum dots were concentrating in areas of the polymer substrate. This non-uniformity sets the stage for experiencing variability when portioning for testing. Improved mixing of the quantum dot solvents with the polymers should negate the high variability.

Determination of hydrogen peroxide in non-aqueous solvents such as isopropanol and glacial acetic using immobilized CdSe quantum dots was not a direct application. The chemistries involved between each solvent with the POCL system showed that glacial acetic actually quenches the POCL reaction as no emission was detected. Moderate concentrations of hydrogen peroxide and the most sensitive setting was still absent of a POCL signal. Isopropanol acted in opposite fashion of glacial acetic

acid. Emission intensities from standards in isopropanol had higher maximum values. The lifetime of the emission curve was much shorter also. The observation of isopropanol to the POCL system suggested that sub-ppm detection may be possible.

The integrities evaluated for the immobilized CdSe quantum dots showed that techniques used created materials suitable for analytical applications in POCL-FIA. Particular preparations of PMMA-QD520-M and LDPE-QD520-E performed the best. Ignoring the portion of LDPE-QD520-E that skewed the variability results, the preparation was deemed fit-for-use. Several opportunities, however, were identified for improvement. Addition of a semiconductor layer to the CdSe quantum dots would increase the photoluminescence efficiency and intensity. Also, improved mixing control while heating the polymers should reduce the variability due areas concentrating with quantum dots. Finally, the crude and laboratory-built FIA instrument had several improvement factors such as tubing length, rigidity of the configuration, and more sensitive electronics.

REFERENCES

1.)   Walters, Keith A.; Bullen, Heather A. Development of a Nanomaterials One-Week

       Intersession Course. *J. Chem. Edu.*. **2008**, *85* (10), 1406-09.

2.)   Klablunde, Kenneth J., ed. *Nanoscale Materials in Chemistry*. Wiley Interscience, New

       York, 2001.

3.)   Storrs Hall, J. *Nanofuture: What's Next for Nanotechnology*. Prometheus Books, Amherst,

       2005.

4.)   Rao, C.N.R., ed. *Nanomaterials Chemistry*. Wiley-VCH, Weinheim, 2007.

5.)   Pagliaro, Mario. *Nano-Age: How Nanotechnology Changes Our Future*. Wiley-VCH,

       Weinheim, 2010.

6.)   Nagarajan, R.; Hatton, Alan T. Nanoparticles: Synthesis, Stabilization, Passivation, and

       Functionalization. *ACS Symposium Series*. **2008**, *996*, 2-14.

7.)   Wiesner, Mark R.; Bottero, Jean-Yves. *Environmental Nanotechnology: Applications and

       Impacts of Nanomaterials*. McGraw-Hill, New York, 2007.

8.)   Sellers, Kathleen, et al. *Nanotechnology and the Environment*. New York: CRC Press,

       2009.

9.)   Kirchner, Christian; et al. Cytotoxicity of Colloidal CdSe and CdSe/ZnS Nanoparticles.

       Nano Letters, **2005**, *5* (2), 331-38.

10.)   Mahendra, Shaily; et al. Quantum Dot Weathering Results in Microbial Toxicity. *Environ.

       Sci. Technol.*, **2008**, *42*, 9424-9430.

11.)   Anderson, Robin E.; Chan, Warren C. W. "Systematic Investigation of Preparing

       Biocompatible, Single, and Small ZnS-Capped CdSe Quantum Dots with Amphiphilic

       Polymers." *ACS Nano*. **2008**, *2*, 1341-52.

12.)   Rogach, Andrey L., ed. *Semiconductor Nanocrystal Quantum Dots: Synthesis, Assembly,

       Spectroscopy and Applications*. Springer-Verlag/Wien, Austria, 2008.

13.) Boatman, Elizabeth M.; Lisensky, George C.; Nordell, Karen, J.. A Safer, Easier, Faster Synthesis for CdSe Quantum Dot Nanocrystals. *J. Chem. Edu.*. **2005**, *82* (11), 1697-1699.

14.) Shukla, Nisha; Nigra, Michael M. Synthesis of CdSe quantum dots with luminescence in the violet region of the solar spectrum. *Luminescence*. **2010**, *25*, 14-18.

15.) Pradhan, Narayan, et al. "Colloidal CdSe Quantum Wires by Oriented Attachment." *Nano Letters*. **2006**, *6*, 720-724.

16.) Bard, Allen J.; Faulkner, Larry R. *Electrochemical Methods: Fundamental s and Applications*. 2nd ed. John Wiley and Sons, Hoboken, New Jersey, 2001.

17.) Houston, Paul L. *Chemical Kinetics and Reaction Dynamics*. Dover Publications, Incorporated, Mineola, New York, 2001.

18.) Rayner-Canham, Geoff; Overton, Tina. *Descriptive Inorganic Chemistry*. 3rd ed W.H. Freeman and Company, New York, 2003.

19.) Miessler, Gary L.; Tarr, Donald, A. *Inorganic Chemistry*. 3rd ed. Pearson Prentice Hall, New Jersey, 2004.

20.) Semiconductor Band Gaps. http://hyperphysics.phy-astr.gsu.edu/hbase/tables/semgap.html. Accessed August 2012.

21.) Li, Liang-shi; Hu, Jiangtao. Band Gap Variation of Size- and Shape-Controlled Colloidal CdSe Quantum Rods. *Nano Letters*. **2001**, *1* (7), 349-351.

22.) Liu, Liping; Peng, Qing; Li, Yadong. Preparation of CdSe Quantum Dots with Full Color Emission Based on a Room Temperature Injection Technique. *Inorg. Chem.* **2008**, *47*, 5022-5028.

23.) Palaniappan, Kumaranand; et al. Water-Soluble, Cyclodextrin-Modified CdSe-CdS Core-Shell Structured Quantum Dots. *Chem. Mater.* **2006**, *18*, 1275-1280.

24.) Pellergino, Teresa; et al.. Hydrophobic Nanocrystals Coated with an Amphiphilic Polymer Shell: A General Route to Water Soluble Nanocrystals. *Nano Letters*. **2004**, *4* (4), 703-707.

25.) Choi, Hyun-Ju,; Yang, Jun-Kyu; Park, Hyung-Ho. Effect of surface capping molecules on the electronic structure of CdSe nanocrystal film. *Thin Solid Films*. **2006**, *494*, 207-210.

26.) Luo, Xiangdong. Photoluminescence Blue-Shift of CdSe Nanoparticels Caused by Exchange of Surface Capping Layer. *J. Phys. Chem. C*. **2011**, *115*, 20817-20823.

27.) Bryant, Garnett W.; Jaskolski, W. Surface Effects on Capped and Uncapped Nanocrystals. *J. Phys. Chem. B*. **2005**, *109*, 19650-19656.

28.) Hao, Encai; et al.. Synthesis and Optical Properties of CdSe and CdSe/CdS Nanoparticles. *Chem. Mater.*. **1999**, *11*, 3096-3102.

29.) Lin, Yang-Wei; et al. Photoassisted Synthesis of CdSe and Core-Shell CdSe/CdS Quantum Dots. *Langmuir*. **2005**, *21*, 728-734.

30.) Myung, Noseung,; Bae, Yoonjung; Bard, Allen J.. Effect of Surface Passivation on the Electrogenerated Chemiluminescence of CdSe/ZnSe Nanocrystals. *Nano Letters*. **2003**, *3* (8), 1053-1055.

31.) Kaniyankandy, Sreejith; et al. Ultrafast Hole Transfer in CdSe/ZnTe Type II Core-Shell Nanostructure. *J. Phys. Chem. C*. **2011**, *115*, 1428-1435.

32.) Talapin, Dmitri V.; et al. CeSe/CdS/ZnS and CdSe/ZnSe/ZnS Core-Shell-Shell Nanocrystals. *J. Phys. Chem. B*. **2004**, *108*, 18826-18831.

33.) Zhang, Wenjin; et al. Design and Synthesis of Highly Luminescent Near-Infrared-Emitting Water-Soluble CdTe/CdSe/ZnS Core/Shell/Shell Quantum Dots. *Inorg. Chem.* **2009**, *48*, 9723-9731.

34.) Hine, Margaret A.; Guyot-Sionnest, Philippe. Synthesis and Characterization of Strongly Luminescing ZnS-Capped CdSe Nanocrystals. *J. Phys. Chem.* **1996**, *100*, 468-471.

35.) Myung, Noseung; Bae, Yoonjung, Bard, Allen J. Enhancement of the Photoluminescence of CdSe Nanocrystals Dispersed in $CHCl_3$ by Oxygen Passivation of Surface States. *Nano Letters*. **2003**, *3* (6), 747-749.

36.) Manner, Virginia W.; et al. Role of Solvent-Oxygen Ion Pairs in Photooxidation of CdSe Nanocrystal Quantum Dots. *ACS Nano*. **2012**, *6* (3), 2371-2377.

37.) Learn About LEDs. http://www.energystar.gov/index.cfm?c=lighting.pr_what_are. Accessed September 2012.

38.) Murphy, Catherine, J.. Optical Sensing with Quantum Dots. *Anal. Chem.* **2002**, *74*, 521A-526A.

39.) Zorn, Matthias; et al. Quantum Dot-Block Copolymer Hybrids with Improved Properties and Their Application to Quantum Dot Light-Emitting Devices. *ACS Nano*. **2009**, *3* (5), 1063-1068.

40.) Bae, Wan Ki; et al. Multicolored Light-Emitting Diodes Based on All-Quantum-Dot Multilayer Films Using Layer-by-Layer Assembly Method. *Nano Letters*. **2010**, *10*, 2368-2373.

41.) Kwak, Jeonghun; et al. Bright and Efficient Full-Color Colloidal Quantum Dot Light-Emitting Diodes Using an Inverted Device Structure. *Nano Letters*. **2012**, *12*, 2362-2366.

42.) Monat, Christelle; et al.. Nanoostructured Current-Confined Single Quantum Dot Light-Emitting Diode at 1300 nm. *Nano Letters*. **2006**, *6* (7), 1464-1467.

43.) Shi, Lifang; Rosenzweig, Nitsa; Rosenzweig, Zeev. Luminsecent Quantum Dots Fluorescence Resonance Energy Transfer-Based Probes for Enzymatic Activity and Enzyme Inhibitors. *Anal. Chem.* **2007**, *79*, 208-214.

44.) Ghadiali, James E.; Cohen, Bruce E.; Stevens, Molly M. Protein Kinase-Actuated Resonance Energy Transfer in Quantum Dot-Peptide Conjugates. *ACS Nano*. **2010**, *4* (8), 4915-4919.

45.) Lowe, Stuart E.; et al.. Multiplex Sensing of Protease and Kinase Enzyme Activity via Orthogonal Coupling of Quantum Dot-Peptide Conjugates. *ACS Nano*. **2012**, *6* (1), 851-857.

46.) Long, Feng; et al. Quantum Dot/Carrier-Protein/Haptens Conjugate as a Detection Nanobioprobe for FRET-Based Immunoassay of Small Analytes with All-Fiber Microfluidic Biosensing Platform. *Anal. Chem.* **2012**, *84*, 3646-3653.

47.) Zou, Zhexiang; et al. Quantum Dot-Based Immunochromatographic Fluorescent Biosensor for Biomonitoring Trichloropyridinol, a Biomarker of Exposure to Chlorpyrifos. *Anal. Chem.* **2010**, *82*, 5125-5133.

48.) Hoyer, Patrick; et al. Quantum Dot Blueing and Blinking Enables Fluorescence Nanoscopy. *Nano Letters*. **2011**, *11*, 245-250.

49.) Nelson, David L.; Cox, Michael M. *Principles of Biochemistry*. 4th ed. W.H. Freeman & Company, New York, 2005.

50.) Yin, W.; et al. Fluorescent Quantum Dot-Polymer Nanocomposite Particles by Emulsification/Solvent Evaporation. *Chem. Mater.* **2007**, *19*, 2930-2936.

51.) Hirai, Takayuki; Saito, Tsuyoshi; Komasawa, Isao. Stabilization of CdS Nanoparticles Immobilized on Thiol-Modified Polystyrene Particles by Encapsulation with Polythiourethane. *J. Phys. Chem. B.* **2001**, *105*, 9711-9714.

52.) Bradley, Melanie; Bruno, Natasha; Vincent, Brian. Distribution of CdSe Quantum Dots within Swollen Polystyrene Microgel Particles Using Confocal Microscopy. *Langmiur*. **2005**, *21*, 2750-2753.

53.) Yan, Xuehai; et al. Organogels Based on Self-Assembly of Diphenylalanine Peptide and Their Application to Immobilize Quantum Dots. *Chem. Mater.* **2008**. *20*, 1522-1526.

54.) Gattas-Asfura, Kerim M.; et al.. Immobilization of Quantum Dots in the Photo-Cross-Linked Poly(ethylene glycol)-Based Hydrogel. *J. Phys. Chem. B.* **2003**, *107*, 10464-10469.

55.) Cho, Eun Chul; et al. Thiol-Induced Assembly of Au Nanoparticles into Chainlike Structures and Their Fixing by Encapsulation in Silica Shells or Gelatin Microspheres. *Langmiur*. **2010**, *26* (12), 10005-10012.

56.) Jeong, Sanghwa; et al. One-Step Preparation of Strongly Luminescent and Highly Loaded CdSe Quantum Dot-Silica Films. *J. Phys. Chem. C.* **2010**, *114*, 14362-14367.

57.) Harvey, E. Newton. *A History of Luminescence from the Earliest Times Until 1900*. American Philosophical Society, Philadelphia, 1957.

58.)   Campaña-García, Ana; Baeyens, Willy G. *Chemiluminescence in Analytical Chemistry*.
        Marcel Dekker, New York, 2001.

59.)   Guibalt, George G. Practical Fluorescence. 2nd ed., Marcel Dekker, New York, 1990.

60.)   Sharma, Ashutosh; Schulman, Stephen G. *Introduction to Fluorescence Spectroscopy*.
        Wiley-Interscience, New York, 1999.

61.)   Albani, Jihad René. *Principles and Applications of Fluorescence Spectroscopy*. Blackwell
        Science, Ames, Iowa, 2007.

62.)   Skoog, Douglas A.; Holler, F. James; Nieman, Timothy A. *Principles of Instrumental
        Analysis*. 5th ed., Brooks Cole Thomson Learning, United States, 1998.

63.)   Parker, C. A. *Photoluminescence of Solutions. With Applications to Photochemistry and
        Analytical Chemistry*. Elsevier Publishing Co., New York, 1968.

64.)   Operating Instructions for the Perkin Elmer Model 650-10S Fluorescence Spectrophotomer.
        http://www.colby.edu/chemistry/PChem/lab/PE650-10S.pdf. Accessed April 2010.

65.)   Seitz, Rudolf W.; Neary, Michael P. Chemiluminescence and Bioluminescence. *Anal.
        Chem.* **1974**, *46* (2), 188A-198A.

66.)   Rauhut, M. M.; et al. Chemiluminescence from Reactions of Electronegatively Substituted
        Aryl Oxalates with Hydrogen Peroxide and Fluorescent Compounds. *J. Am. Chem. Soc.*.
        1967, *89* (25), 6515-6522.

67.)   Ciscato, Luiz F.; et al.. Direct Kinetic Observation of the Chemiexcitation Step in
        Peroxyoxalate Chemiluminescence. *J. Org. Chem.* **2009**, *74*, 8974-8979.

68.)   Rinehart, Jr., Kenneth L.; et al. On the Mechanism of Firefly Luciferin Luminescence. *J.
        Am. Chem. Soc.* **1975**, *97* (1), 198-200.

69.)   White, Emil H. Chemi- and Bioluminescence of Firefly Luciferin. *J. Am. Chem. Soc.* **1980**,
        102 (9), 3199-3208.

70.)   Deluca, Marlene A.; McElroy, William D. *Bioluminescence and Chemiluminescence*.
        Academic Press, New York, 1981.

71.) Lemasters, John J.; Hackenbrock, Charles R. Kinetics of Product Inhibition during Firefly Lucerifase Luminescence. *Biochemistry*. **1977**, *16* (3), 445-447.

72.) Li, Zhong-wei; et al. Color-Tuning Mechanism in Firefly Luminescence: Theoretical Studies on Fluroescence of Oxyluciferin in Aqueous Solution Using Time Dependent Density Functional Theory. *J. Phys. Chem. A*. **2008**, *112*, 9796-9800.

73.) Mohan, Arthur G.; Turro, Nicholas J. A Facile and Effective Chemiluminescence Demonstration Experiment. *J. Chem. Edu.*. **1974**, *51* (8), 528-529.

74.) Chandross, E. A. *Tetrahedron Lett*. **1963**, *4*, 761-765.

75.) Steiger, O. M.. Enhancement of peroxyoxalate chemiluminescence by copper (II) in flow injection analysis; optimization by factorial design analysis. *Analytica Chimica Acta*. **1996**, *320*, 99-105.

76.) Bollyky, L. J.; et al.. Chemiluminescence from Reactions Oxalic Anhydrides with Hydrogen Peroxide in the Presence of Fluorescent Compounds. *J. Am. Chem. Soc.* **1967**, *89* (25), 6523-6526.

77.) Rauhut, M. M.; et al.. A Study of Chemiluminescence from Reactions of Oxalyl Chloride, Hydrogen Peroxide, and Fluorescent Compounds. *J. Am. Chem. Soc.* **1966**, *88* (15), 3604-3617.

78.) Hadd, Andrew G.; et al. Chemiluminescence Demonstration Illustrating Principles of Ester Hydrolysis Reactions. *J. Chem. Edu.* **1999**, *76* (9), 1237-1240.

79.) Jonnson, Tobias; Irgum, Knut. New Nucleophilic Catalystes for Bright and Fast Peroxyoxalate Chemiluminescence. *Anal. Chem.* **2000**, *72*, 1373-1380.

80.) Bos, Richard; et al.. Studies on the mechanism of the peroxyoxalate chemiluminescence reaction, Part 1. Confirmation of 1,2-dioxetanedione as an intermediate using ^{13}C nuclear magnetic resonance spectroscopy. *Analytica Chimica Acta*. **2004**, *502*, 141-147.

81.) Emteborg, Malin; Pontén, Einar; Irgum, Knut. Influence of Imidazole and Bis(trichlorophenyl) Oxalate in the Oxalyldiimidazole Peroxyoxalate Chemiluminescence Reaction. *Anal. Chem.* **1997**, *69*, 2109-2114.

82.) Orlovic, Mirko; et al. A Simplified Model for the Dynamics of Chemiluminescence in the Oxalate-Hydrogen Peroxide System: Toward a Reaction Mechanism. *J. Org. Chem.* **1989**, *54*, 3606-3610.

83.) Hadd, Andrew G.; et al. Stopped-Flow Kinetics Investigation of the Imidazole-Catalyzed Peroxyoxalate Chemiluminescence Reaction. *J. Org. Chem.* **1998**, *63*, 3023-3031.

84.) Izaak Maurits Kolthoff: Father of Analytical Chemistry. http://www.chem.umn.edu/analytical/IMK.html. Accessed June 2012.

85.) Lakowicz, Joseph R. *Principles of Fluorescence Spectroscopy*. Springer, New York, 2006.

86.) Perkin Elmer: Fluorescence Consumables & Accessories. http://www.perkinelmer.com/Catalog/Category/ID/Luminescence%20Consumables Accessed August 2012.

87.) Horiba: FluoroLog and FluoroMax Accessories. http://www.horiba.com/us/en/scientific/products/fluorescence-spectroscopy/accessories/. Accessed August 2012.

88.) Thermo Scientific: Fluorescence. http://www.thermoscientific.com/ecomm/servlet/productscatalog_11152_L10671_81864_-1_4. Accessed August 2012.

89.) Horiba: APOA-370 Ambient Ozone Monitor. http://www.horiba.com/us/en/process-environmental/products/ambient/details/apoa-370-ambient-ozone-monitor-276/. Accessed August 2012.

90.) Cosa+Xentaur: Total Nitrogen Analyzer TN-110. http://cosaxentaur.com/page/562/total-nitrogen-analyzer-tn110. Accessed August 2012.

91.)   Shimadzu: FR-5301PC Fluorescence Spectroscopy.

http://www.shimadzu.com/an/spectro/fluoresence/rf5301.html. Accessed August 2012.

92.)   Ocean Optics: USB4000-FL Fluorescence Spectrometer.

http://www.oceanoptics.com/Products/usb4000fl.asp. Accessed August 2012.

93.)   Agilent: Fluorescence Detector (FLD). http://www.chem.agilent.com/en-US/products-services/parts-supplies/chromatography-spectrometry/lc-and-lc-ms/fluorescence-detector-(fld)/Pages/default.aspx. Accessed August 2012.

94.)   Sigvardson, Kenneth W.; Birks, John W. Peroxyoxalate Chemiluminescence Detection of Polycyclic Aromatic Hydrocarbons in Liquid Chromatography. *Anal. Chem.* **1983**, *55*, 432-435.

95.)   Hanaoka, Nobuaki; et al. Kinetic Study of Background Emission from Peroxyoxalate Chemiluminescence Reaction and Application to the Improvement of Detection Limits in Liquid Chromatography. *Anal. Chem.* **1991**, *63*, 2680-2685.

96.)   Tsunoda, Makoto; Imai, Kazuhiro. Analytical applications of peroxyoxalate chemiluminescence. *Analytica Chimica Acta*. **2005**, *541*, 13-23.

97.)   Emteborg, Malin; et al.. Peroxyoxalate chemiluminescence in aqueous solutions: Coupling of immobilized enzyme reactor and 1,1'-oxalyldiimidazole chemiluminescence reaction to flow-injection analysis and liquid chromatographic systems. *Analytica Chimica Acta*. **1997**, *357*, 111-118.

98.)   van Zoonen, Piet; et al.. Quenched Peroxyoxalate Chemiluminescence as a New Detection Principle in Flow Injection Analysis and Liquid Chromatography. *Anal. Chem.* **1986**, *58*, 1245-1248.

99.)   Ponten, Einar; et al.. Solid Phase Chemiluminescnce Detection Reactors Based on in Situ Polymerized Methacrylate Materials. *Anal. Chem.* **1996**, *68*, 4389-4396.

100.) Stigbrand, Malin; Darlsson, Anders; Irgum, Knut. Direct and Selective Determination of Atomspheric Gaseous Hydrogen Peroxide by Diffusion Scrubber and 1,1'-Oxalyldiimidazole Chemiluminescence Detection. *Anal. Chem.* **1996**, *68*, 3945-3950.

101.) Betteridge, D. Flow Injection Analysis. *Anal. Chem.* **1978**, *50* (8), 832A-846A.

102.) Ranger, Craig B. Flow Injection Analysis: Principles Techniques Applications Design. *Anal. Chem.* **1981**, *53* (1), 20A-32A.

103.) Stewart, Kent K. Flow Injection Analysis: New Tool for Old Assays, New Approach to Analytical Measurements. *Anal. Chem.* **1983**, *55* (9), 931A-940A.

104.) Ruzicka, Jaromir; Hansen, Elo H. *Flow Injection Analysis*. 2nd ed. J. Wiley, New York, 1988.

105.) Leach, Andrew M.; Wheeler, Aaron R.; Zare, Richard N. Flow Injection Analysis in a Microfluidic Format. *Anal. Chem.* **2003**, *75*, 967-972.

106.) Kotormán, Márta; Simon, Mária; Szajáni, Béla. Application of a Flow Injection System in Wine Analysis. *J. Agric. Food Chem.* **1991**, *39*, 909-910.

107.) Nanita, Sergio C.; Pentz, Anne M.; Bramble, Frederick Q. High-Throughput Pesticide Residue Quantuative Analysis Achieved by Tandem Mass Spectrometry with Automated Flow Injection. *Anal. Chem.* **2009**, *81* (8), 3134-3142.

108.) Kiba, Nobutoshi; et al. Chemluminometric Sensor for Simultaneous Determination of L-Glutamate and L-Lysine with Immobilized Oxidases in a Flow Injection System. *Anal. Chem.* **2002**, *74* (6), 1269-1274.

109.) Honda, Kazumasa; Sekino, Jun; Imal, Kazuhiro. Bis(2,4-dinitrophenyl) Oxalate as a Chemiluminescence Reagent in Determination of Fluorescenct Compounds by Flow Injection Analysis. *Anal. Chem.* **1983**, *55*, 940-943.

110.) Milosfsky, Robert E.; Birks, John W. Photoinitiation of Peroxyoxalate Chemiluminescence: Application to Flow Injection Analysis of Chemilumophores. *Anal. Chem.* **1990**, *62*, 1050-1055.

111.) Lee, Hye Jin; et al. Pulse Amperometric Detection of Salt Concentrations by Flow Injection Analysis Using Ionodes. *Anal. Chem.* **2000**, *72*, 5562-5566.

112.) Dai, Quanqin; et al. Temperature Dependence of band gap in CdSe nanocrystals. *Chemical Physics Letters.* **2007**, *439*, 65-68.

113.) Sigma-Aldrich: CdSe quantum dots. http://www.sigmaaldrich.com/catalog/search?interface=All&term=cdse&lang=en&region=US&focus=product&N=0+220003048+219853269+219853286&mode=match%20partialmax. Accessed February 2013.

VITA

CHRISTOPHER S. MOORE

Personal Data: Date of Birth: March 28, 1985

                          Place of Birth: Kingsport, Tennessee

                          Marital Status: Engaged

Education: Daniel Boone High School

                               Gray, Tennessee (2003)

                          East Tennessee State University

                               Johnson City, Tennessee; Chemistry; B.S. (2008)

                          East Tennessee State University

                               Johnson City, Tennessee; Chemistry; M.S. (2013)

Professional Experience: Tutor of Biology, Chemistry, and Calculus

                               East Tennessee State University

                               Kingsport, TN, 2007-2008

                          Undergraduate Lab Instructor

                               East Tennessee State University

                               Johnson City, Tennessee, 2008-2009

                          Analytical Laboratory Technician

                               Eastman Chemical Company

                               Kingsport, Tennessee, 2008-2012

                          Analytical Chemist

                               Eastman Chemical Company

                               Kingsport, Tennessee, 2012-Current